CRJ700 Regional Aircraft Performances Optimization Using Adaptive Winglet Systems

by

Marine SEGUI

MANUSCRIPT-BASED THESIS PRESENTED TO ÉCOLE DE TECHNOLOGIE SUPÉRIEURE IN PARTIAL FULFILLMENT FOR THE DEGREE OF DOCTOR OF PHILOSOPHY
Ph. D.

MONTREAL, JUNE 29TH, 2022

ÉCOLE DE TECHNOLOGIE SUPÉRIEURE
UNIVERSITÉ DU QUÉBEC

BOARD OF EXAMINERS

THIS THESIS HAS BEEN EVALUATED

BY THE FOLLOWING BOARD OF EXAMINERS

Mrs. Ruxandra Mihaela Botez, Thesis Supervisor
Department of Systems Engineering at École de technologie supérieure

Mr. Philippe Bocher, President of the Board of Examiners
Department of Mechanical Engineering at École de technologie supérieure

Mr. Guy Gauthier, Member of the jury
Department of Systems Engineering at École de technologie supérieure

Mr. Jeremy Laliberté, Member of the jury
Department of Mechanical and Aerospace Engineering at Carleton University

Mr. Adrian Hiliuta, External Evaluator
CMC Electronics

THIS THESIS WAS PRENSENTED AND DEFENDED

IN THE PRESENCE OF A BOARD OF EXAMINERS AND PUBLIC

ON JUNE 21ST

AT ÉCOLE DE TECHNOLOGIE SUPÉRIEURE

FOREWORD

The aerospace industry has often been an axis of technological progress and international challenges. Thus, the best aircraft manufacturers have competed to claim the best innovations: the most efficient, the biggest, or the fastest aircraft. Nearly 500 years after Leonardo da Vinci designed the first flying machine, aviation is facing a new challenge: ecological issues.

Several research projects are being conducted to reduce the emission of toxic gases from aircraft into the atmosphere, and this project is part of one of them. Inspired by biomimetics, the "Morphing-Wing" technology has shown much promise. Morphing systems aim at improving the performance of an aircraft by adapting the geometry of the wing during flight. However, is such a system efficient enough to reduce the fuel consumption and the associated emissions of an aircraft? This is the challenge I attempt to address at the Research Laboratory in Active Control, Avionics and AeroServoElasticity (LARCASE).

Preliminary analyses were performed during my master studies. The very interesting results I found led me to further develop this project during the last three years of my PhD. This thesis presents the work done and the conclusive results obtained.

ACKNOLEDGMENTS

I would like to thank my thesis supervisor Ruxandra Botez, head of the LARCASE laboratory at ÉTS. I would like to thank her for her financial support and for many corrections made to all of my publications. I would also like to thank her for all the opportunities and responsibilities she gave me at LARCASE and at ÉTS, many thanks.

Then, I would like to thank Jérémy Laliberté and Salman Shafi for allowing me to join and be funded by the CREATE UTILI program. This program allowed me to enhance my knowledge on unmanned aerial systems. I also met people from the drone industry through meetings, workshops and internships, which was very fulfilling. In this context, I would also like to thank Ian Glenn and the entire ING aviation team for the great work done during my last internship.

I would like to thank Alessandro Ceruti for the opportunity to work on my research with two of his students Federico and Vittorio. This collaboration was enriching, and allowed us to share our knowledge and culture to conduct very good research. Thank you also for your support in editing, it was helpful to me.

Dear jurys, I also would like to thanks you for the time you spent reading and evaluating this thesis.

I would like to thank my colleague at LARCASE, Georges Ghazi, Radu Dancila, Manuel Gurrola-Arrieta, Rojo, Yvan Tondji, Elias Zohreh, and the great trainees I was able to work with during this thesis; Federico R. Abel, Vittorio Rugoli, Maxime Baudier et Clément Biet. We have shared good moments despite the COVID19 crisis, thank you for your good mood.

My deepest feelings go to my parents and my friends who never stop bringing me their joy of life and their support. My parents, thank you for these moments of complicity, of sharing although we are far away, *merci pour tout (et pour les tuto Maurice!)*.

These doctoral studies were difficult for me, especially due to the context of the health crisis. In spite of everything, I always found the courage to continue thanks to your unconditional support. You have always been there to motivate me, make me happy and cheer me up, especially during difficult times. You are a piece of chocolate every day and you know how much I love chocolate! The future still holds challenges and projects, together I have no doubt that we will overcome them, thank you my love.

Finally, this work could not have been written without my dear *Ridsa* and *la bande 13 organisée*, which brought me the necessary concentration, CMBB. Another thought for my animals stayed in France who give me joy and good mood when I can finally hold them close to me.

I wish finally to have one more thought to the stars who watch over me, up there, mon béw, my auntie, my uncle, and my grandparents, I hope you are proud once again.

OPTIMISATION DES PERFORMANCES D'UN AVION À L'AIDE DE SYSTÈMES D'AILES DÉFORMABLES

Marine SEGUI

RESUMÉ

Concerné par l'impact de l'aviation dans le réchauffement climatique, cette thèse vise à montrer les avantages d'équiper les avions d'ailettes adaptatives. Par soucis de validation, l'étude a été appliqué à l'avion régional CRJ700. En effet, le Laboratoire de recherche en commande active, avionique et aéroservoélasticité (LARCASE) dispose d'un simulateur de vol qualifié d'un niveau D pour cet avion. Cet outil est essentiel dans cette recherche car il permet de délivrer des données de vol admettant une erreur maximale de 5% avec les données de vol réelles de l'avion. De plus, un modèle géométrique de l'avion CRJ700 a été fourni par le constructeur Bombardier, ce qui nous a permis de travailler avec la géométrie originale de l'avion exact.

Un système d'ailette adaptative a été développé afin d'être présenté comme une solution à court terme pour améliorer les performances des avions et ainsi réduire leur consommation de carburant. L'ailette est l'une des dernières parties que l'on assemble sur un avion. En conséquence, il a été considéré que changer les ailettes conventionnelles par des ailettes adaptatives devrait être peu couteux d'un point de vue production.

L'ailette adaptative développée dans cette thèse effectue une rotation entre -93 deg et +93 deg, en considérant que pour un angle de 0 deg, l'ailette est parallèle à l'horizon. Pour réaliser l'analyse aérodynamique, un modèle de haute-fidélité a été développé à l'aide du logiciel open-source OpenFoam. Une méthodologie spécifique a été établie afin de rendre le modèle entièrement paramétrique et convergent pour l'ensemble des conditions de vol testées, considérant des angles d'attaque entre -2 deg et +4 deg, ainsi qu'un nombre de Mach allant jusqu'à 0.79 pour une altitude de 30,000 ft. Pour l'ensemble des conditions de vol, le modèle aérodynamique a pu être validé avec précision, notamment en admettant une marge d'erreur maximale de 0.0026 sur l'évaluation du coefficient de trainée.

En utilisant ce modèle, une étude aérodynamique a pu être effectuée. Face au coût de calcul, il a été choisi de réaliser des simulations pour les positions d'ailettes -93, -73, -35, 0, 35, 73 et 93 deg et d'ensuite prédire l'évolution des coefficients aérodynamiques pour les positions d'ailettes intermédiaires grâce à des méthodes d'interpolation. Cette méthodologie a permis d'étudier les coefficients aérodynamiques des différentes positions d'ailette disponible entre -93 et +93 deg, et pour 35 conditions de vols communément utilisées par l'avion CRJ700. En résultats, il a été trouvé que pour une même condition de vol le coefficient de portance d'un avion équipé d'une ailette adaptative été fortement augmenté alors que le coefficient de trainé avait été réduit par rapport à la configuration originale de l'avion. Ceci a permis de démontrer

que pour un coefficient de portance donné, un avion équipé d'une ailette adaptative disposé d'une trainée 2.65% inférieure à la trainée du même avion équipé d'une ailette fixe.

Une étude de performance a ensuite été conduite à l'aide d'un modèle développé et validé au LARCASE. Pour l'utiliser, une méthodologie a été développé afin d'isoler les contributions aérodynamiques du groupement « aile-fuselage » et « aile-horizontal de queue » de l'avion, à partir des calculs globaux effectué avec le logiciel OpenFoam. De plus une méthode pour calculer l'angle de déviation du fluide par l'aile (downwash) a été développé. À l'aide de ces données, des avantages d'équiper un avion avec des ailettes déformables ont pu être mise en avant, notamment avec un temps de monté amélioré de 4.21% (en moyenne), une consommation de carburant réduite de 3.79% en monté (en moyenne) et de 1.99% en croisière (en moyenne).

Mots-clés : Aérodynamique, Modélisation, Morphing-Wing, Optimisation, Performances

AIRCRAFT PERFORMANCES OPTIMIZATION USING MORPHING SYSTEMS

Marine SEGUI

ABSTRACT

Motivated by the impact of aviation on global warming, this thesis aims to show the advantages of equipping aircraft with adaptive winglets. For validation purposes, the study was applied to the CRJ700 regional aircraft. Indeed, the Research laboratory of active control, avionics and aeroservoelasticity (LARCASE) has a level D flight simulator for this aircraft. This tool is essential in this research because it allows to deliver flight data admitting a maximum error of 5% with the real flight data of the aircraft. Moreover, a geometric model of the CRJ700 aircraft was provided by the manufacturer Bombardier, allowing us to work with the exact original geometry of the aircraft.

An adaptive winglet system was developed to be presented as a short-term solution to improve aircraft performance and thus reduce its fuel consumption. The winglet is one of the last parts to be assembled on an aircraft. Therefore, it was considered that changing conventional winglets to adaptive winglets should be relatively cost-effective from a production perspective.

The adaptive winglet developed in this thesis rotates between -93 deg and +93 deg, considering that for an angle of 0 deg, the winglet is parallel to the horizon. To perform the aerodynamic analysis, a high-fidelity model was developed using the open-source software OpenFoam. A specific methodology was established to make the model fully parametric and convergent for all flight conditions tested, considering angles of attack between -2 deg and +4 deg, as well as Mach number up to 0.79 for an altitude of 30,000 ft. The aerodynamic model validated for all these flight conditions with high accuracy, for instance by admitting a maximum margin of error of 0.0026 for the drag coefficient estimation.

Using this model, an aerodynamic study was conducted. Due to the computational cost, it was chosen to perform simulations for the winglet positions of -93, -73, -35, 0, 35, 73 and 93 deg, and to then predict the evolution of the aerodynamic coefficients for the intermediate winglet positions using interpolation methods. This methodology allowed the aerodynamic coefficients of the different winglet positions available between -93 and 93 deg to be studied, and for 35 flight conditions commonly used by the CRJ700 aircraft. It was found that for the same flight conditions the lift coefficient of an aircraft equipped with an adaptive winglet was significantly increased, while the drag coefficient was reduced compared to the original aircraft configuration. This demonstrated that for a given lift coefficient, an aircraft equipped with an adaptive winglet had a drag 2.65% lower than the drag of the same aircraft equipped with a fixed winglet.

A performance study was then conducted to analyze the benefits in terms of fuel consumption using a model developed and validated at the LARCASE. A methodology was developed to isolate the aerodynamic contributions of the "wing-body" and "horizontal-tail" groupings of the aircraft from the global calculations, computed using the OpenFoam software. In addition, a method to calculate the downwash deviation angle of the fluid by the wing was developed. Using these data and methodologies, the advantages of equipping an aircraft with adaptive winglets can be confirmed, particularly with a climb time improved by 4.21% on average, fuel consumption reduced by 3.79% on average during climb and by 1.99% on average during cruise.

Keywords: Aerodynamics, Modelling, Morphing-Wing, Optimization, Performances

TABLE OF CONTENTS

Page

LIST OF TABLES

Page

LIST OF FIGURES

Page

LIST OF ABREVIATIONS

ANCAT	Advisory Council for Aerospace Research in Europe
LARCASE	Laboratoire de Recherche en Commande Active, Avionique et Aéroservoélasticité
CAD	Computer-Aided Design
CRIAQ	Consortium de Recherche et d'Innovation en Aérospatiale au Québec
CO_2	Carbon dioxide
CIRA	Italian Aerospace Research Center
CG	Gravity Center
CORSIA	Carbon Offsetting and Reduction Scheme for International Aviation
CRJ700	Regional Jet 700
EDF	Environmental Defense Funds
GHG	Greenhouse gas
ICAO	International Civil Aviation Organization
FAA	Federal Aviation Administration
NLF	Natural Laminar Flow
IAR-NRC	Institute for Aerospace Research - National Research Council of Canada
TLA	Throttle Lever Angle
CFD	Computationnal Fluid Dynamics
VLM	Vortex Lattice Method
NS	Navier Stokes equations
RAM	Random Access Memory
RANS	Reynolds Averaged Navier Stokes equations

SIMPLE	Semi-Implicit Method for Pressure-Linked Equations
S-A	Spallart-Allmaras turbulence model
SST	Shear Stressed Transport equations
STL	Triangulated geometry file
SHM	snappyHexMesh OpenFoam utility
VSIM	Virtual Simulator product of CAE
VRESIM	Virtual Research Simulator of the CRJ700 at LARCASE
UAV	Unmanned Aerial System
NASA	National Aeronautics and Space Administration
ISA	International Standard Atmosphere
PSO	Particle Swarm Optimization algorithm
PTERA	Prototype-Technology Evaluation and Research Aircraft
ToC	Top of Climb
CI	Cost Index
CAS	Calibrated air Speed
GAMG	Geometric-Algebraic Multi Grid

LIST OF SYMBOLS

General

U	Flow velocity magnitude and direction ($m.s^{-1}$)
p	Kinematic pressure ($m^2.s^{-2}$)
P	Pressure ($kg.m^{-1}.s^{-2}$)
ν	Kinematic viscosity ($m^2.s^{-1}$)
$\tilde{\nu}$	Turbulent kinematic viscosity ($m^2.s^{-1}$)
μ	Dynamic viscosity ($kg.m^{-1}.s^{-1}$)
k	Turbulence parameter for $k-\omega$ model ($m^2.s^{-2}$)
ω	Turbulence parameter for $k-\omega$ model (s^{-1})
C_L	Lift coefficient (aircraft)
C_D	Drag coefficient (aircraft)
C_{M_y}	Pitching moment coefficient (aircraft)
ξ	Adaptive winglet deflection angle (deg)

Aerodynamic symbol relative to the aircraft

L	Lift force (N)
D	Drag force (N)
M_y	Pitching moment (N.m)
C_{L_s}	Lift coefficient (stability axis)
C_{D_s}	Drag coefficient (stability axis)
C_{M_s}	Pitching moment coefficient (stability axis)
ρ	Air density ($kg.m^{-3}$)
S	Reference area (m^2)

$\bar{c}$	Mean aerodynamic chord (m)
α	Angle of attack (deg)
M	Mach number
V	True Air Speed (m/s)
δ_{stab}	Horizontal stabilizer angle (deg)
δ_{elev}	Elevators deflection angles (deg)
ε	Downwash flow deviation angle (deg)
x_{ht} and z_{ht}	Cartesian projections (horizontal and vertical) between the wing aerodynamic center and the tail (m)
F_N	Required thrust force (N)
F_b	Fuel burn (lb)
R/C	Rate of climb (ft/min)
γ	Flight path angle (deg)

Aerodynamic symbols relative to the *wing-body*

$C_{L_{(wb)}}$	Lift coefficient
$C_{D_{(wb)}}$	Drag coefficient
$C_{M_{(wb)}}$	Pitching moment coefficient
S_{wb}	Wing reference area (m^2)

Aerodynamic symbols relative to the *horizontal-tail*

$C_{L(ht)}$	Tail lift coefficient
$C_{D(ht)}$	Tail drag coefficient
α_{ht}	Tail angle of attack (°)
S_{ht}	Tail reference area (m^2)

INTRODUCTION

In today's world of innovation, simplicity and technology, more and more people are concerned about climate change and its short- and long-term effects. Thus, with our eyes fixed on the biological clock of the Earth, we must work towards the future innovations. The aerospace sector, with its 2% of the world's carbon dioxide emissions, represented close to 915 million tons of carbon dioxide (CO_2) emission in 2019 (IATA, 2019) and 859 million tons of CO_2 in 2017 (Aviation: Benefits Beyond Borders, 2018). These figures highlight the need to design a new generation of aircraft, extremely efficient and targeting zero emissions.

0.1 Problem Statement

Fully involved in the global warming studies, the International Civil Aviation Organization (ICAO) has required aircraft manufacturers to reduce their 2005 emissions by half by 2050 (ICAO, 2010). To support the ICAO requests, the Carbon Offsetting and Reduction Scheme for the International Aviation (CORSIA) program, that was initiated in January 2019. This program intends to claim a financial contribution from the polluting operators, dependent on their CO_2 emissions (ICAO, 2020).

These initiatives of the aviation authorities reveal how much the aerospace professionals are now realizing the importance of reducing green-house emissions.

0.2 Solutions

The 30-years margin to reach 2050 is a very short time frame for the aeronautical industry. Indeed, in this industry, the process to design a new aircraft is long, on one hand because of the time length of design and production of an aircraft, and on the other hand because of the high number of safety analyses tests that must be performed before its delivery. Therefore, it is important to act on two temporal levels: short and long terms.

For the long-term period, more environmentally-friendly aircraft are being planned, such as a full electric aircraft. To develop this concept, a bi-plane has been designed to fly using only electrical energy: the “Solar Impulse” (Solar Impulse Foundation, 2016b). The aircraft has successfully completed a world tour (43,000 km) in 23 days, reaching a maximum altitude of 9,102 meters and a maximum indicated airspeed of 49 knots (Solar Impulse Foundation, 2016a). This project has been a real step towards green energy aircraft applications, encouraging engine manufacturers to develop electric and hybrid engines for their use on new aircraft generations. Sixteen years after the launching of the Solar Impulse, Siemens is about to sell its electric and hybrid motor branch “eAircraft” to Rolls Royce, one of the biggest players on the engine market (Rolls-royce, 2019). In partnership with Airbus, Rolls Royce has worked on the design of an engine capable of providing up to 2 MW. That prototype was planned to replace one of the four jet engines required by the “E-FAN X” aircraft for its first flight, planned for 2021 (Airbus, 2020). That project aimed at designing a hybrid-electric aircraft for 50 to 100 passengers (Vittadini, 2020). Even though the project was cancelled in April 2020 due to the COVID19 crisis, it remains a promising project for the development of electrical aircraft engines.

For both short and medium terms, research has also been focused on new trajectory optimizations and procedures to reduce aircraft greenhouse emissions. This research aimed to develop new algorithms to obtain the best route that would burn the least amount of fuel possible to reach the arrival airport. Similarly, some modifications regarding airport departure and arrival procedures were analyzed and further improved to reduce carbon emissions, as well as aircraft noise around airports. These studies have shown that fuel costs have been reduced by up to 7.44% (Murrieta-Mendoza, 2017).

Other solutions consist in improving existing aircraft by enhancing flight dynamics and performance models. On one hand, an on-board performance model could be improved while considering an aircraft’s degradation with time (in terms of drag and related engine performance models). This improvement should ensure that the predicted fuel burn is closer to the real consumption; the improved model may recommend cleaning, or replacing certain parts

prior to maintenance dates in order to keep the aircraft in its optimal condition at all times (Ghazi, Gerardin, Gelhaye, & Botez, 2020). On the other hand, existing aircraft design could be geometrically improved, for instance by replacing its winglets or its horizontal tail surfaces with new, more efficient systems (e.g., using new materials increasing laminar surface of the wings) or by equipping them with a morphing system (Marine Segui, 2018).

Inspired by bird flight, morphing wing technology aims at improving the efficiency of wings by locally adapting their geometries during flight (Concilio, Dimino, Lecce, & Pecora, 2018). Thus, for each flight condition encountered, the geometry of a wing would change with the aim to offer optimal performances (i.e., minimum fuel consumption, minimum flight time, etc.). As a result, the aircraft geometry will be optimized for the entire flight, which will considerably reduce the amount of fuel required, and therefore, it would reduce its associated carbon footprint.

0.3 Global Research Objective

Although all solutions described in the above section appear to be innovative and highly efficient, the morphing wing technique seems to be especially promising, and it would be of particular interest to us. Indeed, among the short- and medium-term solutions, this technique has the greatest potential to improve the performance of existing aircraft.

The main objective of this research is to design, and therefore, to analyze the effect of a morphing wing system in flight on the overall performance of an aircraft. More concretely, using the new system, our main objective is to reduce the fuel consumption of an aircraft over the whole flight, by at least 3%.

The 3% reduction in fuel consumption objective has been estimated from various types of models predicting greenhouse gas (GHG) emissions into the atmosphere. There are different models, that predict the amount of gas that will be emitted by aircraft in the coming years, based on the evolution of the air traffic, and thus, on the evolution of the overall fuel efficiency

of aircraft. Greenhouse gas emissions for the year 2100 are predicted by the Environmental Defense Funds (EDF) model by considering an aircraft fuel efficiency improvement of 0.9% per year. Similarly, the National Aeronautics and Space Administration (NASA), the Abatement of Nuisances Caused by Air Transport (ANCAT), and the Deutsches Zentrum für Luft- und Raumfahrt (DLR) models currently used for the medium-term range are based on a fleet energy improvement of 1% per year. Another model developed by the Advisory Council for Aerospace Research in Europe (ACARE) established forecasts based on a higher improvement in energy optimization of 2% per year (République Française, 2005).

Finally, to reach the target set in 2005, and to decrease the trend of CO_2 emissions under the CORSIA program, the ICAO predicts that the efficiency of new aircraft will have to be 3% better than that of their predecessors (ICAO, 2010). As we only consider here an improvement related to aerodynamics (without considering an additional improvement that could be brought by new engines or by trajectory optimization procedures in avionics systems), the optimized aircraft design proposed in this thesis should demonstrate a fuel saving of at least 3% in order to meet the minimum ecological requirements.

0.4 Global Methodology and Thesis Organization

This research has developed a new morphing system and has performed several analyses to achieve an aircraft performance improvement of at least 3% over a single flight. Thus, this research is multidisciplinary and involves knowledge of several fields, such as mechanical design, aerodynamics, flight mechanics and aircraft performance.

Due to the complexity of this research, it was chosen to focus this thesis on analyses that would demonstrate improved performance, and consequently reduced in-flight fuel consumption. This thesis is organized into five chapters which present the scientific approach used to reach the main objective.

The first chapter presents the state of the art and the specific sub-objectives to be fulfilled in order to reach the research main objective. This first chapter introduces the project, its objectives, including the originality of the new morphing system, and highlights the contributions of this thesis.

The methodology developed in the context of this thesis is outlined in Chapters 2 to 4, where each chapter corresponds to the resolution of each sub-objective of the thesis. These chapters correspond to two published journal papers and a third paper under review.

General remarks and discussions are presented in the fifth chapter, which also includes future work recommendations.

CHAPTER 1

STATE-OF-THE-ART AND RESEARCH CONTRIBUTIONS

To expose all the resources needed to carry out this project, an overview of the state-of-the-art was assembled. This bibliographical research summarizes the studies performed within the framework of morphing wing technologies and presents the tools that we might use to achieve our objective.

This critical review of the literature allowed us to identify the methodologies and the hypotheses required to reach our main objective. In addition, this first chapter presents the specific objectives of the thesis and describes the originality of this work.

1.1 State-of-the-Art – Aircraft Geometry Optimization

As noted above, a complete state-of-the-art was established to introduce the reader to the work. This section covers studies conducted to improve aircraft performance using a geometrical modification. Two kinds of geometrical modifications could be distinguished:

- "Fixed" geometrical modification, which consists of replacing a section of an aircraft, for instance, the wing, by another wing, equipped with new materials to improve its aerodynamic qualities; and
- "Moveable" geometrical optimization, in which an aircraft's surface is replaced by a new one equipped with a morphing control system that will change its geometry during flight. This optimization category is usually called "morphing-wing" or "variable geometry", and sometimes "adaptive geometry".

1.1.1 Optimization using Fixed Geometry

As stated in the 2016 ICAO Environmental Report, advances in materials, structure and aerodynamics are expected to significantly reduce aircraft-induced drag and weight (ICAO, 2016). The ICAO also states that it would be particularly interesting to work on the

optimization of certain aircraft surface geometries, such as wings, engine nacelles, empennages and fuselages.

Many research studies have been undertaken to improve and optimize aircraft structures and aerodynamics, so that they can "glide more", "drag less" or "carry more payload". To reduce aircraft weight, structural materials have been improved, firstly with wood, then with steel, and today with composites. For instance, among the latest aircraft introduced to the market, the Airbus A350 and the Boeing B787 are composed of 53% and 50% carbon fiber, respectively (Cummins, 2019).

To improve aircraft aerodynamics, a significant drag reduction could be achieved by maintaining "Natural Laminar Flow" (NLF) on the leading edges of the wings and nacelles. In addition, applications of "Active Flow Control" could also be implemented, particularly on surfaces with large deflection angles, such as a control surface (the Boeing 757's EcoDemonstrator, for example). It is estimated that a 5% increase of the aircraft lift-to-drag ratio can be achieved if its geometry is optimized to maintain a laminar flow (ICAO, 2016).

The Airbus BLADE project is based on the concept of "Natural Laminar Flow" (NLF). In one study, an Airbus A340's wingtips were cut off and they were replaced by two new wingtips. These new wingtips were equipped with supercritical airfoils, and with an extra-smooth skin allowing a more laminar flow. These new wingtips have a smaller sweep deflection angle than the remaining wing. Using this feature, the supercritical behavior of the new wingtip was analyzed, while the sweep angle did not influence the results. It was expected that the friction between the wing and the flow would be reduced by at least 50%, which should lead to a reduction in fuel consumption of at least 5% according to Airbus. To date, at least 23 flight tests have been carried out, which is equivalent to almost 65 hours of flight time, but no results have yet been published (Goold, 2018).

Another idea concerns the blended wing body (BWB) geometry, currently being analyzed by manufacturers such as NASA, Bombardier and Airbus. Wind tunnel and demonstrator flight

tests found that this geometry is more efficient than conventional aircraft geometry (Duvelleroy, Benquet, & Ramadier, 2020 ; Firdaus Mohamad et al., 2010 ; Galea, Filippidis, Wang, Lawrence, & Ewer, 2011). However, this new design still raises problems in terms of passenger safety, for instance, for emergency evacuation plans or maneuvering loads. Indeed, the development of safety instructions and their certification is a considerable work, which still requires more years of study.

More generally, wings, as well as each surface included in the aircraft geometry, have been sized to offer a global efficient flight over its entire flight envelope (Raymer, 2012a). Indeed, an aircraft must be able to fly with a weight that can vary up to 40% on average from its empty weight, in a variable environment, defined by altitudes varying (roughly) from 0 to 50,000 ft and Calibrated Air Speeds (CAS) ranging from 0 to 350 knots (Mach numbers up to 0.9). Since an aircraft will encounter a large range of flight conditions, we can mention that the geometries of conventional aircraft might not be optimized for each point of the flight envelope. From this point of view, projects dedicated to aerodynamic optimization by laminarity, although innovative and promising, aim at improving the global aircraft aerodynamics.

1.1.2 Optimization using “Morphing-Wing” Techniques

Another technology, aimed at adapting aircraft geometry during flight, could be very interesting to implement as a means to reach the ICAO objectives in the short term. This "adaptive geometry" or “morphing-wing” technology aims to change the shapes of the aircraft's wings to optimize their aerodynamic parameters during flight. The origins of this technique can be traced back to Germany during World War II and to efforts in the United States in the 1950s. This technology was mainly developed on fighter aircraft, using “variable wings”, with the aim to allow optimal flight in both subsonic and supersonic regimes (the Tomcat F14, the Mirage G8 or the Tornado F3 were equipped with the variable sweep technology, for instance). Morphing wing systems can also be found on UAVs, with the goal of reducing the drag of the wings and increasing their operational range.

Other techniques of variable geometry have been observed in aviation. We can note in particular the concept of the oblique wing allowing drag reduction at high speed (in the supersonic domain). This concept was developed by NASA, and tested in flight in 1979 with on AD-1 aircraft.

Variable geometries have been considered to revolutionize supersonic civil aviation by NASA as part of the NASA Aeronautics's University Leadership Initiative (ULI) (Datta & Lagoudas, 2021 ; Schrass, Leal, & Hartl, 2020). Indeed, the supersonic aircraft aims to use variable systems (i.e., structure, skins, actuators, etc.) to optimize flight performance, manage the supersonic boom and therefore to reduce the noise when the aircraft flies over land.

In the morphing wing field, as experts usually aim to precisely reduce the drag of an aircraft, or to slightly increase the lift, a technique aiming to morph the airfoil during flight was developed. Various researches on morphing wings have been explored; in order to apply new systems based on airfoil distortion to civil aircraft. Some of them were described in following paragraphs.

In 2016, together with FlexSys laboratory, NASA proposed the FlexFoil project to replace wing flaps with a morphing wing system (Herrera, Lung, Ervin, & Flick, 2015 ; Kota, Flick, & Collier, 2016). The objective was to manufacture a new wing with flaps integrated into the skin of the wing. A completely flexible wing was then designed with the aim of eliminating all existing junctions between the fixed and moving surfaces of the conventional wing, as they were particularly responsible for the flaps turbulence, noise, and mechanical fatigue. To reproduce the flaps action, the airfoil trailing edge shape of the wing was changed according to its camber parameters. Extremely smooth materials, capable of significantly reducing the friction on the wing surface, were selected to equip the Gulfstream III prototype business aircraft. This change was expected to reduce the noise during takeoff and landing phases by 30%. In addition, this approach made it possible to reduce the drag of an initially fixed long-range wing by 5 to 12%, leading to significant fuel savings (Kota, 2016).

A study based on measuring aircraft performance improvement using morphing wing systems was developed at Michigan University. The methodology consisted of combining the aerodynamic and structural optimization of wing airfoils in order to reduce fuel consumption. The performance studies were carried out on the NASA "Common Research Model" (CRM), an aircraft type close to that of Boeing 777-200ER. Aerodynamic calculations were performed in the transonic domain using a high-fidelity CFD resolution coupled with a Spalart-Allmaras turbulence model. For its long-range mission, it was found that the fuel consumption could be reduced by up of 1% during a flight (climb, cruise and descent phases). By modifying the structural elements, the drag was reduced by up to 5% for several flight conditions, which lead to an additional fuel consumption reduction of up to 2.7% (Burdette & Martins, 2019 ; Martins, 2016 ; Zhang, Khosravi, & Zingg, 2017).

The Research Laboratory in Active Controls, Avionics and Aeroservoelasticity (LARCASE) has found several promising results, notably in the CRIAQ 7.1 and the Canadian-Italian MDO 505 projects, called “Laminar Flow Improvement on an Aeroelastic Research Wing” and “Morphing Architectures and Related Technologies for Wing Efficiency Improvement”, respectively. The results of these projects are mentioned in various LARCASE publications (Koreanschi, Sugar Gabor, & Botez, 2016a ; Sugar Gabor, Koreanschi, Botez, Mamou, & Mebarki, 2016a, 2016b). The control laws for morphing wings using electrical actuators were designed, and experimental validations were performed at the LARCASE Price-Païdoussis and IAR-NRC Wind Tunnels (R. M. Botez et al., 2018 ; Grigorie & Botez, 2018 ; Grigorie, Khan, Botez, Mamou, & Mébarki, 2019 ; Popov, Grigorie, Botez, Mébarki, & Mamou, 2010 ; Tchatchueng Kammegne et al., 2017 ; Tchatchueng Kammegne & Botez, 2019). Numerical simulations as well as wind tunnel tests have shown that by deforming a part of the original wing airfoil, a reduction in drag of up to 14% was possible (Sugar Gabor, Simon, Koreanschi, & Botez, 2014).

Particularly invested in morphing wing research, the LARCASE has also developed methodologies to analyze different morphing techniques applied on the wing leading and trailing edges. All of these have been validated using wind tunnel experiments (Bashir,

Longtin-Martel, Botez, & Wong, 2021 ; Communier, Botez, & Wong, 2019 ; Elelwi, Calvet, Botez, & Dao, 2021).

Thanks to the expertise acquired through these major projects, a new project has been initiated at LARCASE, as part of the Canada Research Chair in Aircraft Modeling and Simulation. This project aims at studying the impacts of morphing systems on Cessna Citation X performance during flight. A morphing system was developed based on the space available onboard, so that fuel tanks could still be located on wings, for instance. As the easiness of this new system implementation was a major constraint, it was decided to install the morphing wing system on the horizontal tail of the Cessna Citation X, as it has no fuel tanks. The morphing system was in charge of balancing (i.e., trimming) the aircraft by changing the horizontal tail airfoil shape instead of changing the horizontal stabilizer angle. Aerodynamic calculations were coupled to optimization processes. Simplified resolution methods, such as the Vortex Lattice Method (VLM), were performed using the NASA open-source software OpenVSP. The airfoil distortion was modeled using a BP3434 parameterization methodology and a Particle Swarm Optimization (PSO) algorithm. This study demonstrated a fuel consumption reduction of 6% to 7% during cruise, which is a fuel reduction equivalent to 100 lbs per hour (Marine Segui, Mantilla, Ghazi, & Botez, 2018).

These recent studies have demonstrated that morphing systems are of great interest to improve aircraft aerodynamics, and therefore to reduce its fuel consumption. To achieve performance results, such as precise fuel consumption values, several models are required, including aerodynamic, structural or performance models. However, obtaining accurate structural data from aircraft manufacturers is a very difficult task because of their confidentiality.

Innovative morphing wing systems, easy to implement in a conventional aircraft geometry (that does not impact fuel tanks), are currently of special interest to efficiently improve the world’s air fleet.

1.2 Winglet Geometry Optimization

The winglet is one of the last assembled surfaces of an aircraft, which makes it especially interesting to study in order to improve aircraft performances in the short-term.

A winglet is a device, introduced in the 1970s by Whitcomb, that reduces the drag induced by marginal vortices at the wing tips. For the same lift, the induced drag generated by a wing equipped with a winglet has been reduced by 8% compared to that of a wing without a winglet (Whitcomb, 1976).

Various winglet shapes have been developed, such as the blended winglet, wingtip fences, split-scimitar winglets, raked wingtips, and others. Each shape has its own advantage; as an example, a blended winglet offers a fuel consumption reduction of 4% to 5% depending on the aircraft type (The Boeing Company, 2009).

The latest winglet (or wingtip) configuration is the one that equips the Boeing 777x aircraft. Developed with an unconventional wing span (approximatively 72 m) that optimizes its performance, the Boeing 777x was a code F airport compatible (airports for aircraft that have wingspans of 65 m to 80 m), therefore it can only access code F-equipped airports (limited to roughly 400 airports worldwide). To expand its scope, Boeing engineers have developed a folding wingtip. Indeed, by folding 3.5 meters of the wing on its each side, the Boeing 777x can operate on the ground as a conventional long-range aircraft (code E airport compatibility, for aircraft wingspan less than 65 m) (Boeing, 2013).

The Federal Aviation Administration (FAA) approved this winglet device in May 2018, with the condition that the manufacturer could prove that the winglet could only be folded while the aircraft was immobilized on the ground (before takeoff, or at the end of the landing process) and never in flight (Federal Aviation Administration, 2018).

Knowing that the mechanism allowing the wing tip shape to move would already be implemented on the B777x, it would be interesting to analyze aircraft performance advantages if the wing tip could also evolve during flight. This question has motivated this thesis research.

An adaptive winglet (controllable or not) during flight is also called a “morphing winglet” or an “active winglet” in the state-of-the-art.

1.2.1 Adaptive winglet: State-of-the-Art

Adaptive winglet projects have shown promising results during the last 10 years. Among these studies, the CLAReT (Control and Alleviation of Loads in Advanced Regional Turbo-Fan Configurations) project was conducted in 2013 by the Clean Sky team, including Bristol university. CLAReT researchers developed a “morphing winglet concept”, that aimed to adapt its winglet cant (i.e., dihedral) and twist angles throughout the flight envelope of a regional jet. For the three tested Mach numbers of 0.48, 0.60 and 0.74, the aircraft operational range was increased by up to 5%. To achieve these results, the CLAReT team conducted structural and aerodynamic studies using Computational Fluid Dynamics (CFD) methods (Cooper, 2020 ; Cooper et al., 2015).

Another adaptive winglet concept was proposed following a collaboration between NASA and Boeing (Ortiz & Alley, 2018). Entitled “Spanwise Adaptive Wing” (SAW), this project was targeted on a wing folded along its spanwise during flight. Flight tests performed using the Prototype-Technology Evaluation and Research Aircraft (PTERA) in 2017 showed that the optimal position angles of the winglet varied between -15 to +15 deg (angle measured between the winglet planform and the ground), while the dihedral angle varied between -75 deg and +75 deg. Dynamics studies have shown that some (not severe) changes could occur in roll damping, but no changes occurred in its original yaw damping or in its longitudinal stability (M. S. Smith, Sandwich, & Alley, 2018).

Teams from Airbus (Wildschek et al., 2015), the Italian Aerospace Research Center (CIRA) (Dimino et al., 2021) and the French aerospace laboratory (ONERA) (Carossa et al., 2016 ; Cedric Liauzun, Le Bihan, David, Joly, & Paluch, 2018) have worked and are working on an adaptive winglet concept to be applied on a regional aircraft within the scope of the Clean Sky 2 European project. The concept included a new controllable surface integrated in the trailing edge of a conventional winglet (such as an aileron located on the winglet). In other words, the winglet was morphed according to its camber during flight. Researchers have presented an important work regarding the mechanism and its structural and control aspects (Gianluca Amendola et al., 2017). Recently, it has been shown that such morphing devices were able to reduce the drag by up to 3% for climb conditions (Dimino et al., 2021).

Airbus and Bristol university collaborated on the Albatross ONE project, in which winglets were free to rotate during flight (Wilson, 2019). Flight tests conducted in 2019 on the Airbus Albatross ONE demonstrator showed some of the benefits, including a lower hinge moment at the wing root during gusts. By bending the whole wing less in gusty winds, researchers believe that an 8% to 9% reduction in fuel consumption was achieved compared to an aircraft with a conventional fixed wingtip (Castrichini et al., 2017 ; Cheung, Rezgui, Cooper, & Wilson, 2018). In addition, by accumulating less load during flight, the wing structure could be lightened, which would result in a significant reduction of the aircraft's empty weight. This free-folding wingtip concept has also led to better roll performance, that was another interesting aspect offered by this system (Healy et al., 2021).

"Telescopic" winglets consist of an enlargement or a shrinking of the winglet span. With this type of device, researchers have successfully reduced the fuel consumption of a transport jet aircraft similar to the Airbus A380 by up to 2% based on the Breguet formula and CFD aerodynamic computations (Daniele, De Fenza, & Vecchia, 2012).

The LARCASE team conducted a study to measure the impact of an adaptive winglet for a Cessna Citation X business aircraft (Marine Segui, Bezin, & Botez, 2018 ; Marine Segui & Botez, 2018b). This study used Vortex-Lattice Method (VLM) aerodynamic computations to

measure the aerodynamic forces and moments of the aircraft in its flight envelope (Marine Segui, Bezin, et al., 2018 ; Marine Segui & Botez, 2018b). In addition, an in-house performance model of the aircraft has shown that the rate of climb could be increased by up to 26 feet/min, and that the fuel flow was reduced by up to 20 pounds (9.1 kg) per hour for cruise by using an adaptive winglet. With such promising results, the authors recommended pursuing this study, and to use Computational Fluid Dynamics (CFD) based on Navier-Stokes equations to confirm results obtained using the VLM (Marine Segui, Bezin, et al., 2018 ; Marine Segui & Botez, 2018b). Indeed, the VLM can predict the induced drag (without the compressibility effects), but not the skin friction and shape (also called “pressure” or “form”) drag. Turbulence effects are also neglected by using a VLM method.

Following the success of this last project, it was recommended to continue these studies using high fidelity computational methods. Thus, by deepening the studies previously carried out, the expected results should demonstrate that an adaptive winglet system can significantly reduce aircraft fuel consumption.

1.2.2 Research Originality

This research consists of the development of a new system that could improve aircraft performance in the short-term (less than 10 years). The global objective consists of reducing the initial fuel consumption of an aircraft by 3% using this new system.

An improvement of the winglet shape was targeted, as several “optimal” shapes of a winglet may exist during a flight. It is important to mention that by improving winglets, fuel tanks installed in wings could be kept, that is one of the main challenges of morphing “wing” systems (due to the space required to install the new system, as well as the risk of electrical fire). Therefore, new adaptive winglets could be developed for existing aircraft, and be easier to test. For a reliable resolution of this thesis, it is important to work with flight test data as representative as possible of the aircraft. Moreover, it is very important to know the geometry of the aircraft precisely to be able to improve it. Both of these motivations led to this research

project being applied on the Bombardier Regional Jet CRJ700, as the LARCASE laboratory has a highly certified flight simulator (Figure 1.1) and an accurate Computer-Aided Design (CAD) drawing of this aircraft (Figure 1.2). The CRJ700 flight simulator is a CAE VSIM product, qualified at a level D (the highest rating) by the Federal Aviation Administration (FAA). This tool is called the Virtual Research Simulator (VRESIM) throughout this thesis.

Figure 1.1 CRJ700 Flight simulator - VRESIM

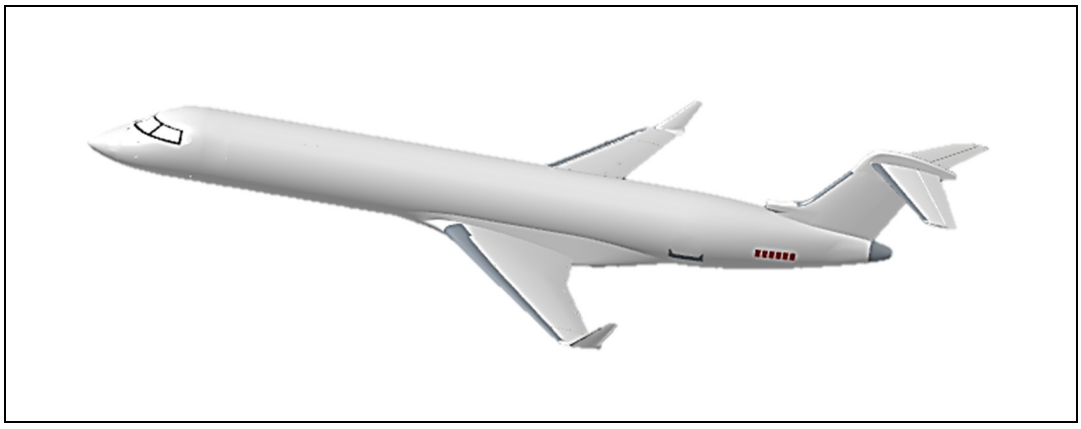

Figure 1.2 CRJ700 Computer Aided Design

The Bombardier Regional Jet CRJ700 is a commercial aircraft used for flights within Europe and the United States. It was designed to carry between 50 and 78 passengers over a range of 2,600 km.

By studying the application or impact of an adaptive winglet system on this aircraft, it will be possible to demonstrate that an airline using aircraft equipped with this morphing wing technology would be able to save fuel, and thus to reduce its carbon footprint.

The originality of the thesis is that it proposes a new strategy to geometrically improve an aircraft design and development that could be representative of the world's air fleet. Therefore, the development of this new technology could improve flight performances in the short term. Indeed, replacing fixed winglets by adaptive winglets will not require a high manufacturing effort. Given that these winglets are surfaces, which, during the assembly of an aircraft, are dissociated from a wing, it would be possible to replace them on the wings of aircraft already in service.

Adding or modifying a surface component on an aircraft obviously requires passing certification tests that may take many years and a huge investment in funds. However, these requirements will be much higher for the complete development of a new aircraft than for the modification of a single surface. This aspect, and the opportunity for fuel consumption improvements in the short term, are two advantages of the improvement or addition of systems on already existing aircraft.

1.3 Specific Objectives

To conduct this project, a multi-disciplinary methodology was established and then presented into three subsections. The first objective was to design a high-fidelity baseline aerodynamic model for its use to compute the aerodynamic forces and moments of a new aircraft geometry. The second objective was to study the aerodynamic benefits of all winglet deflection angles, making it possible to select the most convenient winglet position angle according to several criteria (i.e., lift, drag, lift-to-drag ratio and aerodynamic polar) and flight conditions. Finally, the last objective was to evaluate the flight performances of an aircraft equipped with an adaptive winglet. This objective allowed the performances of conventional and adaptive aircraft configurations (in climb and cruise phases) to be compared.

1.3.1 Aircraft High-Fidelity Aerodynamic Modeling

For the first objective accomplishment an essential tool is developed to complete the aerodynamic analysis. Indeed, as the aircraft geometry should change, it is especially important to develop this tool to be used for the aerodynamic and structural analyses of new aircraft geometries. As structural data of the CRJ700 aircraft are not available, structural analysis was not developed in this PhD thesis. Instead, an aerodynamic study was conducted by considering the aircraft rigid geometry (without its structural flexibility effects).

To compute the aerodynamic forces and moments of the new aircraft geometry (equipped with an adaptive winglet), a high-fidelity aerodynamic model was developed. The preliminary study using VLM computational methods conducted at the LARCASE (Marine Segui & Botez, 2018b) concluded that it would be important to use an aerodynamic model based on Navier-Stokes equations in order to verify the results obtained.

Following this recommendation, a Computational Fluid Dynamics (CFD) software was selected to design a high-fidelity aerodynamic model of the CRJ700 aircraft's baseline geometry. Given that OpenFoam is an open-source software, and that it is becoming more and more well-known, this software was selected to develop the aerodynamic model. Meshes were designed and simulations were conducted based on an OpenFoam code that contained a set of settings. This set of settings was validated by comparing the output forces and moments computed by the aerodynamic model for the baseline geometry of the CRJ700 with those provided by the VRESIM.

Research conducted in this context was published in a first article (included without modifications in CHAPTER 2):

Article 1: **Segui M.**, Abel F.R., Botez R.M., Ceruti A. (2021). High-Fidelity Aerodynamic Modeling of an Aircraft using OpenFoam – Application on the CRJ700. *The Aeronautical Journal*, 126(1298), 585-606.
DOI: https://doi.org/10.1017/aer.2021.86

This article was co-authored with Federico Roberto Abel who was a master student from University of Bologna that made its internship at LARCASE (ÉTS). Mr. Federico Abel has contributed to the development of the aerodynamic model, he was therefore included in the author this research. Dr. Ruxandra Botez has supervised the progress of this research conducted at LARCASE. Dr. Alessandro Ceruti (University of Bologna) has supervised Federico Roberto Abel during its master internship at LARCASE.

In terms of my research contributions, I conducted and organized the number of tests needed to find the optimal OpenFoam parameters to design the aerodynamic model, in terms of meshing and simulations. I performed the necessary flight tests using the VRESIM flight simulator to collect all the data required to validate the aerodynamic model. From these flight tests, I made the selection of interesting and representative flight conditions of the CRJ700 aircraft. Finally, I performed the verifications of the proposed computational method, executed all the simulations and their corresponding validations, and wrote the paper.

1.3.2 Aerodynamic Benefits of an Adaptive Winglet

In order to study the aircraft aerodynamics equipped with an adaptive winglet, it was necessary to design new winglet geometries using Computer-Aided Design (CAD). Then, using the validated high-fidelity aerodynamic model, each of the winglet deflection positions were studied for different flight conditions, step by step (i.e., one deflection angle by another one and one flight condition after the other one). As the computational time using this type of model is not insignificant, the OpenFoam simulations for various winglet deflection angles (7 positions) and various flight conditions representative of the aircraft's flight envelope were performed.

Some aerodynamic advantages, such as increased lift or lift-to-drag ratio, or lowered drag have been found. However, only some winglet positions (7 positions) could be analyzed via this methodology (those computed using the OpenFoam model). As the global objective was to analyze the fuel consumption reduction that could be achieved by equipping an aircraft with adaptive winglets, a new methodology was established to anticipate the aerodynamic performance of all winglet deflection angles (from those computed using the OpenFoam model). Therefore, a large continuity study was conducted to predict the aerodynamic performance of the Bombardier CRJ700 aircraft equipped with an adaptive winglet for its complete flight envelope and for all winglet deflection positions, from -93 deg to +93 deg, in 1-degree steps.

Research conducted in this context was published in a second article (included without modifications in CHAPTER 3).

Article 2: **Segui M.**, Abel F.R., Botez R.M., Ceruti A. (2021). New Aerodynamic Studies of an Adaptive Winglet Application on the Regional Jet CRJ700. *Biomimetics*, 6(4), 54.
DOI: https://doi.org/10.3390/biomimetics6040054

This article was co-authored with same co-authors of the first article. For this second article, Federico Roberto Abel was in charge of designing the adaptive winglet using Computational Aided Design software. Drs. Ruxandra Botez and Alessandro Ceruti have supervised the progress of this research that was conducted at LARCASE (ÉTS).

I performed the selection of the interesting winglet positions to study in the continuity study (in terms of angle of attack, Mach number and winglet deflection angle). I then performed aerodynamic simulations of the different adaptive winglet positions using the developed OpenFoam aerodynamic model. Finally, I performed an aerodynamic analysis and created a

scenario to predict the aerodynamic benefits of equipping an aircraft with an adaptive winglet compared to a conventional and fixed winglet. I also wrote the paper.

1.3.3 Cruise and Climb Benefits of an Adaptive Winglet

The last objective was to analyze the performances gained by the CRJ700 when it was equipped with adaptive winglets with respect to its initial configuration (i.e., fixed winglets). For this study, it was necessary to use an accurate performance model of the CRJ700, including the aircraft's aerodynamic and engine data, to compute the fuel consumption for several flight conditions and several weight configurations.

Based on the methodology developed in-house by the LARCASE team for the Cessna Citation X, a performance model was developed for the CRJ700 aircraft. This model has been validated for cruise and climb phases. Using the performance model developed for the CRJ700, and the aerodynamic data of the CRJ700 equipped with adaptive winglets, it was possible to compute the new aircraft design performances. By simulating different climb and cruise scenarios, we were able to evaluate the fuel quantity that could be saved by the CRJ700 equipped with adaptive winglets with respect to its initial configuration for different flight conditions.

Research conducted in this context was presented in a third article (included without modifications in CHAPTER 4).

Article 3: **Segui M**., and Botez R.M. (2022). Performance Improvement of the Regional Jet CRJ700 Aircraft equipped with Adaptive Winglets. This article was published in the *AIAA Journal of Aerospace Information Systems* in June 2022.

This article was co-authored with Dr. Ruxandra Botez, who also supervised the progress of this research conducted at LARCASE (ÉTS). The performance model presented in this paper was developed in a previous project done by another team also led by Ruxandra Botez.

However, in order to adapt this performance model to an aircraft equipped with an adaptive winglet, it was necessary to develop new materials. I developed the methodology to calculate the downwash from CFD code calculations. I also found the methodology to separate the aerodynamic contributions of the wing-body part from that of the horizontal tail, based on the global aerodynamic coefficient provided by the CFD methods. I also included optimization criteria in the performance toolbox to select a specific winglet position during the climb or cruise segments. I performed all the simulations that led to the results presented in this article. As with the previous two articles, I also wrote this third article in full.

CHAPTER 2

HIGH-FIDELITY AERODYNAMIC MODELING OF AN AIRCRAFT USING OPENFOAM – APPLICATION ON THE CRJ700

Marine Segui [a], Federico Roberto Abel [b], Ruxandra Mihaela Botez [c], Alessandro Certui [d]

[a, c] Department of System Engineering, École de Technologie Supérieure,
1100 Notre-Dame West, Montréal, Québec, Canada H3C 1K3
[b,] School of Engineering and Architecture, University of Bologna, Bologna, Italy
[d] Department of Industrial Engineering, University of Bologna, Bologna, Italy

Paper published in *The Aeronautical Journal*, September 2021, 126(1298), pp. 585-606.
DOI: https://doi.org/10.1017/aer.2021.86

Résumé

Cette étude est axée sur le développement de modèles aérodynamiques longitudinaux pour des conditions de vol stables. Bien que plusieurs solveurs commerciaux soient disponibles pour ce type de travail, nous cherchons à évaluer la précision d'un logiciel libre. Cette étude vise à vérifier et à démontrer la précision du solveur OpenFoam lorsqu'il est utilisé sur des ordinateurs de base (32 à 64 Go de RAM et 8 cœurs). Une nouvelle méthodologie a été développée pour montrer comment un modèle aérodynamique d'un avion peut être conçu en utilisant le logiciel OpenFoam. Le maillage et les simulations ont été conçus uniquement à l'aide des utilitaires OpenFoam, tels que *blockMesh*, *snappyHexMesh*, *simpleFoam* et *rhoSimpleFoam*. Pour l'illustration de la méthodologie, le processus a été appliqué à l'avion Bombardier CRJ700 et les simulations ont été effectuées pour son enveloppe de vol, jusqu'à M0.79. Les forces et les moments obtenus avec le modèle OpenFoam ont été comparés avec une source de données de vol précise (simulateur de vol de niveau D). D'excellents résultats en matière de concordance des données ont été obtenus avec une erreur absolue maximale de 0,0026 pour le coefficient de traînée, validant ainsi un modèle aérodynamique haute-fidélité pour l'avion Bombardier CRJ-700.

Abstract

This study is focused on the development of longitudinal aerodynamic models for steady flight conditions. While several commercial solvers are available for this type of work, we seek to evaluate the accuracy of an open source software. This study aims to verify and demonstrate the accuracy of the OpenFoam solver when it is used on basic computers (32 to 64 GB of RAM and 8 cores). A new methodology was developed to show how an aerodynamic model of an aircraft could be designed using OpenFoam software. The mesh and the simulations were designed only using OpenFoam utilities, such as *blockMesh*, *snappyHexMesh*, *simpleFoam* and *rhoSimpleFoam*. For the methodology illustration, the process was applied to the Bombardier CRJ700 aircraft and simulations were performed for its flight envelope, up to M0.79. Forces and moments obtained with the OpenFoam model were compared with an accurate flight data source (level D flight simulator). Excellent results in data agreement were obtained with a maximum absolute error of 0.0026 for the drag coefficient, thus validating a high-fidelity aerodynamic model for the Bombardier CRJ-700 aircraft.

2.1 Introduction

Aviation has improved over the decades thanks to the use of aircraft modeling techniques and methodologies (Bacchini & Cestino, 2020 ; Bacchini, Cestino, Van Magill, & Verstraete, 2021 ; Cestino, Frulla, Spina, Catelani, & Linari, 2019 ; Antonio Filippone, 2010 ; Antonio Filippone, Zhang, & Bojdo, 2019). Aerodynamics is one aspect of aircraft design that must be very well modeled. Aerodynamic models can be developed from flight data (A. Filippone, Parkes, Bojdo, & Kelly, 2021) or from aircraft design parameters (in the absence of flight test data) (Liem, Mader, & Martins, 2015 ; Marine Segui & Botez, 2018a ; Marine Segui, Ghazi, Botez, & Thompson, 2018 ; Marine Segui, Kuitche, & Botez, 2017 ; Marine Segui, Mantilla, & Botez, 2018 ; Sugar Gabor, Koreanschi, & Botez, 2016). This paper is focused on the latter category. To develop an aerodynamic model from its geometrical characteristics, it is necessary to analyze the fluid behavior around the aircraft from flow equations. Currently, the most accurate equations for modeling the fluid motion around a solid are the Navier-Stokes

equations (NS). To help in NS resolutions, numerical approaches such as Computational Fluid Dynamics (CFD) have been developed (Huvelin, Dequand, Lepage, & Liauzun, 2018a ; Cédric Liauzun, 2006a).

While the most commonly-used CFD commercial software packages are StarCCM+ and ANSYS Fluent (Zou, Zhao, & Chen, 2018), open source and free software have also been released, and they are now available on a significant part of the market. The "editable" aspect of open-source codes is particularly appreciated by companies to develop in-house algorithms, adapted to their computer resources and to their customer research and development projects (He, Mader, Martins, & Maki, 2018 ; Mangano & Martins, 2021 ; Secco, Kenway, He, Mader, & Martins, 2021).

Among open-source CFD software, OpenFoam software is the most widely used (« Comparing CFD Software - Part 2: Open Source CFD Software Packages », s.d.), and it is becoming more and more popular in the industry as it has gained considerable credibility in recent years (since 2016) (« Comparing CFD Software - Part 2: Open Source CFD Software Packages », s.d.). OpenFoam has an impressive number of settings that can be tuned to set up a mesh design or a simulation case (i.e., choice of the solver, turbulence model, resolution scheme, etc.).

From the literature review, it has been observed that the OpenFoam toolbox was used for a wide range of applications, such as gas flow modeling (Mach number from 6 to 12.7) (Le, Greenshields, & Reese, 2012), incompressible flows (Sorribes-Palmer et al., 2017), high lift modeling (Ashton & Skaperdas, 2019), ice accretion modelling (Li & Paoli, 2019), landing gear noise (Hou, Angland, & Scotto, 2017), etc. Despite the general applications available using OpenFoam toolbox, the OpenFoam meshing tools are still very little used. Generally, the mesh is imported from an external application. Otherwise it is designed using OpenFoam meshing utilities only when studies shape are not geometrically complex, such as a basic wing (Behrens, Grund, Ebert, Luckner, & Weiss, 2020). Indeed, as the mesh designed with OpenFoam is unstructured, many “severe” non-orthogonality cells should be measured which is not advised when a low y+ grid is required (Ashton, Unterlechner, & Blacha, 2018).

Moreover, most of these studies have demonstrated that very large computational resources, such as super-computers, are often required to obtain a high level of accuracy modeling (He et al., 2018).

There is no study that estimates the accuracy of the OpenFoam software in the aeronautical sector. Among the published studies, many of them do not use the complete OpenFoam package; indeed, sometimes the mesh is realized using external software. Furthermore, these types of studies were realized using super computers, rendering them quite expensive.

This paper seeks to present the accuracy of OpenFoam software in computing the aerodynamic forces and moments of a conventional aircraft using limited computer resources (no more than 32 GB to 64 GB of RAM memory, and no more than 8 cores) and no symmetrical plane (for future studies reasons). More precisely, the methodology aims to develop an aerodynamic model of an aircraft, such as the regional jet CRJ700.

To verify the values of longitudinal aerodynamic forces and moments that the aerodynamic model (OpenFoam) provides as output, we used the Virtual Research Simulator (VRESIM) located at the Research Laboratory in Active Controls, Avionics and AeroServoElasticity (LARCASE) (Bardela, Botez, Bournisien, & Rusovici, 2018 ; R. Botez, 2018 ; Ruxandra M. Botez, Bardela, & Bournisien, 2019 ; Ghazi, Bosne, Sammartano, & Botez, 2017 ; Ghazi, Botez, & Messi Achigui, 2015 ; Koreanschi, Sugar Gabor, & Botez, 2016b ; Kuitche, Botez, Guillemin, & Communier, 2020). The VRESIM is a Virtual Simulator (VSIM) product designed and assembled by CAE Inc., that deliver flight test data of the CRJ700 aircraft. This VRESIM was delivered to the LARCASE with a level D qualification for its flight dynamics. Level D is the highest qualification level delivered by the Federal Aviation Administration (FAA) (Federal Aviation Administration (FAA), 1991a), and ensures that the aircraft flight dynamics behavior differs by less than 5% from the real flight tests delivered by Bombardier

2.2 Methodology

This section presents the methodology (i.e. the 'Simulation case') used to design an aerodynamic model using OpenFoam software. The complete methodology is applied to the Bombardier Regional Jet CRJ700. However, the same methodology could be adapted for all other aircraft by changing the relevant parameters. The main steps of the methodology are illustrated in Figure 2.1.

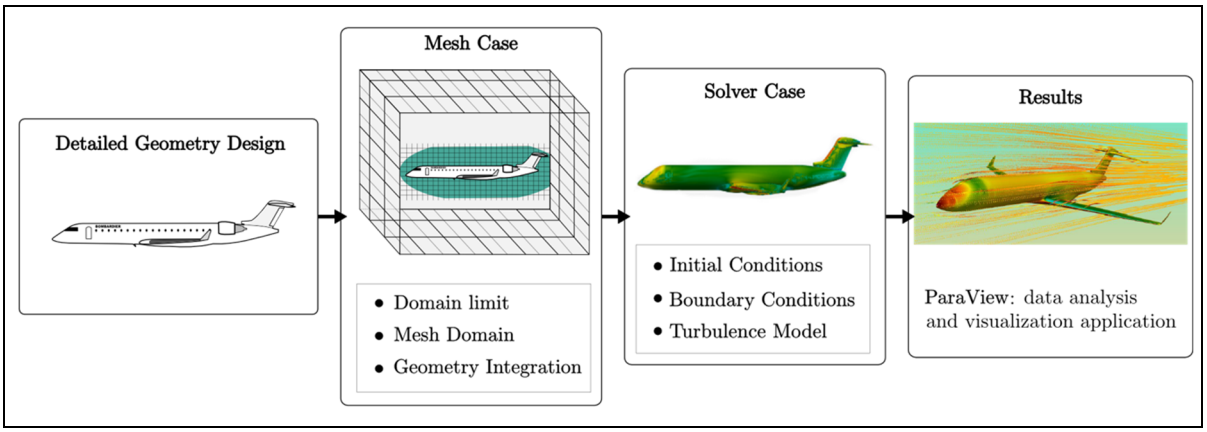

Figure 2.1 Overview of a "Simulation case" using OpenFoam

2.2.1 Bombardier CRJ700 Geometry Preparation

A three-dimensional model of the aircraft external geometry must be designed using a modelling software package such as Computer-Aided Design (CAD), as a watertight surface. For this study we use a CAD drawing of the CRJ700 delivered by the manufacturer Bombardier. To prepare the CAD for CFD analysis, some patches were added to fill in the spaces, for example to fill the gaps between each wing and its slat and flap surfaces. Moreover, some details were removed, such as windows and door outlines, as they created unnatural disorder at this level during mesh design.

The engines were also removed from design to avoid unnecessary computational costs. It was expected that this deletion would not have a significant impact on the lift coefficient. However,

it would impact the drag coefficient computation by up to ΔC_D = 0.002 on average. This difference was estimated for the Bombardier CRJ700 from several conceptual design studies (Lee & Pendergraft, 1985 ; Raymer, 2012a ; Stańkowski, MacManus, Sheaf, & Christie, 2016). Figure 2.2 shows the CRJ700 drawing used to build the aerodynamic model of the aircraft.

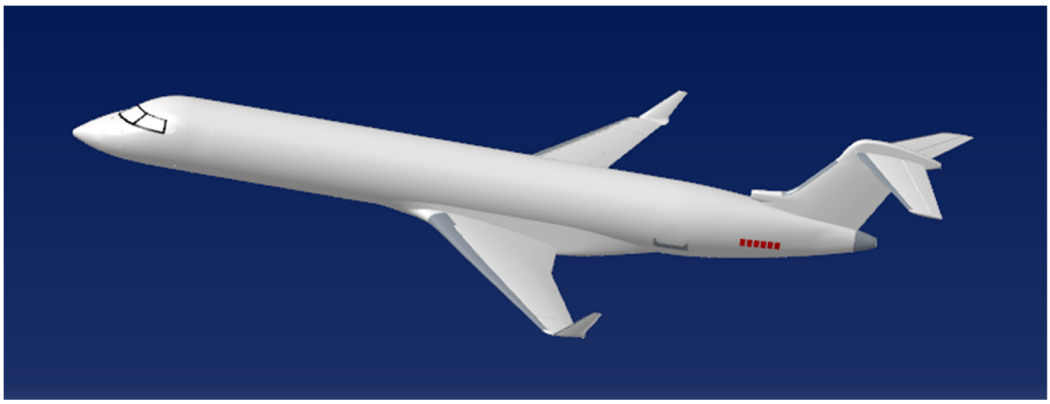

Figure 2.2 CRJ700 CAD drawing used to design the aerodynamic model

2.2.2 Mesh Design

From this geometry file (Figure 2.2), it was necessary to design a mesh for any chosen test case. The mesh was generated by using OpenFoam tools: *blockMesh* and *snappyHexMesh*, mainly for their fully parameterized properties. However, a very wide range of parameters must be set in dictionaries that control *blockMesh* and *snappyHexMesh* applications, by making the mesh design very complex.

In order to find a good combination of *blockMesh* and *snappyHexMesh* parameters that match with the objective computing resources, we used a trial-and-errors methodology. Different mesh settings were tested and their impact on mesh qualities and numeric solutions were analyzed. As analysis of all combinations of parameters may be too exhaustive, the authors have preferred to only highlight *blockMesh* and *snappyHexMesh* pertinent settings. Indeed, there parameters settings lead to stable and accurate solutions, that were used to design the mesh.

The mesh design was mainly constrained by the available number of elements, because of the fact that our computing power was limited. Then, by using an unstructured mesh, the parameters of the mesh generators were modified with the aim to refine a particular surface or zone using a "specific treatment". *BlockMesh* and *snappyHexMesh* parameters finally used to design the mesh were described using the six steps below.

2.2.2.1 Prepare the aircraft surface

The first step of the mesh design consists in providing the 3D geometry with the solid which is desired to study (i.e., the aircraft) to the software. Using OpenFoam, the solid can be defined from triangulated surface geometries in Stereolithography (STL) or Wavefront Object (OBJ) files formats. In this paper, an STL file was derived from the modified CAD drawing of the CRJ700 presented in Figure 2.2. Using this type of file assures that all details of the geometry considered in the CAD have been considered, including the initial coordinate system.

To produce simulations with an angle of attack α different than zero, we decided to rotate the geometry instead of rotating the flow direction (during simulations). This solution was preferred as it kept the flow in the "length" direction of the domain; more explanation is given in subsection 2.2.2.4. Consequently, a STL geometry must be designed for each angle of attack α considered by rotating the geometry around its span axis by an α angle. The aircraft rotation was made around its aerodynamic center.

2.2.2.2 Generate the background mesh using OpenFoam

The second step consists in defining the domain in which the plane is studied. Following the dimensions of the STL surface, a parallelepiped domain with dimensions 44 m × 44 m × 70 m has been set up using the *blockMesh* tool. According to the aircraft dimensions, the domain is 1.89 times larger than its wingspan, 7.18 times larger than its height, and 2.16 times larger than its length. The definition of the domain was a trade-off between time required for

simulations and need for capturing effects due to wakes and flow deflections induced by the aircraft.

It was important to design and divide the background mesh, so that the cells respect a three-dimensional (3D) unit aspect ratio as much as possible. Consequently, a division of 44 cells were set along the vertical and lateral axis, and 70 cells along the length axis.

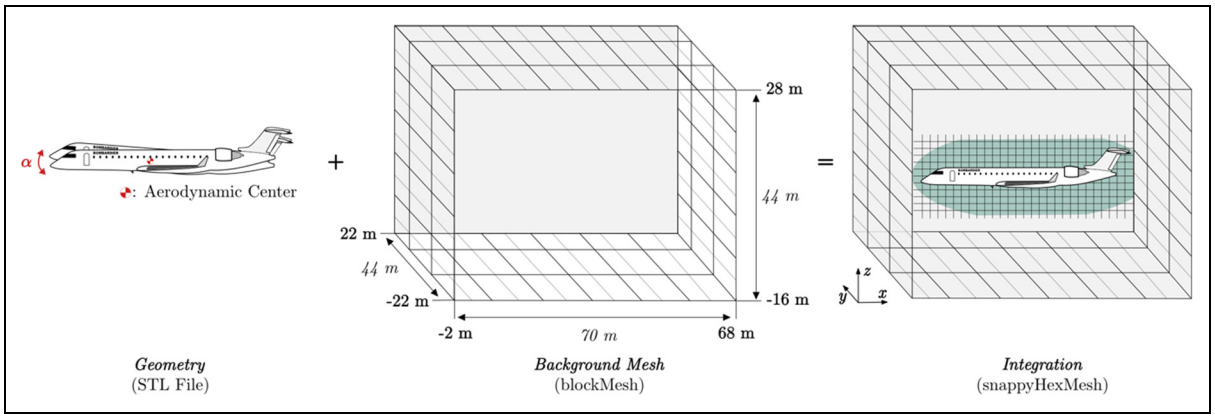

Figure 2.3 Integration of the STL surface geometry in background mesh

After generating the background mesh, the incorporation of the aircraft geometry into this block-domain has been conducted using another OpenFoam tool: *snappyHexMesh (SHM)*. This step was illustrated on Figure 2.3. Hence, at this level, the whole domain is divided by a hexahedral grid extending through the solid wall (i.e., the aircraft) within the computational domain. Integrating the STL geometry into the domain is equivalent to create a vacuum inside the geometry of the aircraft.

Consequently, the global strategy consists in refining or re-aligning cells close to solid wall, corresponding to the green zone on Figure 2.3, in order to well define the outline of the aircraft. For that, we used a Cartesian-grid method which one of the advantages is that the geometry integration can be fully automated (i.e., cells division, removal of re- alignment). All operations of cells division, deletion or re-alignment of the background mesh cells around the STL geometry were made using *SHM* tool. There were two successive refinements steps

necessary for the STL geometry integration into the background mesh, called the “castellated mesh” and the “snapping step”.

2.2.2.3 Development of the castellated mesh

The castellated mesh consists in dividing and removing some cells around the aircraft using a chimera technique. As background cells were large, the highest level of refinement available (level 4) has been defined (cells were split 2^4 times in each direction). The smaller the cells, the better is the outline of the geometry. However, the smaller the cells, the more there are, which will require more memory and longer computational time.

It is important to mention that for any specified level of refinement, the *SHM* algorithm stops dividing cells if either the number of *maxLocalCells* or *maxGlobalCells* is reached. These variables correspond to the maximum number of cell attributes per parallel processor and globally, respectively. Using a system of 8 processors, and 32GB of RAM memory, we have set that the *maxGlobalCells* can be 10 times the number of the *maxLocalCells* (*maxLocalCells* = 12,000,000). Using parallel calculation, it can happen that each processor has an unbalanced task, consequently, by using a *maxGlobalCells* that is slightly larger than number of processors × *maxLocalCells*, it could help in the uniformity of the tasks. Those maximum elements settings were the most restrictive in the mesh design as we used limited computing resources

2.2.2.4 Smooth the mesh using snapping functionalities

To completely match the aircraft’s outline, it was necessary to smooth the surface of the castellated mesh using an iterative process that also been controlled through *SHM* tool. This process involves moving cell vertex points onto the surface geometry to remove the jagged castellated surfaces from the mesh, until mesh design reached the “mesh quality controls” presented in Table 2.1.

Table 2.1 Mesh Quality Controls

Parameters	**Value**
maxNonOrtho	65
maxBoundarySkewness	5
maxInternalSkewness	1

The maximum non-orthogonality *maxNonOrtho* is the maximum angle tolerated to define non-orthogonal cells, while the maximum boundary skewness *maxBoundarySkewness* and the maximum internal skewness *maxInternalSkewness* are the maximum number of faces tolerated with a high skewness for a boundary face or in the internal mesh, respectively.

Table 2.2 Snap Controls

Parameters	**Value**
nSmoothPatch	15
Tolerance	1.0
nSolveIter	250
nRelaxIter	40

The most important settings that control the snapping algorithm of *SHM* were highlighted in the Table 2.2. The combination of settings that control the snapping algorithm of *SHM* highlighted in the Table 2.2 was very efficient for the CRJ700 case.

2.2.2.5 Addition of the layers around the solid to improve the boundary layer

Finally, three layers were added, with an expansion ratio of 2 for the CRJ700. Even if it is an optional step, adding layers is important to “standardize” cells located around the aircraft and to facilitate the wall computations.

The three layers thickness do no exceed 8.5 mm of distance from the solid. The number of layers was set to three because it was the best compromise between the cells resolution and skewness. Indeed, we noticed that adding layers could improve accuracy of solutions but

induced mesh disorder and thus could cause problems for convergence. As for execution time, the mesh process took on average 8h18min using a computer equipped with 8 cores and 32 GB of RAM memory.

2.2.2.6 Final step: Check the mesh

To conclude on the mesh design process, a final verification was performed using the OpenFoam internal application *checkMesh*. By running *checkMesh* application for all the designed meshes, i.e., for angles of attack from -2 degrees to +4 degrees, the user could have access to mesh qualities information.

The non-orthogonality value measured for the 7 meshes was from 65.003 to 65.340 degrees, which was less than 70 degrees, and therefore these meshes could be used to perform properly flow analysis (« cfdsupport », 2020). Moreover, for the skewness, a maximum value of 5.0068 was obtained for all meshes. As the smallest value is targeted to maintain the greatest accuracy possible for the simulations steps the skewness score of meshes was validated. Globally, meshes have on average 11.14 $\times 10^{+6}$ cells and showed an y+ value between 100 and 200, which could be considered as “medium” or “coarse” mesh. However, this range of y+ values is convenient to design an aerodynamic model dedicated to preliminary design analysis.

For the next simulations steps, a solver had to be chosen from among those offered by the OpenFoam toolbox. Commonly, a single solver is used. As the CRJ700 can fly up to Mach number 0.85, a compressible solver is recommended to consider compressibility effects (Wilcox, 2006). However, many flow parameters need to be estimated by the compressible solver, mainly due to the fact that the density is not constant. In addition, the computations are often unstable and convergence is sometimes difficult to obtain, particularly when low computational resources are used (i.e., coarse or medium mesh).

To overcome this problem, an original methodology that consists of using two successive computations was developed in this paper. The first computation will use an incompressible

solver (*simpleFoam*) that will help in the initialization of the second computation with a compressible solver (*rhoSimpleFoam*). Moreover, this selection highlights the accuracy of each solver in its specific fluid domain (i.e., incompressible and compressible). This methodology allows the simulation to remain stable and increases the guarantees to achieve convergence of the compressible solver especially for the type of mesh we used (medium mesh).

The following two sub-sections (2.2.3 and 2.2.4) describe the simulations settings dedicated to *simpleFoam* and *rhoSimpleFoam*, respectively. For this purpose, given the case of an airplane flying in an environment that can be considered as uniquely incompressible, lower than Mach number 0.6, only part 2.2.3 of the methodology is necessary.

2.2.3 Computations using an incompressible solver: *simpleFoam*

SimpleFoam tool is a solver implemented with a method that solves Navier-Stokes equations under the hypothesis of a steady and incompressible fluid. To solve the system of the RANS equations (Anderson, 2017a), *simpleFoam* uses a well-known guess-and-correct procedure, the Semi-Implicit Method for Pressure-Linked Equations (SIMPLE) (Caretto, Gosman, Patankar, & Spalding, s.d. ; Moukalled, Mangani, & Darwish, 2016). To avoid instability in the SIMPLE algorithm, relaxation factors were used. One set to 0.7 for pressure values and another one set to 0.3 for the velocity. Moreover, the convergence was assumed to be obtained when all residuals have reached the value of 1.10^{-4}.

In addition to the resolution algorithm, other parameters are important to specify in order to reach a successful solution. They include the turbulence model, the finite volume solution controls, and the boundary conditions. OpenFoam offers its users the possibility of modifying all these resolution parameters in order to personalize, and thus to optimize the computations. Hence, settings that were used for *simpleFoam* simulations are presented below and numbered from 2.2.3.1 to 2.2.3.3.

2.2.3.1 Turbulence Model Selection: Spalart-Allmaras

To compute the turbulence effects, several turbulence models were available, but two of these models are likely to be better adapted to the flow around the CRJ700 aircraft: the Spalart-Allmaras (S-A) and the $k-\omega$ SST (Shear Stressed Transport) turbulence model (Menter, 1994)(Rumsey, 2020).

As mentioned in specific bibliographical research, the S-A is an appropriate turbulence model for solving aircraft aerodynamics problems (subsonic and transonic studies) (Spalart & Rumsey, 2007). Among its advantages, the S-A model solves the turbulence term of the NS equations with a single equation versus two equations for other models, such as the $k-\omega$ SST (Grisval & Liauzun, 1999).

It is important to mention that in each simulation case that we performed, we used wall functions. These wall functions were used because of the fact that designed meshes were not small enough close to the wall (i.e., the aircraft), especially because of our limited computing resources. In these cases, it is common to use a wall function in order to "approximate" the turbulence effects close to the wall. In order to make a model choice, we have performed some simulations using *simpleFoam* coupled with S-A or $k-\omega$ SST turbulence model (i.e., and their corresponding wall functions). Then, we have compared aerodynamic coefficients computed by models with the VRESIM data (reference), we have noticed that simulations using S-A turbulence model have converged more often than those using $k-\omega$ SST for same initial conditions. From this observation, we assumed that the S-A model offered a larger stability in the computation of aerodynamic coefficients, certainly due to its one turbulence-equation. However, we observed that with accurate initial conditions (closest to the solution), simulations using $k-\omega$ SST turbulence model provided the aerodynamic coefficients closest to the reference data, as shown on Figure 2.4.

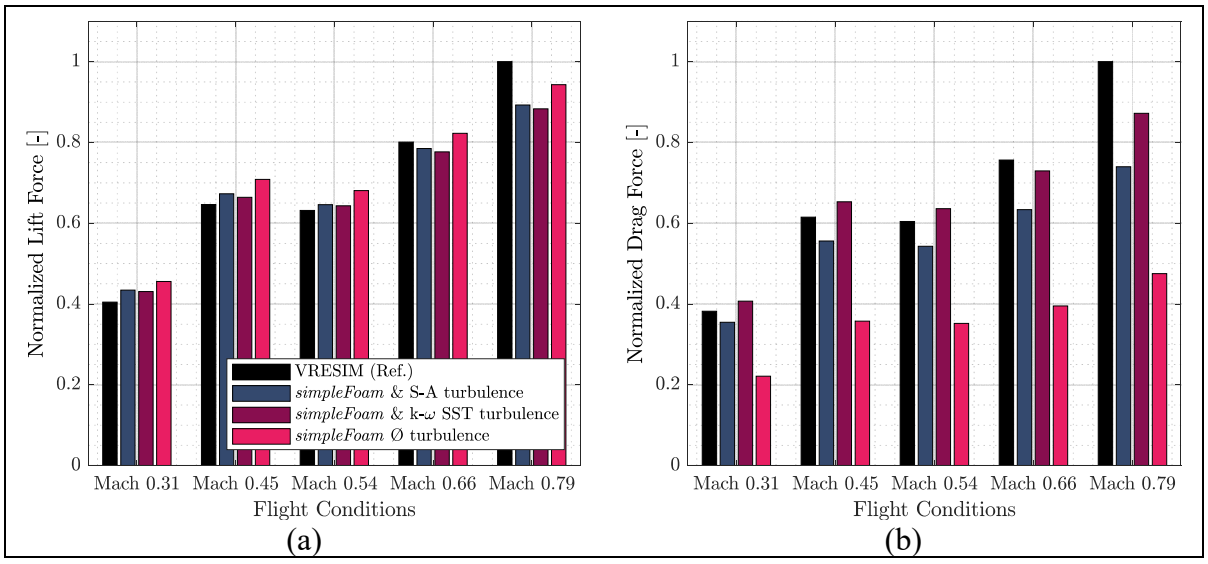

Figure 2.4 Overview of the Turbulence Model Influence (α = 0 deg)

Figure 2.4 shows a comparison of the forces values obtained with *simpleFoam*: those obtained with the Spalart-Allmaras (S-A) turbulence model in "blue", with the $k-\omega$ SST model in "purple", and with no turbulence model in "pink". The normalized lift and drag forces obtained for the 3 models are displayed in Figure 2.4 (a) and (b), respectively, and compared with their normalized reference forces obtained from the VRESIM (in "black"). Simulations were performed for different Mach numbers from M0.31 to M0.79 and for a fixed angle of attack α = 0 deg.

For the lift prediction (Figure 2.4 (a)), it could be observed that both the S-A and $k-\omega$ SST turbulence models give a good approximation of the reference lift value for all Mach numbers (from M0.31 to M0.79). The $k-\omega$ SST turbulence model simulation gives the closest lift forces results to their reference values for Mach numbers M0.31 to M0.54. For higher Mach numbers than 0.6, the trend changes and simulations using the S-A turbulence model give closer lift values to their reference values than the $k-\omega$ SST turbulence model. It is important to remember that *simpleFoam* is a solver that does not consider the fluid compressibility; therefore, it is normal to obtain for this solver, large errors for Mach numbers higher than 0.6.

The effect of the presence or not of a turbulence model is visible on the drag force comparison (Figure 2.4 (b)). For simulations made with no a turbulence model (in "pink"), the drag force estimated by *simpleFoam* is practically half that of the reference force. The lift force is less affected by the turbulence model selection. From these observations, it seems obvious that a turbulence model must be defined, as expected, to predict the aerodynamic forces of the CRJ700 with a very good accuracy.

The main effects affecting the drag force are: the shape (predominant in blunt bodies), friction (significant in streamlined bodies) and induced drag (noticeable only when there is a lift). Concerning the drag prediction (Figure 2.4 (b)), a remark similar to that for the lift prediction can be made. The $k-\omega$ SST turbulence model gives a closer drag value to its reference value than the S-A model. In fact, for Mach numbers M0.31 to M0.54, the $k-\omega$ SST turbulence model over-estimated the drag force while the S-A turbulence model under-estimates it. The overestimation could be explained by the fact that the engine design had been removed from the CAD. This overestimation trend changed for Mach numbers M0.66 and M0.79, and it could be explained by the fact that *simpleFoam* did not compute compressibility effects, and thus simulations in this range of Mach numbers were not enough reliable (for *simpleFoam*). For this reason, it was expected that for Mach numbers higher than 0.6, simulations converged toward a solution that was far away from the reference (real) one due to the incompressibility assumption.

Based on the observations made for Figure 2.4, *simpleFoam* simulations for the CRJ700 were performed with the S-A turbulence model (while solution stability is a priority). For compressible simulations with *rhoSimpleFoam*, the $k-\omega$ SST turbulence model was preferred in order to achieve a better step of accuracy (while solution stability was maintained due to its initialization, that will be explained in section 2.2.4)

2.2.3.2 Initial and Boundaries Conditions

The SIMPLE procedure is a very robust method, but it exhibits a quite low asymptotic convergence rate (Moukalled et al., 2016). In order to remain within an acceptable convergence rate, it is important to define the initial and boundary conditions for the flow parameters with enough accuracy. Using *simpleFoam*, two parameters must be initialized: the kinematic pressure p and the velocity magnitude and direction U. If a turbulence model is desired for the simulation, its parameters need to be initialized as well (e.g., there are two parameters for a S-A model).

For the CRJ700, *simpleFoam* simulations with a freestream kinematic pressure at the inlet and at the outlet of the domain were set with a value p. To initialize each case, the kinematic pressure p (in $m^2.s^{-2}$) was computed using Eq. (2.1), where P and ρ are the pressure and the air density, respectively, obtained from International Standard Atmosphere (ISA) equations at a given altitude. On the surface of the aircraft, the kinematic pressure was defined using a zero gradient of kinematic pressure.

$$p^{(0)} = \frac{P}{\rho} \tag{2.1}$$

The velocity was defined as freestream flow for the inlet and the outlet faces. The magnitude of the flow velocity was always fully defined in the length direction because the mesh was already rotated according to the angle of attack α. The value of the flow speed (in $m.s^{-1}$) was determined from the imposed Mach number M and the speed of sound at a given altitude using Eq. (2.2).

$$U^{(0)} = U_z^{(0)} = M \times a \tag{2.2}$$

As the Spalart-Allmaras turbulence model introduces two parameters: the kinematic viscosity ν and the turbulent kinematic viscosity $\tilde{\nu}$, it is important to set initial conditions for these

values. Both of these parameters are introduced as freestream types for each face of the domain. Values of ν and $\tilde{\nu}$ (in $m^2.s^{-1}$) were initialised using Eq. (2.3) with the dynamic viscosity μ and the density ρ known at a given altitude.

$$\nu^{(0)} = \tilde{\nu}^{(0)} = \frac{\mu}{\rho} \tag{2.3}$$

For the aircraft boundary modelling, a wall function was set as *nutUSpaldingWallFunction* for both ν and $\tilde{\nu}$ parameters. This wall function modified the velocity profile close to the wall (i.e. the aircraft) by taking into account the Spalding equation (Fangqing, 2016 ; Launder & Spalding, 1974). The use of a wall function approach allows the user to impose the flow field close to the wall without having to use a large number of mesh cells, which is much more efficient from the perspective of memory use. As a reminder, y+ values of designed meshes were found to be between 100 and 200 and OpenFoam advised to use these wall functions for high Reynolds numbers conditions, which is the case of targeted simulations (OpenCFD ltd (ESI Group), 2019).

2.2.3.3 Solution Controls

The solution computed by the solver is controlled by two important dictionaries: *fvSolution* and *fvScheme*. Both dictionaries characterize how the user wants to integrate flow properties between cells, and, if an accurate or a stable mathematical treatment is preferred for the resolution.

The *fvSolution* dictionary helps the user to set how the iterative process should work by specifying the linear solver that OpenFoam needs to linearize each equation being solved. The pressure matrix is symmetrical, consequently, the Geometric-Algebraic Multi Grid (GAMG) solver was chosen, along with a *GaussSeidel* run-time "smoother" to reach the tolerance fixed at 1.10^{-6} for the study (relative tolerance of 0.01). The GAMG has a good reputation for this

kind of resolution; it offers rapid convergence and is the most stable solver available (« Finite Volume Method: A crash introduction », s.d.).

To compute the velocity solution, *SmoothSolver*, an iterative solver, was selected. Indeed, *SmoothSolver* is usually used to solve symmetric and asymmetric matrices (the velocity here is an asymmetric matrix). *SmoothSolver* was coupled with the run-time "smoother" *GaussSeidel,* set with a two "sweeps" to reach the tolerance, fixed at 1.10^{-6} (relative tolerance of 0.1 on residuals). The kinematic turbulent viscosity (i.e., $\tilde{\nu}$) was set with the same settings.

The *fvScheme* dictionary allows the user to define the properties linked to the finite volume approach that need to be considered. These properties are linked to the divergence theory (Moukalled et al., 2016). In this study, all properties were set by default, except the divergence scheme criteria, which were set using a bounded Gauss linear upwind method (i.e., second-order bounded). This type of method was selected because of its offered accuracy, even if it may lead to a small oscillatory behavior (along computation iterations).

Most settings were kept by default, as they were already specified for our type of computation. For example, the Laplacian scheme was set by default using a corrected linear Gauss method. This setting is generally better for meshes that have a nonlinear grading (i.e., with an expansion ratio not equal to 1) and that are non-orthogonal. Even if mesh cells in this study have been defined using same size, the refinement operation creates very small-volume cells around the aircraft while background cells remain within a big volume. At computation level, the layout of our mesh could be equivalent to a nonlinear mesh grading. Consequently, using this type of scheme to work with a Laplacian scheme is practical.

Finally, *simpleFoam* simulations were carried out with the same computer setup as for the mesh (8 cores and 32GB of RAM memory). Therefore, computations were also realized using "parallel decomposition". On average, a simulation with *simpleFoam* took 14 hours and 21 minutes, with a minimum and a maximum time of execution of 12h29 and 16h54, respectively.

This computation time appears to be totally acceptable, depending on the hardware used and the expected level of accuracy.

In the case in which a compressible simulation of the fluid was required (i.e., for an aircraft flying higher than M0.3), the last part of the methodology was performed in order to obtain accurate results. Therefore, in order to account for the compressibility effects that appear in the transonic fluid domain, a second computation using a compressible solver is recommended. In this paper, the compressible solver used is *rhoSimpleFoam*.

2.2.4 Computations using a Compressible Solver: *rhoSimpleFoam*

The *rhoSimpleFoam* is a pressure-based solver that uses the same resolution process as the *simpleFoam*, which is the SIMPLE algorithm. However, *rhoSimpleFoam* solves the compressible Navier-Stokes equations in their conservative form.

2.2.4.1 Initials and Boundaries Conditions

Due to the large number of parameters that must be estimated by the *rhoSimpleFoam* solver, the initialization of this solver was optimized using the converged solution obtained by the incompressible flow solver *simpleFoam*. Using this process allows to conserve the stability of the incompressible solver and therefore, increases the guarantees to achieve convergence for compressible simulations.

The last iteration of computation realized using the incompressible solver *simpleFoam* provides a stable solution of the kinematic pressure $p^{(end)}$, the velocity $U^{(end)}$, the kinematic flux $\phi^{(end)}$ and the turbulence variables $\nu^{(end)}$ and $\tilde{\nu}^{(end)}$. In order to initialize the compressible flow solver *rhoSimpleFoam*, it is necessary to provide the pressure *P*, the velocity *U*, and the turbulence parameters. This initialization requires to manage the solution of $p^{(end)}$ (in $m^2.s^{-2}$) obtained from *simpleFoam* in order to include the density value and define *P* (in $kg.m^{-1}.s^{-2}$) for *rhoSimpleFoam*, using Eq. (2.4).

$$P^{(0)} = p^{(end)} \times \rho \quad (2.4)$$

Concerning the velocity *U*, no modifications are required, so that the solution file obtained from *simpleFoam* can be placed directly in the *rhoSimpleFoam* initialization folder.

In addition to the pressure and velocity, compressible simulations using *rhoSimpleFoam* need to be initialized using the temperature *T*. Therefore, for the CRJ700 simulations, the walls of the domain (using *inletOutlet* boundary condition) were initialized using the temperature value *T* (in Kelvin) calculated from the ISA atmosphere for a specific altitude. On the surface of the aircraft, the temperature was defined using a *zeroGradient* boundary condition.

2.2.4.2 Turbulence Model Selection: $k-\omega$ SST (Shear Stressed Transport)

From the observation made from Figure 2.4, simulations performed using a $k-\omega$ SST turbulence model have provided the closest aerodynamic coefficients with respect to the reference (VRESIM) when the solution is precisely initialized. Because of the fact that *rhoSimpleFoam* simulations were initialized using the converged field solution provided by *simpleFoam*, the $k-\omega$ SST turbulence model was preferred to be used for *rhoSimpleFoam* simulations.

The $k-\omega$ SST turbulence model is governed by two transport equations, one equation for the turbulent kinetic energy *k* and another equation for the specific turbulence rate of dissipation ω. The turbulence model equations are not developed in this paper because it is not within the scope of this study. The version of the $k-\omega$ SST turbulence model implemented in OpenFoam is based on (Menter, Kuntz, & Langtry, 2003), and the constants dedicated to the model are detailed in the OpenFoam manual (OpenCFD ltd (ESI Group), 2019).

For *rhoSimpleFoam* simulations, wall functions *kqRWallFunction* and *omegaWallFunction* were used as boundaries conditions at the aircraft level for turbulence parameters *k* and ω, respectively (Moukalled et al., 2016 ; OpenCFD ltd (ESI Group), 2019). This type of function

computes k and ω values from a universal profile, close to the solid (i.e., the aircraft), even if the mesh is not extremely thin at this level. Side boundaries of the domain wet set using a *slip* type for turbulence parameters. As for the Spalding wall function, the OpenFoam manual advised to use them for high Reynold numbers, which is convenient for our cases (OpenCFD ltd (ESI Group), 2019).

Turbulence model ($k-\omega$ SST) parameters, k and ω were initialized at the inlet and at the outlet. Due to the complexity of these parameters, they are usually unknown however, different equations could give an approximation of their values (Moukalled et al., 2016). In this study, the initial values of k (in $m^2.s^{-2}$) and ω (in s^{-1}) were computed from equations (2.5) and (2.6), respectively.

$$k^{(0)} = \left(\frac{\nu}{l}\right)^2 \tag{2.5}$$

$$\omega^{(0)} = \sqrt{\frac{k}{l}} \tag{2.6}$$

where ν is the kinematic viscosity and l is the reference length. The length of the mean aerodynamic chord of the CRJ700 was used for its reference length l.

2.2.4.3 Solution Controls

Solution controls used to set *rhoSimpleFoam* solver simulations were globally the same of those that were used for *simpleFoam* solver simulations. However, *rhoSimpleFoam* is a compressible solver that needs to deal with temperature and energy variables (that were neglected for incompressible simulations). Therefore, to predict the onset of shocks, it was necessary to select a temperature dependent transport model. For its general applications, the Sutherland viscosity model has been set in the *thermophysicalProperties* dictionary using the default constants (White, 2006). Using the Sutherland Eq. (2.7), the dynamic viscosity μ (in

kg.m^{-1}.s^{-1}) is estimated from the temperature T, and the Sutherland constants are $A_s = 1.458 \times 10^{-6}$ and T_s= 110.4 °K for the air.

$$\text{(Sutherland viscosity Model):}\quad \mu = \frac{A_s\sqrt{T}}{1+\frac{T_s}{T}} \tag{2.7}$$

Furthermore, additional information was added to *fvSolution* and *fvScheme* dictionaries due to the compressible solver (such as parameters related to energy or $k-\omega$ SST turbulence model).

For the *fvSolution* dictionary, the same settings as those used to compute the velocity solution with the *simpleFoam* solver (i.e., the *SmoothSolver* solver coupled with *GaussSeidel* run-time "Smoother") were used to compute the solutions for k, ω, and the energy e.

The turbulence divergence scheme was expressed with a Gauss upwind method. This kind of numerical method of resolution is also called a "forward" integral method (Moukalled et al., 2016). Computing the next iterations using the previous ones is a very efficient and economical computation method. Most interesting aspects with this method is the compromise between speed of resolution and stability. This numerical method of resolution (Gauss upwind) was also been used to compute the divergence control criteria of energy parameters.

The complete simulation case for *rhoSimpleFoam* was designed utilizing all these specifications. Simulations were done for different flight conditions in order to cover the whole CRJ700 flight envelope. *RhoSimpleFoam* simulations were also accomplished with a computer with a limited capacity (8 cores and 32GB of RAM memory). To save execution time, computations were parallelized on the 8 processors of the computer using the "Scotch" method (Chevalier & Pellegrini, 2008). On average, the 35 computations using the *rhoSimpleFoam* solver were processed 2 hours faster than those processed with the *simpleFoam* solver. However, the convergence was not reached "directly" in some cases because of the fact that the initial state was too far from the solution (due to the compressibility effects), and thus, the

solution had a slightly oscillatory trend, and the computation time went up to 30 hours until the solution would reach a stable state.

2.2.5 Force estimations and post-treatment

Aerodynamic forces and moments acting on the CRJ700 were computed with *simpleFoam* or *rhoSimpleFoam* by use of an internal function *forcesCompressible* programmed in OpenFoam software. The forces and moments presented as results were obtained from the last computation iteration by adding the pressure and viscous aspects together. The aerodynamic coefficients of lift C_L, drag C_D were computed from lift L and drag D forces using Eq. (2.8), and pitching moment coefficient C_{m_y} were computed using pitching moments M_y according to Eq. (2.9):

$$C_{L,D} = \frac{2 \times \left[F_{L,D}^{(end)}(\text{pressure}) + F_{L,D}^{(end)}(\text{viscous})\right]}{\rho \,.\, S \,.\, V^2} \tag{2.8}$$

$$C_{m_y} = \frac{2 \times \left[M_y^{(end)}(\text{pressure}) + M_y^{(end)}(\text{viscous})\right]}{\bar{c} \,.\, \rho \,.\, S \,.\, V^2} \tag{2.9}$$

where ρ is the air density for the selected altitude (following ISA atmospheric model), S is the wing area of the aircraft, V is the aircraft True Air Speed (TAS) (i.e. the fluid speed in the simulation context) and $\bar{c}$ is the mean aerodynamic chord of the aircraft wing.

2.3 Simulation Results

To give an overview of the aerodynamic model's validity, CFD simulations were performed for the five combinations of Altitude-Mach that are the most representative for the CRJ700. The combinations are shown in Table 2.3. These flight conditions were selected after performed several flight plans using the VRESIM flight simulator of the CRJ700.

Table 2.3 Flight conditions selected to test the aerodynamic model

Flight conditions	**Altitude**	**Speed**	**Angle of Attack**
1	5,000 ft	M0.31	$\alpha \begin{cases} -2.0 \text{ deg} \\ -1.0 \text{ deg} \\ 0.0 \text{ deg} \\ 1.0 \text{ deg} \\ 2.0 \text{ deg} \\ 3.0 \text{ deg} \\ 4.0 \text{ deg} \end{cases}$
2	10,000 ft	M0.45	
3	20,000 ft	M0.54	
4	25,000 ft	M0.66	
5	30,000 ft	M0.79	

2.3.1 Convergence Study

To demonstrate the stability of the solutions given by the *simpleFoam* solver, Figure 2.5 shows the residual convergence obtained for all the cases evaluated. This figure presents the simulation cases using two colors: “magenta” for cases when the angle of attack is equal to zero, and the “blue” for cases when angles of attack within the range -2 to 4 degrees, except zero. Figure 2.5 shows that the residual convergence criteria of 10^{-4} (a “dashed red” line) is not reached at the same time, as meeting this goal depends on the nature of the parameter (pressure or velocity) and its axis (*x*, *y* or *z*). The *z*-velocity is the parameter that converges the quickest as seen on Figure 2.5 (d). In this study, the *z*-axis is located along the wing plan; this observation could signify that the fluid behavior is easier to predict in the axis that is not directly affected by the flow direction. All the other parameters have residuals that reached convergence after 1000 iterations of computations.

Another observation can be made concerning the dependency of the angle of attack in residual convergence. Indeed, cases where angles of attack are equal to zero converged sooner than those for other angles of attack. This could be explained by the alignment of the aircraft in the mesh domain, as the aircraft is not perfectly aligned with the length axis (*x*- axis) for angles of attack that are not zero, which renders the computation more difficult and less stable. Consequently, convergence is reached a bit later for these cases than for cases where angles of attack are zero.

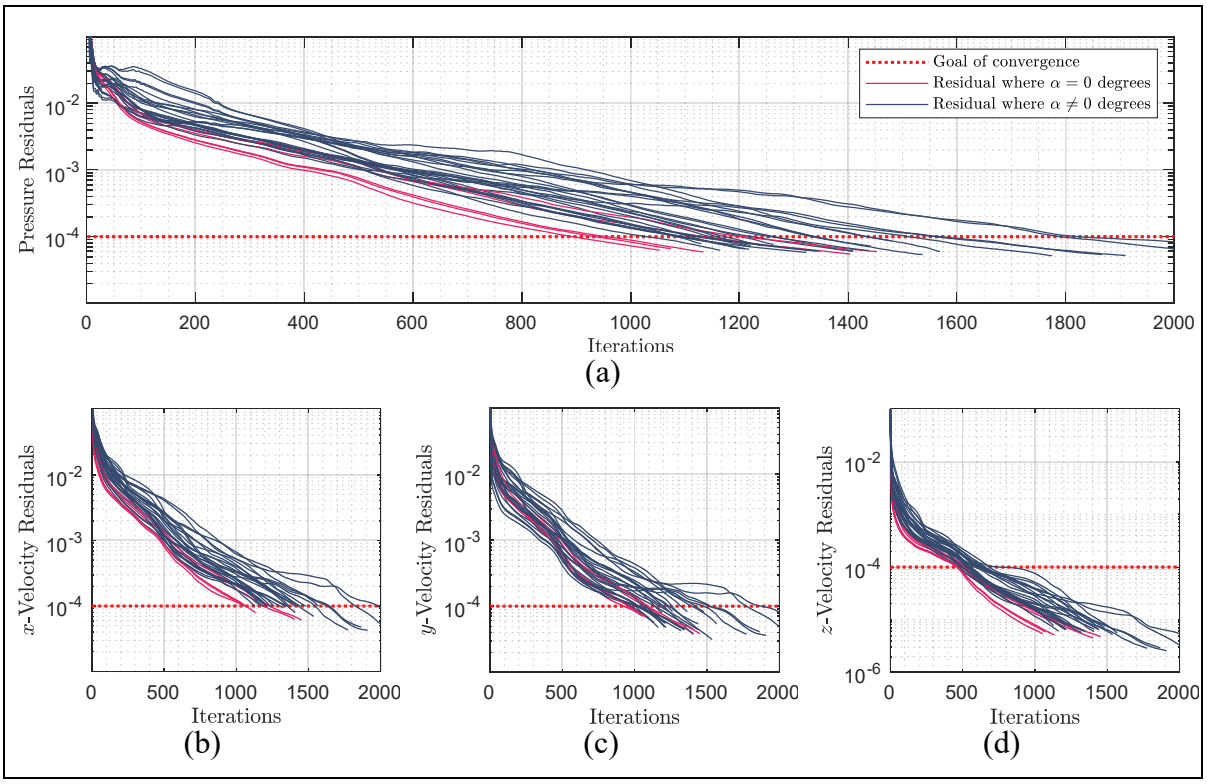

Figure 2.5 Residual convergence of pressure and velocity obtained for *simpleFoam* computations

Figure 2.6 shows the residual convergence achieved with *rhoSimpleFoam* solver computations. Contrary to the observations in Figure 2.5 for *simpleFoam* solver computations, straight convergences can be observed here for both the pressure and the velocity. The convergence is especially straight at the beginning, due to the initialization of the solver using the previous computation results that were performed with *simpleFoam*. This initialization could also explain why fewer than 1000 iterations are required to reach convergence with *rhoSimpleFoam* than with *simpleFoam* (where twice as many iterations are required to observe convergence in all cases). However, the pressure residuals are also the "limiting condition of convergence" for *rhoSimpleFoam* computations, as the velocity in each direction has already reached the convergence criteria.

This first overview of the convergence results reveals that there are flight conditions that allow the simulation to find a convergence more quickly than others. For instance, *simpleFoam*

simulations with an angle of attack of 0 degrees converged faster than those for other angles of attack, whatever the Mach number selected. Concerning the *rhoSimpleFoam* simulations, solutions converged rapidly (in less than 1000 iterations), as they were initialized with last iteration results of the *simpleFoam* computation.

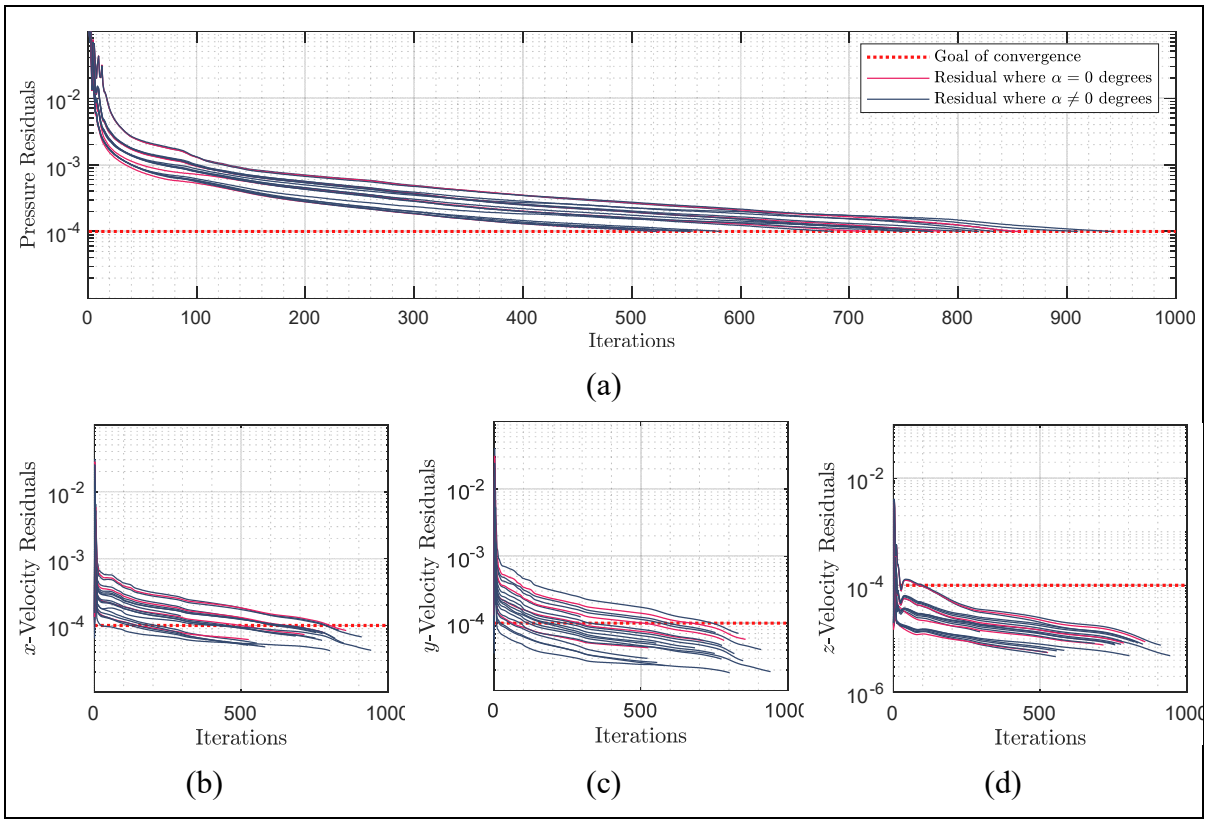

Figure 2.6 Residual convergence for *rhoSimpleFoam* computations

2.3.2 Comparison of the lift coefficient C_L between the aerodynamic models and the reference (VRESIM)

The lift coefficient (C_L) is the first aerodynamic parameter analysed and compared. The lift coefficient values with angles of attack from -2 to 4 deg were computed and compared at Mach number values from 0.31 to 0.54 (low values) and at 0.66 and 0.79 (high values). The results obtained with the *simpleFoam* model (in "pink"), and the *rhoSimpleFoam* model (in "purple") were compared to the reference (provided by VRESIM) values (in "black"), in Figure 2.7 (for

low Mach values) and Figure 2.8 (for high Mach values). It is important to specify that for confidentiality reasons, the y- axes of these graphs have been hidden. We also want to mention that *simpleFoam* results were presented in the paper as "intermediary" results obtained through the methodology (until reaching *rhoSimpleFoam* results). Consequently, it was out of scope to improve *simpleFoam* results. However, according to the level of accuracy required, and the flight conditions that the reader want to simulate, results provided by *simpleFoam*, could be corrected using a Prandtl-Glauert equation to reach a "convenient" level of accuracy (and low computational resources).

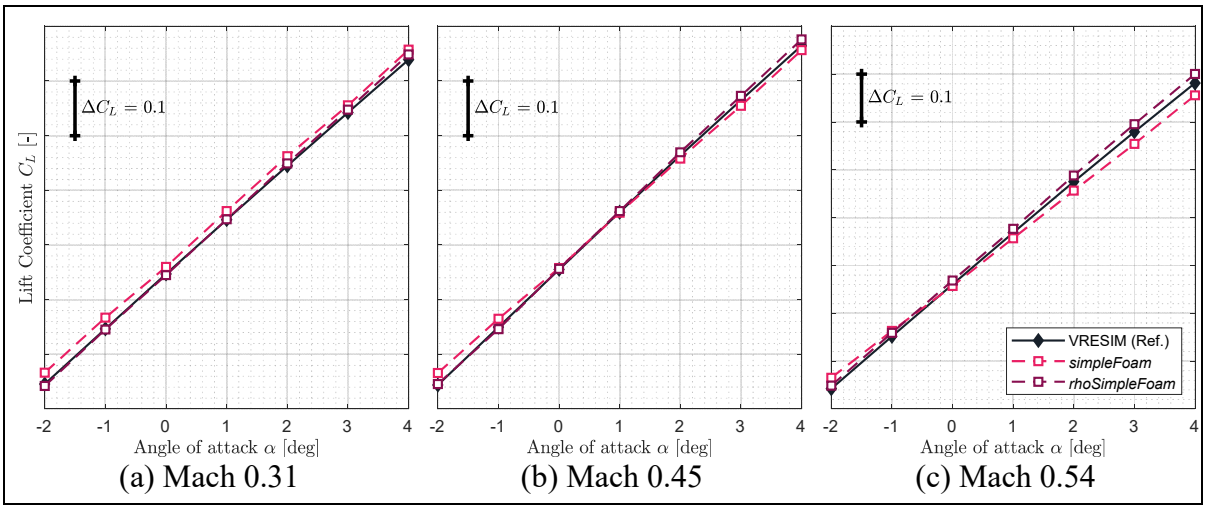

(a) Mach 0.31 (b) Mach 0.45 (c) Mach 0.54

Figure 2.7 Lift coefficient comparison for low Mach numbers value

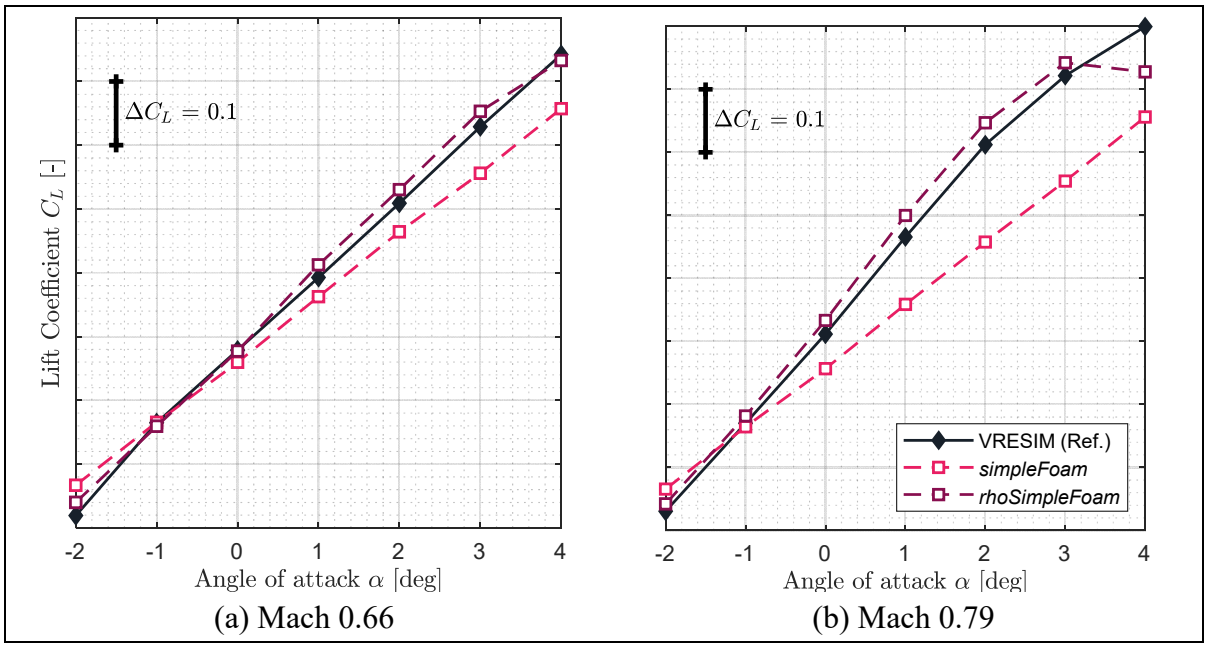

(a) Mach 0.66 (b) Mach 0.79

Figure 2.8 Lift coefficient comparison for high Mach numbers values

The lift coefficient comparisons versus the angle of attack for two high Mach number values, M0.66 and M0.79, are displayed in Figure 2.8 (a) and (b), respectively. In this Mach number range, the effects of compressibility are no longer negligible. Indeed, this can be easily observed from the results obtained with the *simpleFoam* solver, shown in "pink". Despite the incompressibility hypothesis, the *simpleFoam* solver offered acceptable results for M0.66, with a maximum absolute error of 0.085 observed for the angle of attack of 4 deg. However, for M0.79, *simpleFoam* converges towards solutions that are very different to reference values (with a margin of error higher than 0.1). Consequently, as expected, *simpleFoam* could be considered as less optimal than *rhoSimpleFoam* for high Mach value of M0.66 and M0.79.

Meanwhile, the compressible solver, *rhoSimpleFoam*, does account for the compressible effects of the fluid, and therefore its results match closely those of the VRESIM reference. For angles of attack from -1 to 3 deg, *rhoSimpleFoam* can predict the CRJ700 VRESIM lift coefficient within a maximum margin error of 0.035.

2.3.3 Comparison of the drag coefficient C_D between the aerodynamic models and the reference (VRESIM)

Similarly, drag coefficients obtained from simulations performed using *simpleFoam* and *rhoSimpleFoam* solvers were compared to those of the reference VRESIM according to the angle of attack. These results are presented for five Mach numbers values in Figure 2.9 and Figure 2.10. Comparisons for low Mach number (from 0.31 to 0.54) are displayed in Figure 2.9 (a), (b) and (c), and those for high Mach number (M0.66 and M0.79) are presented in Figure 2.10 (a) and (b).

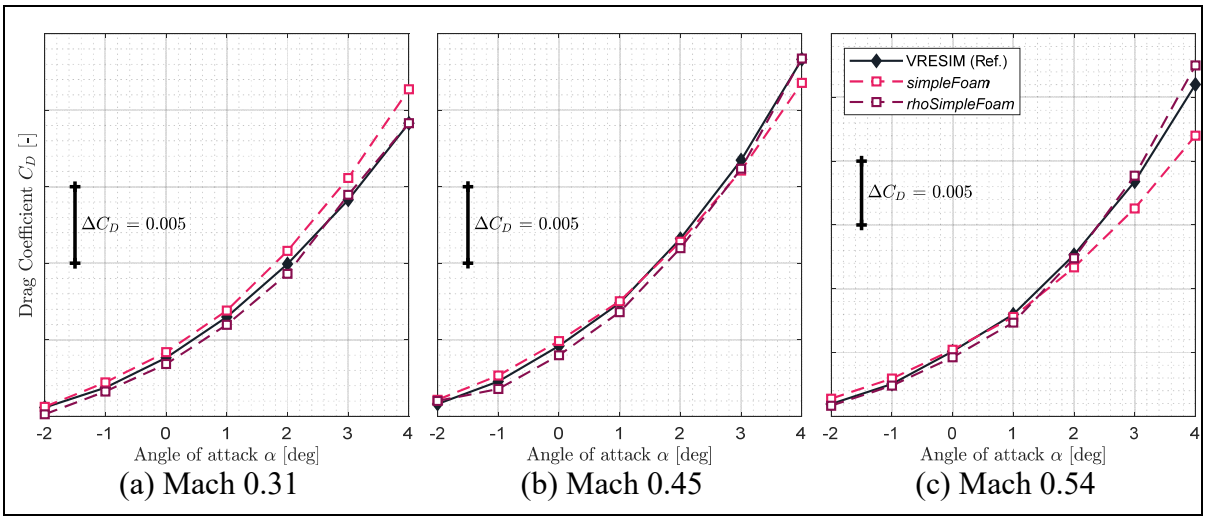

Figure 2.9 Drag coefficient comparison for low Mach numbers value

Figure 2.9 (a) and (b) show that the *simpleFoam* solver can predict the drag coefficients for angles of attack from -2.0 to 4.0 deg with a maximum absolute error of 0.0022 with respect to VRESIM values, while the compressible solver, *rhoSimpleFoam*, can predict the drag coefficient with a maximum absolute error of 0.0006 with respect to the reference (VRESIM). Thus, for Mach numbers 0.31 and 0.45, it was observed that *rhoSimpleFoam* was 3.5 times better than *simpleFoam* to predict drag coefficients.

For Mach number 0.54, on Figure 2.9 (c), it was observed that maximum absolute errors for both solvers were slightly higher, especially for the angle of attack of 4 deg (0.004 for

rhoSimpleFoam and 0.0015 for *simpleFoam*) than those observed for lower Mach numbers on Figure 2.9 (a) and (b). This observation could be explained by the fact that the angle of attack could increases the compressibility effect. Because Mach number 0.54 is situated at the limit of compressibility, and *simpleFoam* does not consider compressibility effects, it was expected that the results provided by this solver could be less representative for these flight conditions. For the second solver, *rhoSimpleFoam*, a range of errors close to 0.0015, could be explained by the fact that engines design was removed from the CAD model. Indeed, in the literature, it was found that this removal could affect the drag coefficient up to 0.002 according to empirical techniques (Lee & Pendergraft, 1985 ; Stańkowski et al., 2016). In consequence, results obtained using *rhoSimpleFoam* are acceptable.

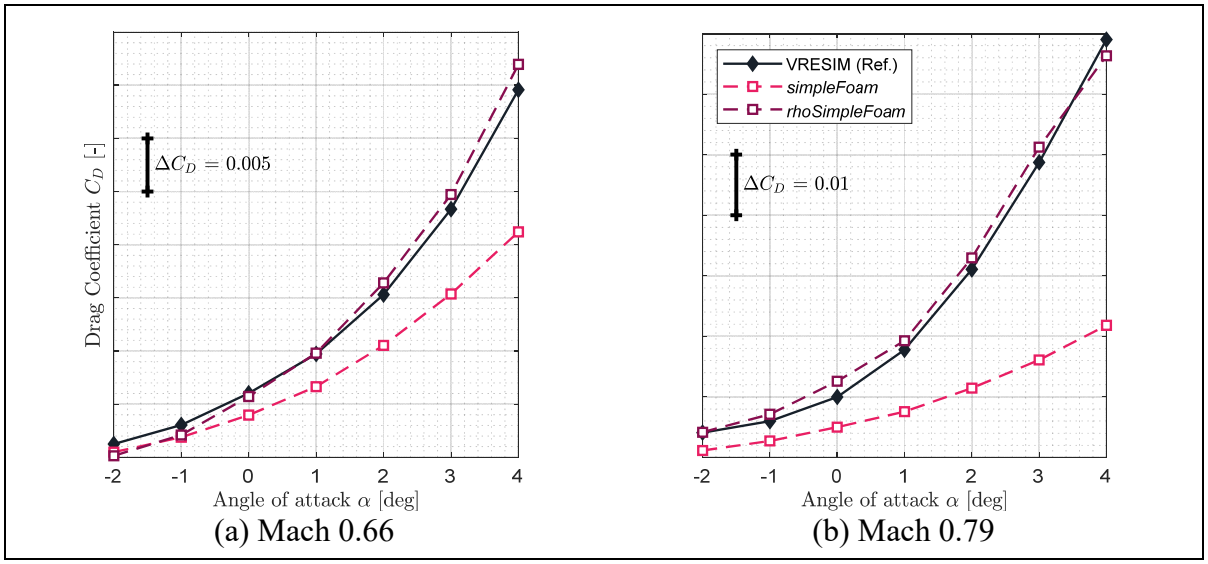

Figure 2.10 Drag coefficient comparison for high Mach numbers values

An observation similar to those made for the lift coefficient comparison for high values of Mach can also be made for the drag coefficient comparison for same Mach numbers. Indeed, the compressibility effect cannot be neglected for Mach numbers M0.66 and M0.79, and thus the *simpleFoam* solver is not really appropriate to use for these flight conditions. However, for M0.66 and angles of attack very close to 0 deg, the *simpleFoam* solver delivered drag coefficients with less than 0.002 of absolute error, which indicates that it performs well.

Meanwhile, the compressible solver (*rhoSimpleFoam*) estimated the drag coefficient of the CRJ700, within a maximum error of 0.0015 with respect to the reference (VRESIM), except for angles of attack of 0 and 4 deg at Mach number M0.79 (Figure 2.10 (b)) and for 4 deg at M0.66 (Figure 2.10 (a)) where the maximum absolute error is less than 0.0026. This exception appears to be due to a small "deviation" in the convergence, a situation that has occurred occasionally for simulations with *rhoSimpleFoam*. In this case, the convergence is quite oscillatory and sometimes not enough iterations are allowed for the solver to converge within the imposed minimum residual limit (10^{-4}). Finally, to overcome this situation, the simulation should be completed using close to 100 more iterations.

It is important to notice that a maximum absolute error of 0.0015 for the drag coefficient prediction is a small error as the model aims to be used for preliminary design studies. Thus, the mesh of the model was designed as "coarse" as possible due to the limited computing resources. Moreover, this level of error is largely acceptable as some assumptions were initially made, as for instance, the engines removal from the CAD drawing.

2.3.4 Comparison of the pitching moment coefficients C_{M_y} between the aerodynamic models and the reference (VRESIM)

Lastly, the pitching moment coefficients computed by OpenFoam solvers were compared to those of the reference (VRESIM) versus lift coefficients. It is important to mention that the pitching moment coefficient is generally very difficult to predict from aerodynamic perspective, because it is very sensitive to the aerodynamic center position. To avoid the projection of forces and moments from an axis to another one, the same aerodynamic center coordinates were set for the CAD drawing (the design of the *.STL files for each angle of attack), and for the OpenFoam *force* function of computation. Pitching moment coefficient versus the lift coefficient were compared for low Mach numbers (M0.31 to M0.54) on Figure 2.11 (a), (b) and (c), and for Mach numbers M0.66 and M0.79 on Figure 2.12 (a) and (b), respectively.

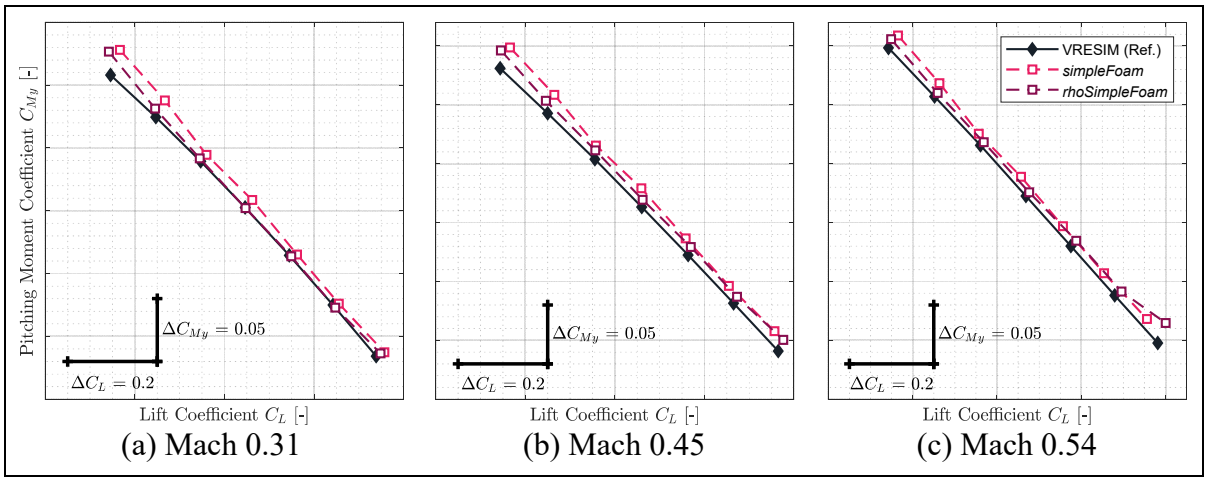

(a) Mach 0.31 (b) Mach 0.45 (c) Mach 0.54

Figure 2.11 $C_{M_y} = f(C_L)$ comparison for low Mach numbers value

Globally, the pitching moment coefficient is less well-estimated than the lift and drag coefficients. However, both the *simpleFoam* and *rhoSimpleFoam* computations found pitching moment coefficients with a maximum absolute error of 0.017 of error, except for negative angles of attack (where maximum absolute errors are close to 0.072). For positive angles of attack (i.e., 0 deg to 4 deg), the *rhoSimpleFoam* solver well estimated the pitching moment coefficient with a maximum absolute error of 0.017 from the reference.

The difficulty involved in predicting the pitching moment coefficients for negative angles of attack could be related again to the fact that the engines of the CRJ700 were removed from CAD drawing for the aerodynamic computations. However, normally a part of the total pitching moment of the aircraft is due to the engines' geometry (and this aspect was considered in the VRESIM values).

The engine part of the total pitching moment depends evidently on the engine geometry and on the aircraft's angle of attack. Indeed, the engine lift and drag forces generated a moment at the aerodynamic center. Because of the fact that the engines attachments to the fuselage rear has a certain fixed pitch angle, the absence of engines design in the simulations mainly impacts the analysis results for negative angles of attack.

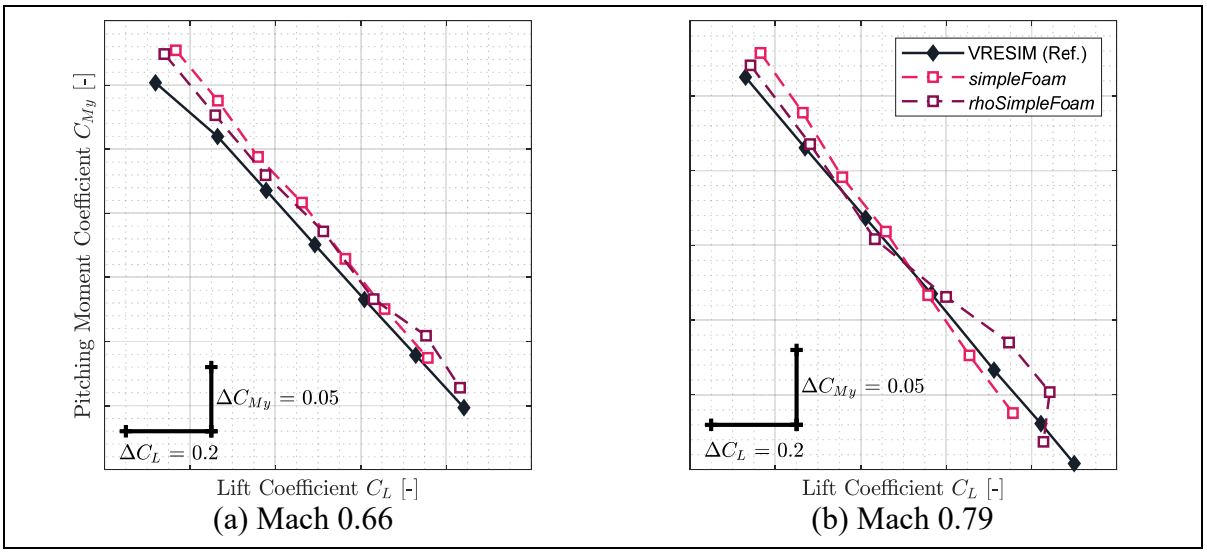

Figure 2.12 $C_{M_y} = f(C_L)$ comparison for high Mach numbers values

Similar observations can be made for Mach numbers M0.66 and M0.79. From Figure 2.12 (b), it seems that the compressible solver *rhoSimpleFoam* has some difficulties to match the reference (VRESIM), but the incompressible solver *simpleFoam* did not, which was surprising. Despite of the special shape of the *rhoSimpleFoam* results, the pitching moment coefficients were fairly well-estimated, with a maximum absolute error of 0.015 for positive angles of attack. The *simpleFoam* solver estimated the pitching moment coefficients with a slightly larger error (0.035 of error from the VRESIM). This last observation was expected, as *simpleFoam* is an incompressible solver, and thus this hypothesis could not be applied for cases where Mach numbers is over M0.6 (Friedlander & Serre, 2007a).

2.3.5 Results summary obtained using the compressible solver *rhoSimpleFoam*

In order to summarize results obtained for the compressible solver *rhoSimpleFoam*, a statistical study was finally performed. Thus, for the three longitudinal aerodynamic coefficients (i.e., C_L, C_D and C_{My}), absolute errors recorded for all flight conditions tested previously have been displayed in Figure 2.13 (a), (b) and (c), respectively.

Errors are displayed following the *x*-axis, while the *y*-axis is dedicated to show the number of instances. The bars show the number of predicted flight conditions with the in corresponding absolute errors displayed on the *x*-axis. The red curve describes the normal distribution of these values. The normal distribution shape allows to define if the distribution of errors is narrow or wide.

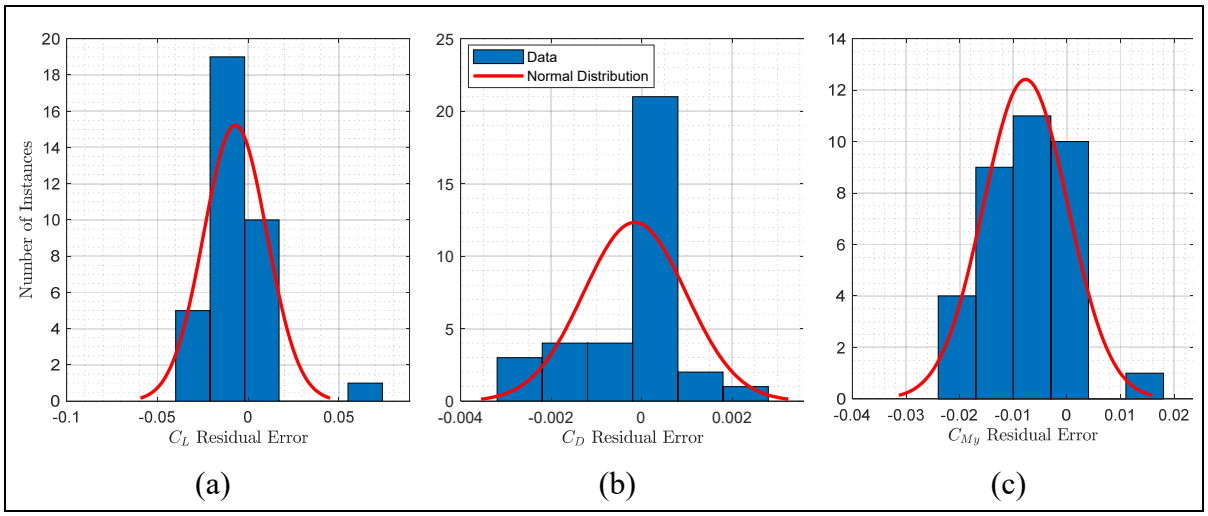

Figure 2.13 Statistical study concerning *rhoSimpleFoam* prediction errors over the 35 flight conditions

On Figure 2.13 (a), it was observed that the solver *rhoSimpleFoam*, was able to predict the lift coefficient with less than 0.05 of absolute error from VRESIM values, for 34 flight conditions (over 35). Globally, *rhoSimpleFoam* has predicted the lift coefficient with an average error of -0.007 (top of the red curve) and a standard deviation of ±0.045. This aspect means that *rhoSimpleFoam* was able to predict lift coefficient of the Bombardier CRJ700 within a margin error of -0.007 ± 0.045 in 95% of cases.

On Figure 2.13 (b), it was observed that *rhoSimpleFoam* was able to very well predict the drag coefficient for the 35 flight conditions tested. For over 20 conditions, the drag coefficient was estimated by the solver with an absolute error less than 0.001 which is an excellent result for a model dedicated to perform preliminary design analysis. More generally, the drag coefficient

of the Bombardier CRJ700 was predicted within a margin error of -0.00015 ± 0.00114 in 95% of cases.

Finally, Figure 2.13 (c) showed prediction error of *rhoSimpleFoam* at the pitching moment level. It has been observed that error bars were a little bit more spread out on the space for the pitching moment coefficient than for lift (Figure 2.13 (a)) and drag coefficients (Figure 2.13 (b)). This aspect comes from the fact that pitching moment coefficient is more sensible to the engine deletion in the model, as previously explain. Nonetheless, *rhoSimpleFoam* predicted the pitching moment coefficient of the Bombardier CRJ 700 within a margin error of -0.0077 ± 0.0079 in 95% of cases, which was more than acceptable for an aerodynamic model dedicated to be used in the conceptual or preliminary design phases.

2.4 Conclusion

The study presented here has demonstrated that it is possible to obtain accurate results with an aerodynamic model based on open source CFD methods. The originality of this study is its premise that low-power computation resources had been used such as computers equipped with 8 processors and 32 GB of RAM memory. In order to measure the accuracy and precision of the results, an aircraft simulation tool with real flight data was used. The Virtual Research Simulator (VRESIM) the CRJ700 is a high-level flight simulator; its flight dynamic has been qualified with the level D, the highest level of qualification delivered by the Federal Aviation Administration (FAA) for a simulator.

With OpenFoam toolbox, it was possible to design a complete aerodynamic model, including the mesh and simulation steps. While many mesh and simulation settings are proposed by OpenFoam are a great advantage for computation optimisation, they are also representing a significant amount of time to gather the optimum settings to design a very good model.

The model proposed in this paper was designed through two successive steps. The first step used a more stable rather than a more accurate model to compute a first flow state. A

computation coupling of the SIMPLE algorithm of resolution for incompressible conditions (*simpleFoam*) with the Spalart-Allmaras (SA) turbulence model was parameterised for this purpose. Then, based on the state found by the first computation, the computation of the flow state was continued with a compressible solver (*rhoSimpleFoam*) and a more accurate turbulence model: $k-\omega$ SST. By coupling both solvers (for incompressible and compressible flow), a more stable solver and more accurate results were obtained than it would have been possible using only one solver.

A statistical study has shown that the lift coefficient (C_L) was predicted within a margin error of -0.007 ± 0.045 in 95% of cases. Similarly, the drag coefficient (C_D) was predicted within a margin error of -0.00015 ± 0.00114 in 95% of cases and the pitching moment coefficient (C_{M_y}) was estimated within a margin error of -0.0077 ± 0.0079 in 95% of cases. According to these excellent results, the resulting model (coupling *simpleFoam* with SA turbulence model and then *rhoSimpleFoam* with $k-\omega$ SST turbulence model) was validated for the complete flight envelope simulated in this paper, for Mach number range M0.31 – M0.79.

Finally, OpenFoam codes have shown that they can lead to a high level of accuracy for longitudinal coefficient predictions (by using reference data very close to real flight tests data). The methodology presented here was applied to a regional aircraft to better understand its functioning; however, it could be applied for other aircraft geometries. Moreover, this paper has also shown that while having access to a high-level computational resource is important to perform quick computations, a very good level of accuracy could also be reached by using lower-level computer resources which are commonly available in academic and industrial environments.

CHAPTER 3

NEW AERODYNAMIC STUDIES OF AN ADAPTIVE WINGLET APPLICATION ON THE REGIONAL JET CRJ700

Marine Segui [a], Federico Roberto Abel [b], Ruxandra Mihaela Botez [c], Alessandro Certui [d]

[a, c] Department of System Engineering, École de Technologie Supérieure,
1100 Notre-Dame West, Montréal, Québec, Canada H3C 1K3
[b,] School of Engineering and Architecture, University of Bologna, Bologna, Italy
[d] Department of Industrial Engineering, University of Bologna, Bologna, Italy

Paper published in *Biomimetics*, Vol. 6, No. 4, September 2021, pp. 54-76.
DOI: https://doi.org/10.3390/biomimetics6040054

Résumé

Cette étude vise à évaluer comment une ailette marginale adaptative en vol peut améliorer les caractéristiques aérodynamiques de l'avion CRJ700. La géométrie de l'avion a été légèrement modifiée pour intégrer une ailette adaptative, mobile suivant un axe de rotation. Les caractéristiques aérodynamiques de la nouvelle conception d'ailette ont été calculées à l'aide d'un modèle aérodynamique de haute-fidélité, validé et développé avec le code open-source OpenFoam. Le modèle aérodynamique utilise successivement les deux solveurs *simple-Foam* et *rhoSimpleFoam* basés sur les équations « Reynold Averaged » de Navier Stokes (RANS). Les caractéristiques aérodynamiques de l'ailette adaptative ont été étudiées pour 16 conditions de vol représentatives de la montée et de la croisière habituellement franchies par le CRJ700. Il a été trouvé que l'ailette adaptative pouvait augmenter le rapport portance/traînée jusqu'à 6,10% et réduire le coefficient de traînée jusqu'à 2,65%. Les polaires aérodynamiques du Bombardier CRJ700 équipé d'ailette adaptative ont été comparé à celles du CRJ700 équipé d'ailette fixes. Similairement, cette étude montre aussi une comparaison des moments de tangage obtenu entre les deux configurations.

Abstract

This study aims to evaluates how an adaptive winglet during flight can improve aircraft aerodynamic characteristics of the CRJ700. The aircraft geometry was slightly modified to integrate a one-rotation axis adaptive winglet. Aerodynamic characteristics of the new adaptive design were computed using a validated high-fidelity aerodynamic model developed with the open-source code OpenFoam. The aerodynamic model uses successively the two solvers simple-Foam and rhoSimpleFoam based on Reynold Averaged Navier Stokes equations. Characteristics of the adaptive winglet design were studied for 16 flight conditions representative of climb and cruise usually considered by the CRJ700. The adaptive winglet can increase the lift-to-drag ratio by up to 6.10% and reduce the drag coefficient by up to 2.65%. This study also compared the aerodynamic polar and pitching moment coefficients variations of the Bombardier CRJ700 equipped with an adaptive versus a fixed winglet.

3.1 Introduction

With the substantial increase in carbon dioxide (CO_2) emissions into the atmosphere over the past several years (Air Transport Action Group (ATAG), 2018 ; International Air Transport Association (IATA), 2019), the aerospace sector has to limit its figures in the near future (ICAO, 2018 ; International Civil Aviation Organization (ICAO), 2010). For that, some solutions are available such as working on trajectories optimization (B. Dancila, Beulze, & Botez, 2019 ; R. Dancila & Botez, 2019 ; Murrieta-Mendoza & Botez, 2020 ; Murrieta-Mendoza, Botez, & Bunel, 2018 ; Murrieta-Mendoza, Romain, & Botez, 2016 ; Murrieta-Mendoza, Ternisien, Beuze, & Botez, 2018), or improve aircraft models to design reliable flight simulators (Ghazi & Botez, 2017, 2019 ; Ghazi, Gerardin, et al., 2020 ; Huvelin, Dequand, Lepage, & Liauzun, 2018b). It has been shown that trajectory optimization can save up to 2% of the cost of flights. Moreover, the use of reliable flight simulators could replace real flights related to pilot training or aircraft launch (certification, optimizations, etc.) and consequently could also help to reduce CO_2 emissions. To complement these efforts, solutions involving the optimization of aircraft geometry could also be interesting.

3.1.1 Literature Review: Aircraft Geometry Improvement

Other solutions aim to improve the aircraft geometry and reduce the drag as a means to reduce fuel consumption (Ameduri & Concilio, 2020 ; G. Amendola, Dimino, Concilio, Pecora, & Amoroso, 2019 ; Concilio, Dimino, & Pecora, 2021 ; Dimino et al., 2021). Among the notable advances, the arrangement of a winglet at the wingtip is considerate as one of the most important. When an aircraft is flying, the high-pressure flow (below the wing) joins the low-pressure flow (over the wing) by generating a vortex and therefore creating undesired drag. By introducing a winglet device at the wingtip, Whitcomb improved the cruise efficiency from 6% to 9% and increased the mileage by 6.5% for a National Aeronautics and Space Administration (NASA) test aircraft (Freestone, 1988). Various winglet shapes have been developed, such as the blended winglet (The Boeing Company, 2009), wingtip fences (Hitchens, 2015), split-scimitar winglets (United Airlines, 2014), and raked wingtips (Heathers, 2002). Each shape has its own advantage; as for example, a blended winglet offers a reduction of the fuel consumption from 4 to 5% depending on the aircraft type (The Boeing Company, 2009).

The latest winglet (or wingtip) configuration is the one that equips the Boeing 777x aircraft (« How the 777X's folding wing tips work », 2018, p. 777). Developed with an unconventional wing span that optimizes its performance, the Boeing 777x is code F airport compatible (wingspan is from 65m to 80m), therefore it can only access F-equipped airports (limited to roughly 400 airports worldwide). To expand its scope, Boeing engineers have developed a folding wingtip for use in ground phases. Indeed, by folding 3.5 meters of the wing on each side, the Boeing 777x can operate on the ground as most conventional long-range aircraft (code E airport compatibility) (Boeing, 2013, p. 777). According to the Federal Aviation Administration (FAA), to be certified, this device must be completely folded for taxi phases and unfolded for flight phases (Federal Aviation Administration, 2018). However, it would be interesting to measure how the Boeing 777x performances can be influenced by the fact the wingtip will also move (under control) during flight. Furthermore, the winglet mechanism is

already installed; making it active during the flight will not add any significant weight at the wing tip.

Some studies have been already done under the name of “adaptive winglet”, “morphing winglet” or “active winglet”, and these studies have indicated promising ideas. Among these studies, the project CLAReT (Control and Alleviation of Loads in Advanced Regional Turbo-Fan Configurations) was conducted in 2013 by the Clean Sky team and Bristol university (« Welcome to the Clean Sky | Clean Sky », 2020). CLAReT researchers developed a “morphing winglet concept” that aims to adapt the winglet cant (i.e., dihedral) and twist angles throughout the flight envelope of a regional jet. For the three speed conditions studied, Mach numbers 0.48, 0.60 and 0.74, the aircraft operational range was increased by up to 5%. To achieve these results, the CLAReT team conducted structural analysis and aerodynamic studies using Computational Fluid Dynamics (CFD) methods (Cooper, 2020 ; Cooper et al., 2015). Bristol university and the aircraft manufacturer Airbus have also conducted a “free winglet” project called “AlbatrossOne” able to reduce bending moments absorbed by the wing during the flight, and therefore could lead to a weight reduction (Castrichini et al., 2017 ; Cheung et al., 2018 ; Healy et al., 2021).

Teams from Airbus (Wildschek et al., 2015), and the French aerospace laboratory (ONERA) (Carossa et al., 2016 ; Cedric Liauzun et al., 2018) are also working on an adaptive winglet applied to a regional aircraft. The device imagined is in fact a new control surface integrated in the trailing edge of a conventional winglet. In other words, the winglet is morphed according to its camber during the flight. Researchers have presented an important work regarding the mechanism and structural aspects, but to date, no significant aerodynamic results were obtained (Gianluca Amendola et al., 2017).

The state-of-the-art also offers a “telescopic” winglet that consists of an enlargement or a shrinking of the winglet span. With this device, researchers have successfully reduced the fuel consumption of a transport jet aircraft similar to the Airbus A380 by up to 2% based on the Breguet formula and CFD aerodynamic computations (Daniele et al., 2012).

Contributing to the work on global warming, recent studies performed by the Laboratory of Applied Research in Active Controls, Avionics and AeroServoElasticity (LARCASE) were targeted to improve aircraft aerodynamics characteristics using adaptive structures (i.e., “morphing wings” or “adaptive wings”) (Concilio et al., 2018). The knowledge and skills of LARCASE in this discipline were notably highlighted in 2014 by winning the Consortium for Research and Innovation in Aerospace in Québec (CRIAQ) runner-up award for the CRIAQ MDO505 project entitled "Morphing Architectures and related Technologies to improve the Wings Efficiency" (R. M. Botez, 2018 ; R. M. Botez et al., 2018 ; Koreanschi et al., 2017a, 2017b, 2016a ; Marine Segui & Botez, 2018c ; Marine Segui, Gabor, Koreanschi, & Botez, 2017 ; Sugar Gabor, 2015 ; Tchatchueng Kammegne, Botez, & Grigorie, 2016).

In 2018, the LARCASE team conducted a preliminary study to measure the impact of an adaptive winglet for a Cessna Citation X (Marine Segui, Bezin, et al., 2018 ; Marine Segui & Botez, 2018b). This study used Vortex-Lattice Method (VLM) aerodynamic computations to measure the aerodynamic characteristics of the aircraft in its flight envelope (Marine Segui, Bezin, et al., 2018 ; Marine Segui & Botez, 2018b). In addition, an in-house performance model of the aircraft has shown that rate of climb could be increased by up to 26 feet/min during climb segments and fuel flow reduced by up to 20 pounds (9.1 kg) per hour for cruise segments, using an adaptive winglet. With such promising results, the authors recommended to pursue this study and use Computational Fluid Dynamics (CFD) based on Navier-Stokes equations in order to confirm results obtained using VLM (Marine Segui, Bezin, et al., 2018 ; Marine Segui & Botez, 2018b). Indeed, VLM can predict induced drag (without compressibility effects), but not skin friction and shape (called also “pressure” or “form”) drag. Turbulence effects are also neglected with a VLM method.

3.1.2 Paper Objectives

The literature shows that several researches have been interested in adaptive winglet structural studies, but only a few of them have measured aerodynamic characteristics. Similarly, the

literature lacks studies which would lead to predict performance inflight of an aircraft equipped with an adaptive system.

The goal of this research is to continue the work realized using the VLM methods by the LARCASE team (Marine Segui, Bezin, et al., 2018 ; Marine Segui & Botez, 2018b). The adaptive winglet design is investigated in terms of a complete aerodynamic study over the whole flight envelope of a regional jet. A further study will then evaluate the benefits of an adaptive winglet in terms of "flight performance", for this reason, only longitudinal aerodynamic characteristics were studied in this paper. As structural data of the aircraft is not available, mechanical and aero elastic aspects were not studied in this paper. However, this study should highlight all the information to further design the winglet motion mechanism.

This research will evaluate the aerodynamic efficiency of an adaptive winglet in flight with respect to a fixed (i.e., conventional) winglet. Among the benefits considered, a winglet is one of the last parts assembled onto an aircraft wing, and thus it can be quite easily replaced on a fleet. Given that the surface of the winglet would need to be controllable, certification phases would be necessary, but these phases would be shorter and less expensive than for a new aircraft certification.

Adaptive winglets could therefore present a significant ecological aspect, as they could allow the improvement of aircraft performance already on the market, without the need for replacing them. Moreover, by applying this winglet change to a whole fleet, the International Civil Aviation Organization (ICAO) objectives could be realized in a relatively short time, while limiting the related expenses.

To perform this present study, the Bombardier CRJ700 (Bombardier, 2019) was chosen because the LARCASE has a high-quality flight simulator for this aircraft. The Bombardier CRJ700 flight simulator located at LARCASE, called the Virtual Research Simulator (VRESIM), is a simulator designed and assembled by CAE Inc. for research needs of LARCASE.

The VRESIM is a level D flight simulator that is able to simulate flight test data with less than 5% of error with respect to those of the real aircraft (Federal Aviation Administration (FAA), 1991b). Indeed, the level D is the highest degree delivered by the Federal Aviation Administration (FAA) to qualify the flight dynamics of a simulator. In addition, aerodynamic data provided by the VRESIM was simulated based on original aerodynamic data tables delivered by the aircraft designer Bombardier for the CRJ700. In consequence, the VRESIM is a very reliable source for validation.

3.2 Methodology: Adaptive Winglet Analysis

The methodology aims to quantify the advantages and disadvantages of equipping an aircraft with an adaptive winglet from an aerodynamic point of view. For this purpose, an adaptive winglet has been designed for the CRJ700 aircraft. Then, a high-fidelity aerodynamic model of the aircraft was used to compute lift, drag and pitching moment forces for several flight conditions and several winglet deflection angles.

3.2.1 Adaptive Winglet Design

The adaptive winglet considered in this research was designed based on the original winglet of the CRJ700. Winglets that equipped the original Bombardier CRJ700 are commonly called “canted winglets”. As a signature of Bombardier aircraft, “canted winglets” have a curved part at the trailing edge.

Due to the mechanical difficulties involved in moving the original winglet showing a thin thickness (0.15 m at the root), we decided to slightly modify the original shape of the winglet by incorporating a “pod” at its root. The use of this component shape was inspired by the Airbus Blade project (AIRBUS, 2020) and the Boeing *777x* winglet motion (« How the 777X’s folding wing tips work », 2018).

The pod's exposed surface is 0.654 m^2, its length is 1.372 m and its maximum diameter is 0.173 m. It was designed to allow enough space inside of the pod to install a gear mechanism or a similar actuation device, as in the case of the Boeing *777x* winglet motion. Given that this study is targeted to aerodynamic analysis and further, performance benefits, the hypothesis that this was pod could accommodate an adequate mechanism using current technology was made.

Figure 3.1 shows the Bombardier CRJ700 equipped with the adaptive winglet. It can be observed that the winglet of this proposed aircraft configuration has the capability of moving following one rotation axis. When the adaptive winglet makes an angle ξ of 73 deg, it can be superimposed onto the original Bombardier winglet. The winglet angle ξ is measured between the winglet axis and the ground.

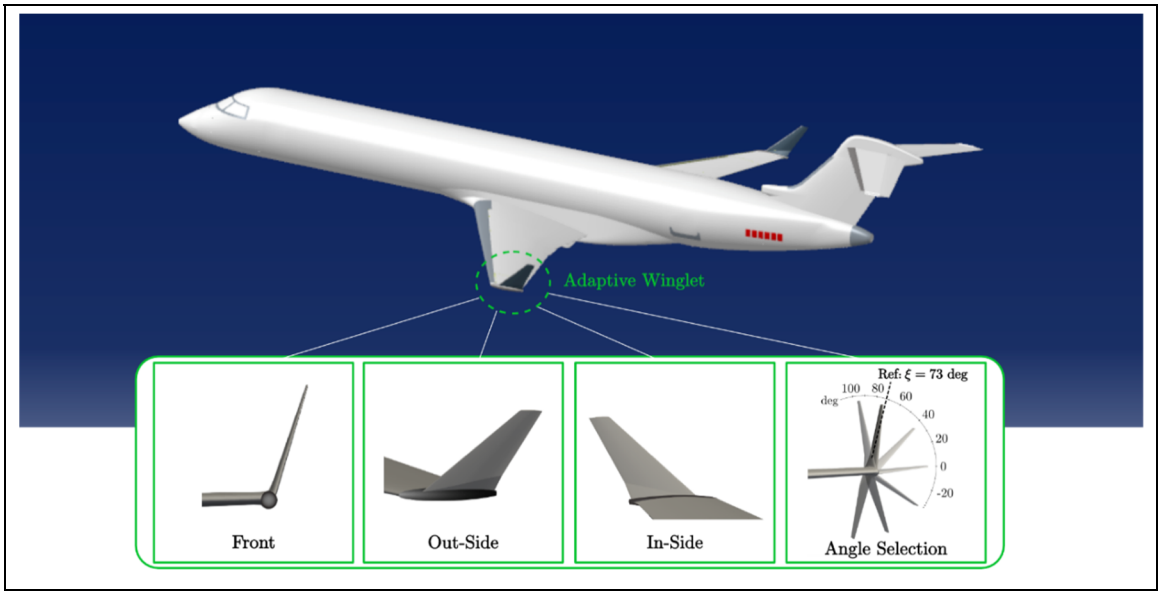

Figure 3.1 Bombardier CRJ700 adaptive winglet

3.2.2 Presentation of the Aerodynamic Model

In order to analyze the new aerodynamic characteristics brought by the adaptive aspect of the winglet, a high-fidelity aerodynamic model was used as recommended by previous work (Marine Segui, Bezin, et al., 2018 ; Marine Segui & Botez, 2018b). The method here consisted

in using the aerodynamic model designed and validated for the original Bombardier CRJ700 to perform simulations of the aircraft equipped with the adaptive winglet. As this model was developed in a previous study, all details and design justifications such as mesh analysis or turbulence model choice were not being covered in this paper. For more details, please refer to the work that consisted on developing the original aerodynamic model of the CRJ700 (Marine Segui, Abel, Botez, & Ceruti, 2021a).

The aerodynamic model of the Bombardier CRJ700 used in this study was implemented using the open-source CFD code OpenFoam (i.e., mesh and simulations utilities) in such a way as to limit computation expenses. Indeed, computers that have limited computation capacity were used to design the mesh and perform computations (computers equipped with 8 processors and 32 GB of RAM memory). Meshes were designed as coarse as possible while they provide acceptable qualities. In addition, new simulation process consisting of using two successive solvers was developed in order to optimize solution convergence and stability (i.e., especially required for coarse/medium mesh).

3.2.2.1 Mesh Design

The mesh of the aerodynamic model was designed using *blockMesh* and *snappyHexMesh* OpenFoam utilities (Figure 3.2). For simulations using an angle of attack different from zero, it was preferred to rotate the aircraft instead of the flow. In consequence, one mesh was developed for each combination of angle of attack (from -2 degrees to 4 degrees) and winglet deflection angle (for the adaptive winglet version of the aircraft).

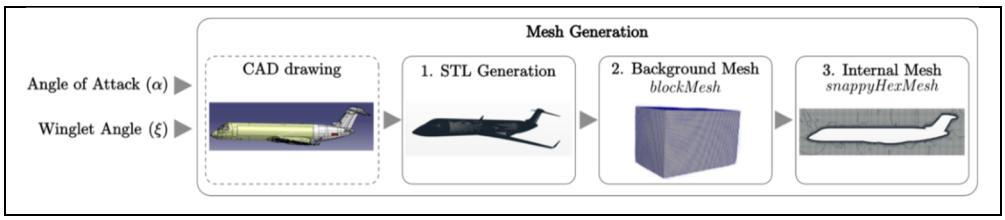

Figure 3.2 Mesh design outlines

The aircraft shape (i.e., including angle of attack and winglet deflection angle) was designated using a triangulated file (STL), from the CAD model (Figure 3.1). The *blockMesh* utility was used to design the "background mesh" which is a domain of 44 m × 44 m × 70 meters composed of hexahedral cells of 1 m^3 (1×1×1 meters). Then, the *snappyHexMesh* (*SHM*) tool was used to made the aircraft integration (i.e., the aircraft shape defined using the STL file) into the "background mesh". In order to perfectly smooth the wall of the plane, *SHM* use an algorithm that made refinement, smoothing and re-alignment treatments using several techniques such as chimera technics and curvilinear mesh (OpenCFD ltd (ESI Group), s.d. ; Marine Segui, Abel, et al., 2021a). The *SHM* algorithm perform mesh re-arrangement until mesh quality criteria have been reached. In this study, the maximum non-orthogonality was set to 65 and the maximum skewness was set to 5. The refinement near wall was set using three layers measuring a maximum of 8.5 mm in total. The first layer, the closest to the wall did not exceed 1.55 mm.

Meshes obtained for the original CRJ700 design were composed on average by 11.14×10^6 cells, and showed an y+ value between 100 and 200 which has been considerate as "medium" mesh.

3.2.2.2 Simulation Settings

The CRJ700 flies up to Mach number 0.85, in consequence, a compressible solver is required in order to consider compressibility effect (Friedlander & Serre, 2007b). Moreover, the model was designed to study the CRJ700 in steady-state situations and therefore it exploited solvers using time-averaged Navier-Stokes equations (RANS) (OpenCFD ltd (ESI Group), s.d.).
As meshes were designed as coarse as possible while keeping an acceptable quality level due to computer resources limitations, it was necessary to take that aspects into account for simulations steps. Indeed, with the "medium" mesh designed, it was difficult to reach a good rate of convergence using a compressible solver (such as *rhoSimpleFoam*, for instance). In order to avoid this problem, a special process was developed for the CRJ700 aerodynamic model. It consists of using two successive OpenFoam solvers, as illustrated in Figure 3.3. We

observed that instability in solutions has been avoided during design and validation studies of the aerodynamic model (Marine Segui, Abel, et al., 2021a).

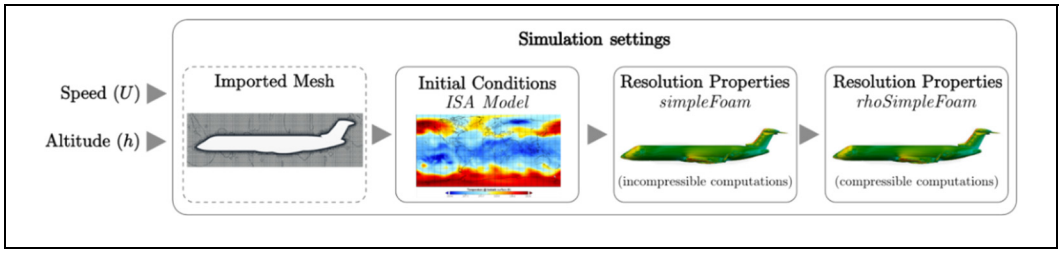

Figure 3.3 Simulation process summary

A first estimation of the flow properties was computed using the incompressible solver *simpleFoam* initialized using atmospheric data issued from an International Standard Atmosphere (ISA) model. ISA equations give the theoretical properties of an atmospheric flow in terms of its pressure, air density, dynamic viscosity, temperature, etc., according to the altitude (without any temperature deviations).

The converged solution obtained with *simpleFoam* (the first simulation) was then used to initialize the flow for the compressible solver *rhoSimpleFoam* (density-based) (Marine Segui, Abel, et al., 2021a). This second simulation is "stable" especially due to the fact that it was initialized using a converged solution of pressure and speed flow. New parameters that were necessary to estimated such as turbulent parameters and the temperature were then predicted in a more stable way than without a "pre-simulation" (i.e., *simpleFoam*).

Concerning the choice of turbulence model, it was found that coupling the solver *simpleFoam* with Spalart-Allmaras (S-A) turbulence model was the most stable option, especially due to its 1-equation representation. For the second simulation, where accuracy was more important than computation stability (because stability was maintained due to flow initialization), the turbulence model $k-\omega$ Shear Stress Transport (SST) was selected (Marine Segui, Abel, et al., 2021a).

3.2.2.3 Validation of the CRJ700 Aerodynamic Model

Finally, the aerodynamic model was tested for 35 flight conditions frequently flown by the Bombardier CRJ700, for which the altitude ranges from 5,000 ft to 30,000 ft, the Mach number from M0.31 to M0.79 (normal cruises are operated between M0.78 and M0.82), and the angle of attack from -2 degrees to 4 degrees. Figure 3.4 indicates the statistical study of the errors obtained between aerodynamic coefficients computed by the OpenFoam model versus the reference (i.e., VRESIM). Figure 3.4 (a), (b) and (c) show the results in terms of lift, drag and pitching moment coefficients absolute errors, respectively.

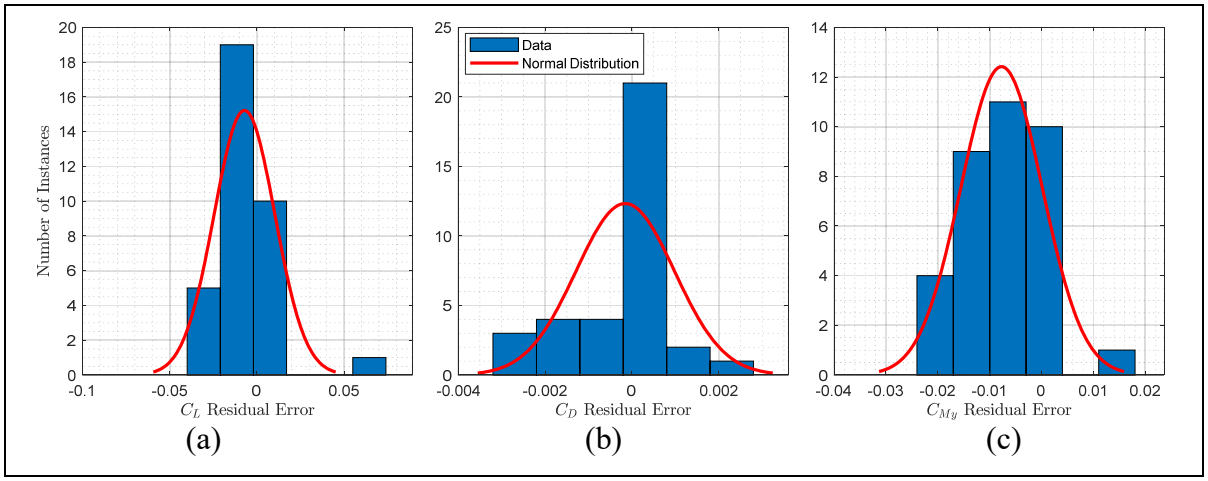

Figure 3.4 Statistical analysis of errors obtained between the reference (VRESIM) and the validated aerodynamic model of the CRJ700 using OpenFoam. Residual errors are presented in terms of lift (a), drag (b) and pitching moment (c) coefficients

Lift coefficients of the CRJ00 were predicted by the aerodynamic model design within an error margin of -0.007±0.045 in 95% of cases. Similarly, the drag and the pitching moment coefficients were estimated within error margins of -0.00015±0.00114 and -0.0077±0.0079 in 95% of cases, respectively. Based on these low errors (Figure 3.4), it was assumed that the aerodynamic model of the Bombardier CRJ700 designed using OpenFoam was highly accurate, and has therefore been validated to perform the adaptive winglet study (Marine Segui, Abel, et al., 2021a).

By considering the validated aerodynamic model as accurate, all its properties, hypotheses and settings were re-used to compute the aerodynamic characteristics of the adaptive configuration of the airplane (i.e., equipped with the adaptive winglet) by changing the input geometry.

3.2.3 Comparison of the Original and the Adaptive Winglet Designs of the CRJ700

This section aims to compare the original and the adaptive winglet design of the CRJ700. Indeed, to design the adaptive winglet version of the CRJ700, some modifications were made at the winglet level. To use the CRJ700 validated aerodynamic model to study the characteristics of the aircraft equipped with the adaptive winglet, the context, such as mesh qualities must remain similar.

Indeed, similar mesh qualities allow the use of the same solver settings as those used for the validation of the aerodynamic model. In this context, the same level of confidence (of the validated model) can be expected in the results of the simulations.

3.2.3.1 Geometric Comparison

Firstly, a geometric comparison was made on Figure 3.5. The original winglet shape that equipped the original Bombardier CRJ700 is represented in “dark grey” color and the adaptive winglet design is shown in “pink” color.

From Figure 3.5, it can be observed that the original and the new adaptive designs are very similar. The main difference is located around the winglet root with the addition of the pod. Indeed, the pod is slightly bigger than the original winglet at the junction between the wing and the winglet.

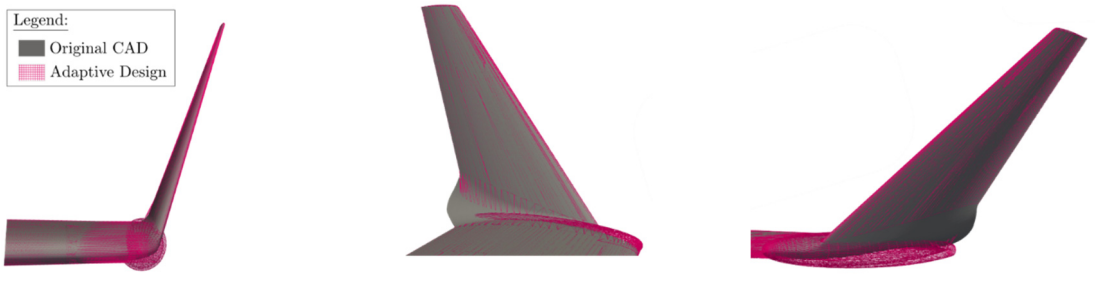

(a) Front view (b) View inside of the wing (c) View outside of the wing

Figure 3.5 Superposition of the Computer-Aided-Design (CAD) of the original model and the new adaptive model of the CRJ700 aircraft

As the adaptive winglet geometry is larger than the original winglet geometry, it was expected that this new design including the pod would slightly increase the drag.

3.2.3.2 Aerodynamic Comparison

Firstly, the mesh qualities obtained for both aerodynamic models (for the validated and for the new adaptive model of the CRJ700 aircraft) were compared and described in Table 3.1 in terms of cell's "maximum non-orthogonality", "maximum skewness" and "number of cells".

Table 3.1 Average mesh qualities of validated and new aerodynamic models

Mesh quality parameters	**Validated model (no pod)**	**New model (with pod)**
Max. non-orthogonality (deg)	65.060	65.020
Max. skewness	5.0006	4.9925
Number of cells ($\times 10^{+6}$)	11.14	11.12

As a reminder, one mesh was generated per angle of attack studied using the validated model which represent 7 meshes. The average qualities of these 7 meshes were added on the second column of Table 3.1. Concerning the new aerodynamic model (to study the adaptive winglet), as the winglet deflection angle would change; a new mesh is also needed for each winglet

deflection angle. In order to check the validity of meshes generated for the new adaptive design, it was chosen to analyze meshes generated for the combination of the seven angles of attack and the winglet deflection angles $\xi = \{-93, -73, -35, 0, 35, 73 \text{ and } 93\}$ deg. Meshes qualities obtained for these 49 meshes (for the new adaptive design model), have been displayed in the third column of Table 3.1.

Globally, the figures displayed in Table 3.1 reveal that all the meshes have qualities in the same order of magnitude. For the "maximum non-orthogonality" criteria, it was observed that 65.06 deg (for the validated model) and 65.02 deg (for the new model) are extremely close. Similarly, cells' maximum skewness values were also very close such as 5.00 for the validated model and 4.99 for the new model that includes pod design. In addition, meshes were designed using similar number of cells: close to $11.14 \times 10^{+6}$ cells for validations cases and using approximatively $11.12 \times 10^{+6}$ cells for adaptive cases (equipped with the pod). Therefore, it seems that the "pod" designed in order to integrate the adaptive winglet was not linked to a degradation of the mesh qualities, which is very favorable to pursue the study.

As the meshes have shown qualities very similar to those of the original model, same solver (*simpleFoam* and *rhoSimpleFoam*) settings as those used for the validated aerodynamic model were kept.

As a second verification study, the aerodynamic characteristics of the original (without a pod) and the adaptive aircraft configuration (equipped with a pod and a winglet fixed set at angle $\xi = 73$ deg) of the CRJ700 were compared in order to assess how the pod affects the aerodynamic coefficients values.

Figure 3.6 shows the lift and drag coefficients delivered from the aerodynamic model for the original CRJ700 design (data validated with the VRESIM) and for the adaptive winglet configuration of the aircraft. These results are given for 25 different flight conditions for which the aerodynamic model have been validated.

As the differences in terms of pitching moments are very small (0.0031 on average), it was considered that the pod does not have a high influence on this aerodynamic characteristic. Generally, the results of both models are “close enough” (Figure 3.6 (a) and (b)), which indicates that the aerodynamic model used for both models correctly computes the aerodynamic performance of both aircraft designs.

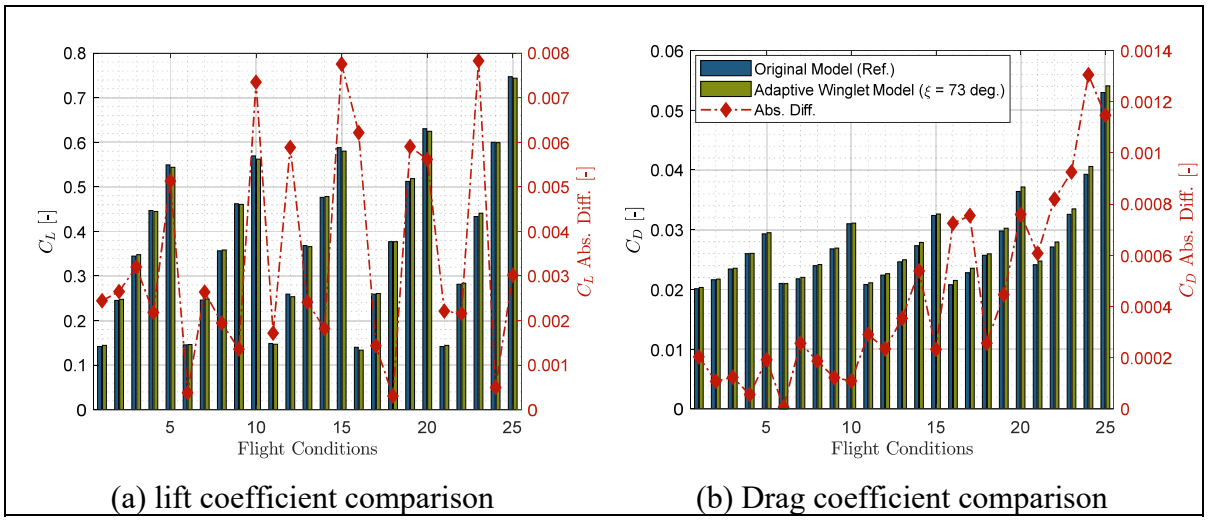

(a) lift coefficient comparison (b) Drag coefficient comparison

Figure 3.6 Comparison of aerodynamic coefficients obtained using the aerodynamic model for the original and the adaptive winglet design of the CRJ700 aircraft

It is important to clarify that it is normal that the two models do not overlap, as it is not exactly the same aircraft being considered (one has the original Bombardier CRJ700 winglet, in “blue” color, the other has an adaptive winglet with a pod, arranged at 73 deg, in “green” color). It can be observed on Figure 3.6 (a) and (b) that there is a “gap” of error between the aerodynamic characteristics of the two models which reflects the impact of the pod integration.

Depending on the flight condition, the pod seems to have a different impact on the lift coefficient (Figure 3.6 (a)). Indeed, sometimes, the pod induced an increase on the lift coefficient, and sometimes a decrease, but the difference is always less than 0.008, which is very small. This non-constant trend seems to be determined by the turbulence computation as its variation is very complex according to flight conditions.

The drag coefficient (Figure 3.6 (b)) for the adaptive winglet configuration (in “green” color) is higher than the drag coefficient obtained for the original design (in “blue” color) by 0.0005 on average. It was expected that the drag would be larger for the adaptive winglet configuration because the pod is larger than the original winglet at the root level and thus it induces higher drag. Moreover, we noticed that the drag coefficient error increases as the Mach number increases.

This section has highlighted that the adaptive winglet design does not have a strong impact on the mesh qualities nor on the aerodynamic characteristics. Therefore, the same solution settings of the validated aerodynamic model can be kept and the same level of accuracy can be expected to compute characteristics of the new adaptive design.

However, small differences were observed from the aerodynamic point of view, especially due to the “pod” integration in the design. In order to carefully analyze benefit of the adaptive winglet compared to a fixed one, it was chosen to define that the reference of the study should be the adaptive winglet design set with a deflection angle of 73 deg. This choice allows to consider pod disadvantages of the adaptive winglet design and well highlighted the adaptive aspects of the winglet.

It is important to highlight that the new junction (i.e., the “pod”) was not geometrically optimized in this first study. Indeed, as this research aims to measure advantages of an adaptive winglet versus a fixed winglet, it was preferred to compared the aerodynamic characteristics of two versions of the “same” winglet (one version fixed at 73 deg, and one able to move). Therefore, if an improvement is noticed with this adaptive winglet, an even greater improvement is expected in the case where an optimized junction is implemented.

3.2.4 Aerodynamic Simulations

Aerodynamic characteristics of the new adaptive design of the CRJ700 were computed using the validated aerodynamic model presented in section 3.2.2.

To study the widest range of winglet deflection angle, it was assumed that the adaptive winglet limits its angle ξ variation between -93 deg and 93 deg. Since conducting CFD analysis in such a wide range can be time consuming, the strategy consists in studying the aerodynamic characteristics for specific winglet positions and then perform a continuity analysis to predict aerodynamic characteristics between these positions.

3.2.4.1 Aerodynamic Simulations for Specific Winglet Deflection Angles

The aerodynamic characteristics of the Bombardier CRJ700 equipped with the different winglet deflection angles $\xi = \{-93, -73, -35, 0, 35, 73 \text{ and } 93\}$ deg were evaluated for various flight conditions, the most representative of the whole flight envelope of the aircraft. This range of winglet deflection angle was chosen arbitrarily except for $\xi = 73$ deg, which was considered as the reference angle.

Flight conditions choices were achieved by performing a wide range of flight tests (climb, cruise and descent segments) on the whole flight envelope using the VRESIM flight simulator. Moreover, only "clean" configurations of the aircraft (i.e., no slats, no flaps, no gears) were considerate.

Table 3.2 Flight conditions selected for the adaptive winglet study

Altitude	Mach number	Angle of attack
5,000 ft	M0.31	-2 deg to +2 deg
10,000 ft	M0.45	-2 deg to +2 deg
20,000 ft	M0.54	-2 deg to +2 deg
25,000 ft	M0.66	-2 deg to +2 deg
30,000 ft	M0.79	-2 deg to +2 deg

The flight conditions selection was made from conditions often used during flight tests, as well as according to flight conditions that were validated using the original aerodynamic model of the CRJ700. A recap of the tested flight conditions is presented in Table 3.2.

For each set of flight conditions (combinations of an altitude, Mach number and angle of attack) described in Table 3.2, winglet positions $\xi = \{-93, -73, -35, 0, 35, 73 \text{ and } 93\}$ were studied. It is important to add that for all flight conditions simulated, the horizontal tail of the CRJ700 aircraft was set at its neural position (0 deg).

3.2.4.2 Continuity Study

As a second step, a continuity study was required to predict values of the lift and drag forces and pitching momentum between the selected flight conditions (Table 3.2) and between two positions of winglet deflection angles ξ studied (i.e., the range: $\{-93, -73, -35, 0, 35, 73 \text{ and } 93\}$).

The variation of the aerodynamic coefficients ($C_L, C_D,$ and C_{My}) with the Mach number, and winglet deflection angle ξ, for a fixed angle of attack was analyzed. Figure 3.7 and Figure 3.8 show the variation of the aerodynamic coefficients ($C_L, C_D,$ and C_{My}) when $\alpha = 0$ deg, the winglet deflection angle varies from -93 deg to 93 deg and the Mach number changes from 0.31 to 0.79.

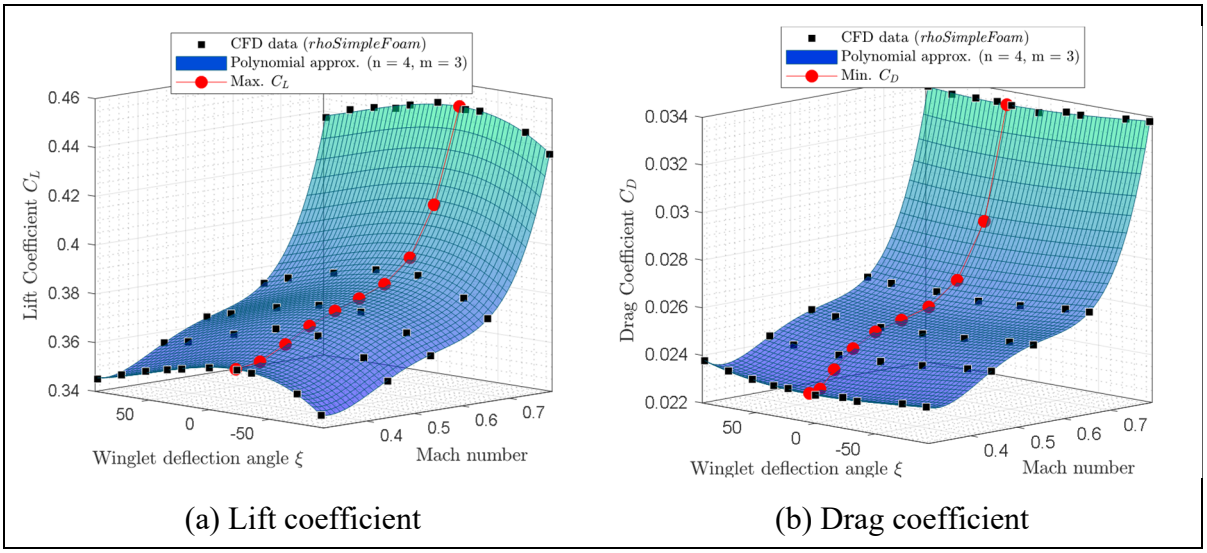

(a) Lift coefficient (b) Drag coefficient

Figure 3.7 Lift and drag coefficients variations with the winglet deflection angle and Mach number for an angle of attack of 0 deg

Aerodynamic coefficients obtained by *rhoSimpleFoam* CFD simulations are represented using black squares on Figure 3.7 and Figure 3.8. Then, these graphs shown a fitting polynomial surface that were investigated in order to determine the variation of aerodynamic coefficients between CFD measures.

For the three longitudinal aerodynamic coefficients, the fitting surfaces with the closest R^2 to 1 (R^2>0.96) were polynomial surfaces corresponding to a fourth order for the Mach number inputs, and to a third order for the winglet deflection angle inputs. As a reminder, R is the correlation factor usually used in identification methods, such as linear regression (Yan & Su, 2009).

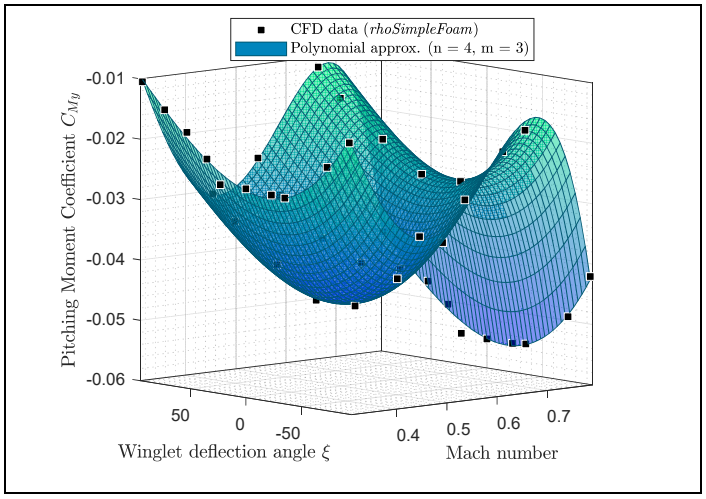

Figure 3.8 Pitching moment coefficient variation versus the winglet deflection angle and Mach number for angle of attack of 0 deg

The polynomial fitting surface equations for $C_L, C_D,$ and C_{My} are presented in Eq. 3.1, where $a_{i,j}$ are polynomial coefficients, and M and ξ designate the Mach number and the winglet deflection angle, respectively.

$$C_{L,D,M_y}(M,\xi) = \sum_{i=0}^{n=4} \sum_{j=0}^{m=3} a_{ij}.M^i.\ \xi^j \qquad (3.1)$$

It is important to add that due to the fact that an order 3 was necessary to model aerodynamic coefficient surfaces versus the winglet deflection angle, it means that the variation of aerodynamic coefficients ($C_L, C_D,$ and C_{My}) is non-symmetrical on both sides of the 0 deg winglet position. This non-symmetrical behavior is attributed to the winglet planform, that originally had a very small camber in the adaptive winglet design. It could also be attributed to the loading distributions changes, particularly as the effective span changes (i.e., the aspect ratio).

Using fitting surfaces, the winglet deflection angles corresponding to the maximum value of C_L and minimum values of C_D for each Mach number was analyzed. These results are displayed on Figure 3.7 (a) and (b), using "red" dots. Figure 3.7 (a) shows that the winglet deflection angle that is corresponding to the maximum of C_L depends on the Mach number. In other words, the winglet deflection angle that gives the maximum of C_L is a function of the Mach number (for a fixed angle of attack). This observation can also be done for the minimum value of C_D on Figure 3.7 (b). However, the winglet deflection angle that corresponds to the maximum value of C_L is not necessarily the same that offered the minimum value of C_D (for a given Mach number and angle of attack).

3.3 Results

This third section presents the results obtained for the aerodynamic study of an adaptive winglet application for the Bombardier Regional Jet CRJ 700.

3.3.1 Aerodynamic Benefits of an Adaptive Winglet

In order to highlight benefits of an adaptive winglet, it is important to select an optimization criterion. Usually, the optimization criteria concern inflight parameters such as a flight time or the fuel consumption. Since this study deals only with the aerodynamic aspects, improvement performed using an adaptive winglet do not allow to conclude on the final performances that could be offered during flight.

Figure 3.9, Figure 3.10 and Figure 3.11 show benefits observed in terms of lift, drag, and lift-to-drag ratio, respectively. These results highlight how a specific winglet deflection position ξ should improve the fixed winglet configuration (set at ξ = 73 deg). Benefits were computed using two statistical tools; the maximum benefit value on sub-figures (a) and the averaged benefit value on sub-figures (b), obtained among all the flight conditions tested.

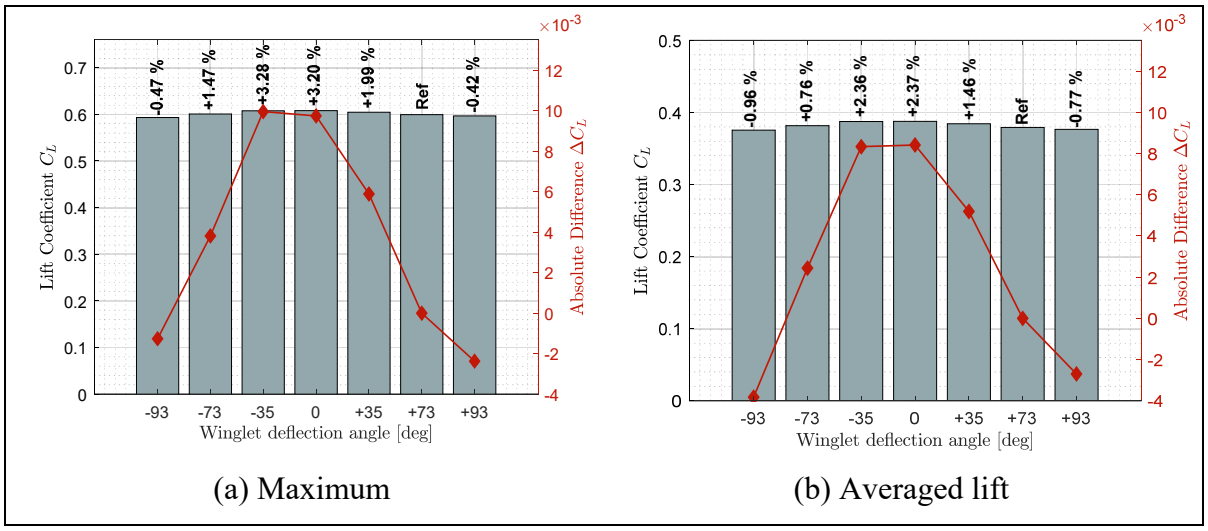

Figure 3.9 Maximum and averaged lift benefits observed for different winglet deflection angle and different flight conditions

Figure 3.9 shows the lift (left axis) and the lift difference (right axis) obtained for each winglet deflection angle from ξ = -93 to 93 deg. As an additional information, the relative difference obtained between a specific winglet deflection and the reference position was displayed above the corresponding bars.

On Figure 3.9, it could be noticed the negative difference obtained for winglet deflection angles ξ = -93 deg and ξ = +93 deg. This demonstrate that ξ = ± 93 deg degrade (i.e., reduce) the lift coefficient with respect to the reference position (ξ = 73 deg). On the other hand, other winglet deflection angles (ξ = -73 deg to ξ = +35 deg) have shown a lift benefit (i.e., increase) with respect to the reference position. Indeed, a maximum lift increase of 3.28% have been obtained for the winglet position ξ = -35 deg (Figure 3.9 (a)). Similarly, a winglet position ξ = 0 deg (close to horizontal) have shown an average lift improvement of 2.37% (Figure 3.9 (b)).

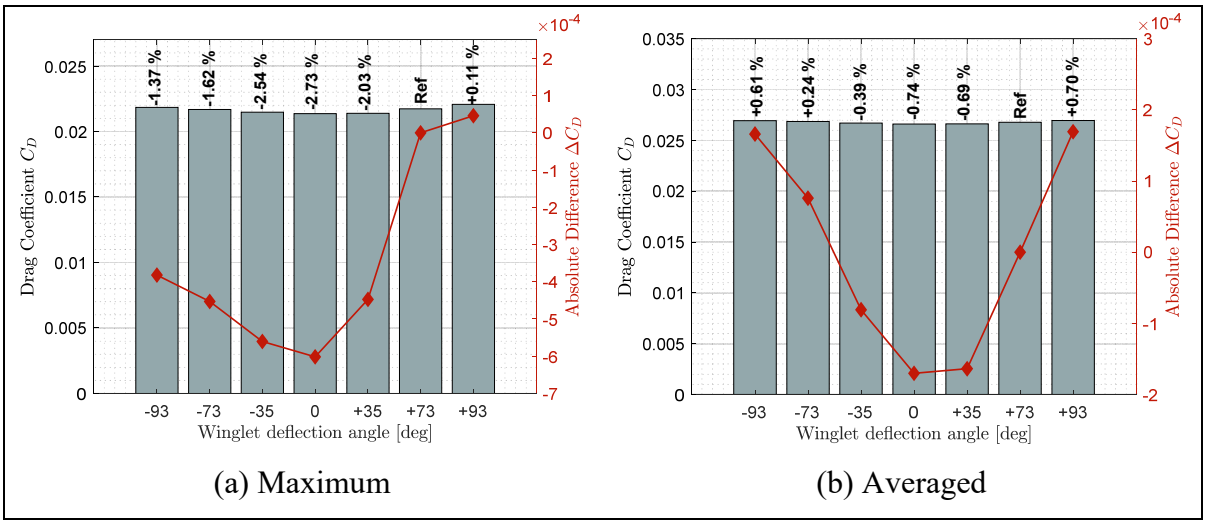

Figure 3.10 Maximum and averaged drag benefits (reduction) observed for different winglet deflection angle and different flight conditions

Concerning the drag, it was noticed that the different winglet deflection angle could reduce the drag (i.e., benefit) differently. For specific flight conditions that conducted to the maximum drag improvement (minimization) (Figure 3.10 (a)), it was shown that all winglet deflection except the position ξ = +93 deg have shown a drag reduction from 1.37% to 2.73%. However, it was observed that only winglet deflection angles ξ = -35 deg to +35 deg could reduce the drag coefficient of the aircraft on average for all the flight conditions tested (Figure 3.10 (b)). This observation allows us to highlight the advantage of an adaptive winglet. Indeed, for specific flight conditions (such as the ones that offered the maximum drag difference on Figure 3.10 (a)), certain winglet position can offer really advantageous aerodynamic performance such as a drag reduction up to 2.73%.

The last aerodynamic criterion is the lift-to-drag ratio. As it was observed some advantages of an adaptive winglet in terms of lift and drag coefficients, good improvements were also expected in terms of lift-to-drag ratio on Figure 3.11. Since the improvement of using an adaptive winglet in terms of lift coefficient was higher than the improvement in terms of drag, the lift-to-drag results follow a similar trend as the lift results (Figure 3.9).

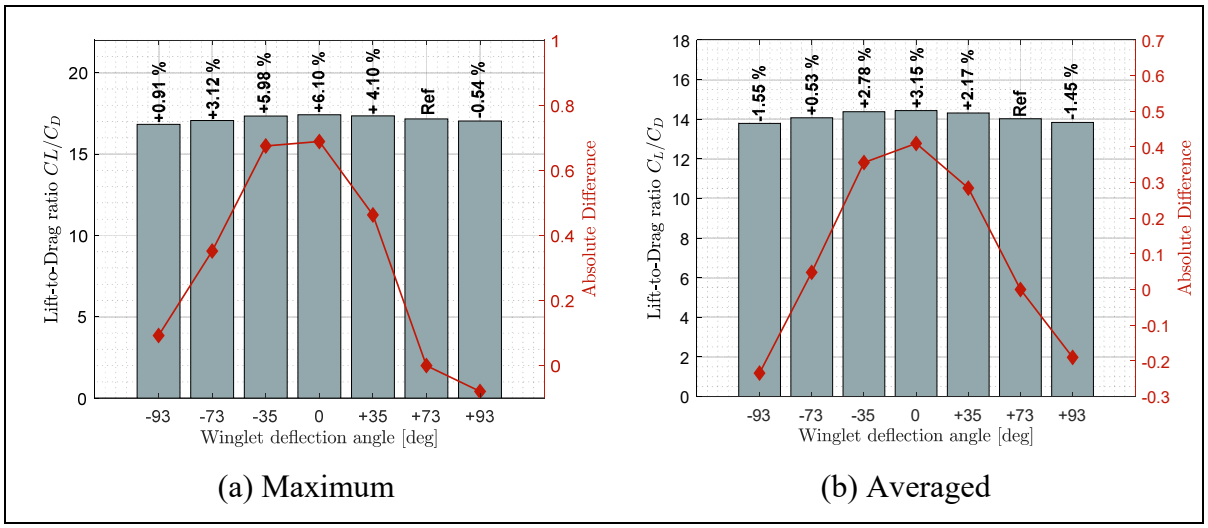

Figure 3.11 Maximum and averaged benefits observed on the lift-to-drag ratio for different winglet deflection angle and different flight conditions

By this way, on average, winglet deflection angles from ξ = -73 deg to +35 deg show a lift-to-drag increase (i.e., benefit) up to 3.15% (Figure 3.11 (b)). For specific flight condition, it was observed that the winglet position ξ = -93 deg could increase the lift-to-drag ratio up to 0.91% (Figure 3.11 (a)). Similarly, for specific flight conditions, other winglet deflection position could increase the lift-to-drag value by up to 6.10%.

Results shown on Figure 3.9 to Figure 3.11 have shown the advantage of using an adaptive winglet as different winglet deflection position could offer lift, drag or lift-to-drag ratio improvement with respect to the reference configuration of the aircraft. Generally, winglet positions $\xi = \pm$ 93 deg offered the "worst improvement", and in reverse, winglet positions ξ = -35 deg to ξ = +35 deg shows the best aerodynamic characteristics.

Most of the best improvements were corresponding to the winglet deflection position of ξ = 0 deg, which may affect the choice of using an "adaptive" winglet instead of a fixed one set at ξ = 0 deg. This result was expected as the position ξ = 0 deg is corresponding to the highest aspect ratio of the wing, and consequently it is the "ideal" position to increase the lift and reduce the induced drag. As a reminder, usually, the pilot needs to fly at different optimum criterion such as the maximum speed, the minimum flight time, etc., which are not necessarily

corresponding to an optimal aerodynamic criterion such as lift, drag or lift-to-drag ratio (all along the flight).

In this study, using aerodynamic criteria, we have shown that the adaptive winglet allows to improve aerodynamic characteristics for several flight conditions thanks to its adaptive aspect. Consequently, it could be expected that during the flight, the "optimal" winglet deflection position should be different from the $\xi = 0$ deg position as the optimal flight criteria should be based on aircraft performances instead of aerodynamic characteristics.

3.3.2 Comparison of the Characteristics of the CRJ700 Equipped with Fixed Versus Adaptive Winglets in Terms of Aerodynamic Polar and Pitching Moment

Based on the optimization criteria of the "maximum lift-to-drag ratio", the aerodynamic polar of the aircraft equipped with an adaptive winglet has been computed using polynomial interpolation shown on section 3.2.4.2. In this section, aerodynamic polar of the new and the reference configuration of the CRJ700 (fixed winglet) were compared for five Mach numbers representative of the flight envelope of the aircraft.

Moreover, effects observed on the pitching moment are displayed in this same subsection. The pitching moment behavior is fundamental because it affects the position of the horizontal tail necessary to trim the aircraft, the limits in the variation of the Center of Gravity (CG) to avoid commands saturation or poor stability, and the flight qualities. Consequently, it was important to analyze how the pitching moment change between the two configurations of the aircraft (fixed and adaptive winglet) in order to verify that the adaptive configuration maintains a certain stability.

The results obtained for Mach numbers 0.31, 0.45, 0.54, 0.66 and 0.79 are presented in Figure 3.12 to Figure 3.16, respectively. Each of these figures are divided into two subfigures (a) and (b). The sub-figures (a) show the comparison in terms of aerodynamic polar between a CRJ700

aircraft equipped with a fixed (in “black” color) versus an adaptive winglet (in “pink” color). Similarly, sub-figures (b) show the comparison of the fixed versus adaptive winglets’ results in terms of pitching moment coefficients versus lift coefficients.

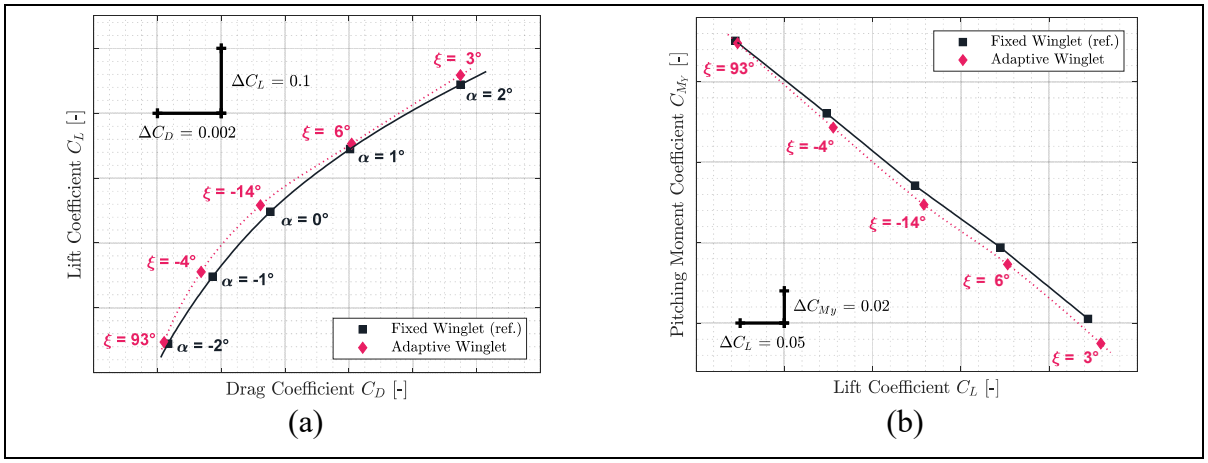

Figure 3.12 Aerodynamic polar (a) and pitching moment coefficient (b) comparison between a CRJ700 equipped with fixed and adaptive winglets at Mach number 0.31

It is important to add the fact that due to the discontinuous aspects of the adaptive winglet geometry (the winglet angle is changing during flight, according to the flight condition), it was preferred to first predict punctually aerodynamic coefficients and display them using “diamond” shapes markers. Then, between aerodynamic coefficients predicted, as the winglet angle could change due to the adaptive configuration, it was preferred to predict intermediate aerodynamic coefficients using spline equations and display it using “dotted” lines.

Globally, for each flight condition, it was observed in sub-figures (a) that the adaptive winglet allows the aircraft to reach an aerodynamic polar located at the left-hand side of the reference polar. Shifting the aerodynamic polar of an aircraft to the left signifies that the drag generated for a given lift has been reduced.

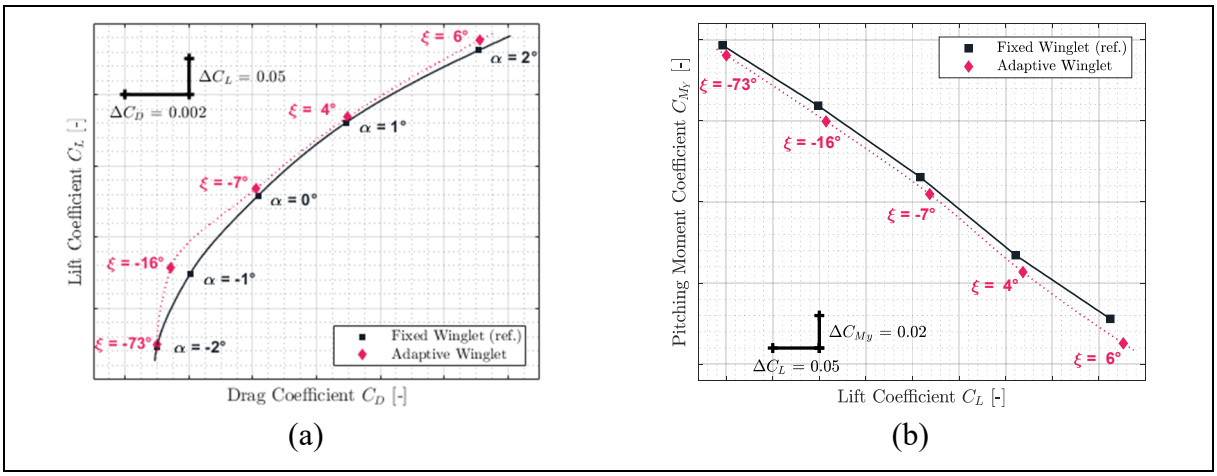

Figure 3.13 Aerodynamic polar (a) and pitching moment coefficient (b) comparison between a CRJ700 equipped with fixed and adaptive winglets at Mach number 0.45

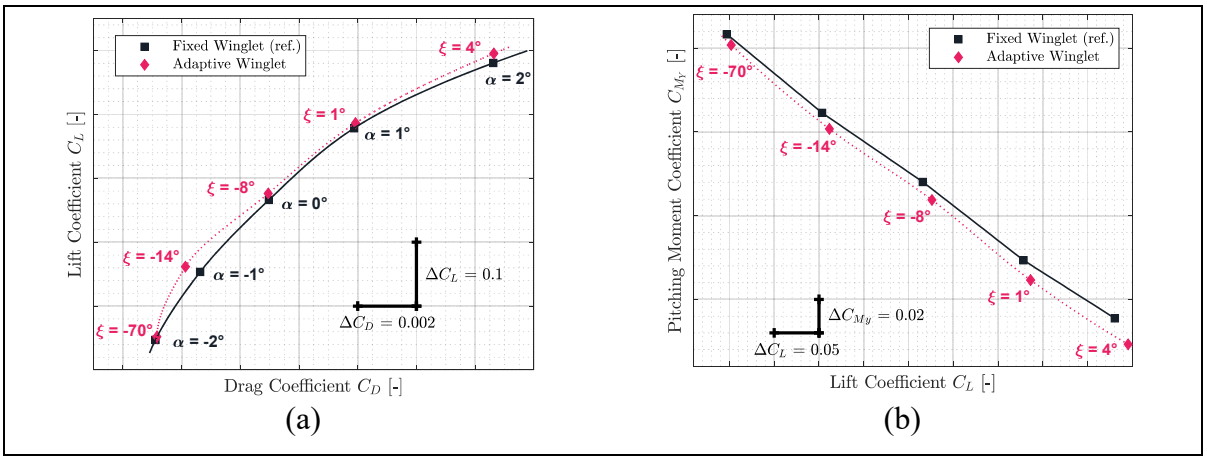

Figure 3.14 Aerodynamic polar (a) and pitching moment coefficient (b) comparison between a CRJ700 equipped with fixed and adaptive winglets at Mach number 0.54

Moreover, by selecting the best winglet deflection angle as the one that offered the maximum fitness to the aircraft, the pitching moment coefficient was impacted (sub-figures (b)). Indeed, it was observed that the pitching moment coefficients obtained by an aircraft equipped with an adaptive winglet were shifted to negative values (downside) with respect to their reference values (shown in “black” color).

As example, for Mach 0.31 on Figure 3.12 (a), the aerodynamic polar corresponding to the aircraft equipped with an adaptive winglet is located on the left-hand side of the aerodynamic

polar corresponding to the aircraft equipped with the fixed winglet. For angles of attack α of 1 deg and 2 deg, “pink” markers were located on the right-hand side of the reference marker (in “black”). This signifies that, locally, for a given angle of attack, the aircraft equipped with an adaptive winglet generates more drag than with a fixed winglet.

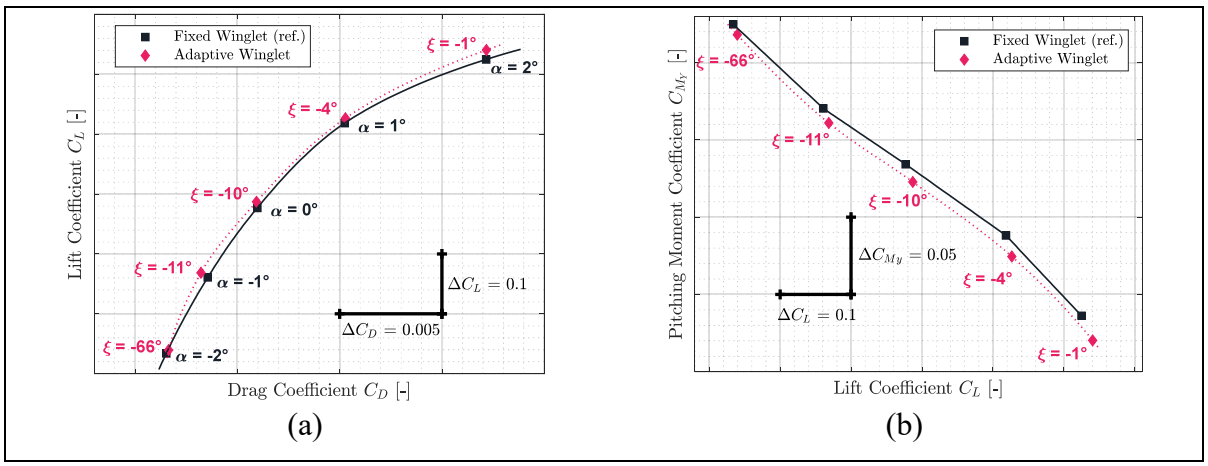

Figure 3.15 Aerodynamic polar (a) and pitching moment coefficient (b) comparison between a CRJ700 equipped with fixed and adaptive winglets at Mach number 0.66

However, for these angles of attack (1 deg and 2 deg), “pink” markers are also located upside of the reference markers. Consequently, while there is more drag generated by an aircraft equipped with an adaptive winglet, there is also more lift. Nevertheless, it is important to combine these two characteristics of lift and drag using an aerodynamic polar. Indeed, to fly an aircraft requires a given lift that depends essentially on its weight (the angle of attack is in fact a consequence and not a requirement to maintain a cap, or hold an altitude for example). The corresponding drag is deducted by the aerodynamic polar, according to the lift required.

From this interpretation, as the adaptive winglet polar is located on the top or on the left-hand side of the reference aerodynamic polar, it signifies that for a given lift required, the drag generated by the aircraft equipped with an adaptive winglet would be less than originally (i.e., aircraft equipped with a fixed winglet).

Figure 3.12 (b) shows that the pitching moment coefficient obtained for the adaptive winglet configuration is approximatively reduced by 0.0067 (from 0.0061 to 0.0074) with respect to the reference value.

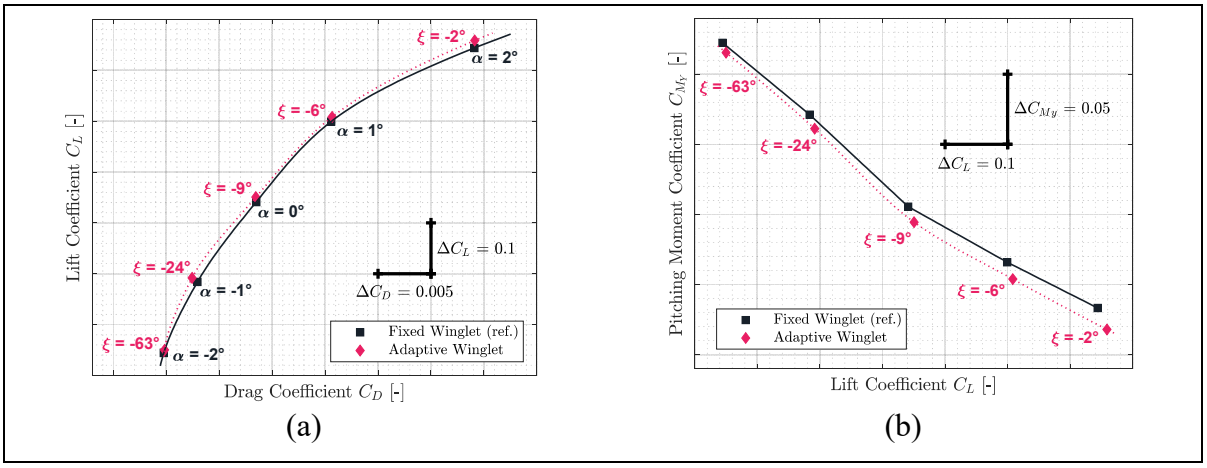

Figure 3.16 Aerodynamic polar (a) and pitching moment coefficient (b) comparison between a CRJ700 equipped with fixed and adaptive winglets at Mach number 0.79

From the stability point of view, original aircraft properties could be conserved. Indeed, since the slope of the pitching moment versus the lift coefficient for an adaptive winglet is similar to that of the reference, the aircraft's neutral point of stability (aft center of gravity) has been conserved. The only difference that could be noted concerns the fact that C_{M_y} at origin (C_{M_0}) has changed, which could affect the aircraft trim status; for instance, the trimmed angle of attack should be lower for the adaptive than for the reference configuration. There is a high probability (because the difference is small) that the C_{M_0} difference can be completely "corrected" by the trim operation or it would slightly increase the flight speed.

In the case where it could not be corrected by the trim operation, the fact that the C_{M_y} was shifted could have an impact on the static margin of the aircraft, and on the forward limit of its center of gravity. In this case, the slope of the pitching moment coefficient versus the angle of attack can be tuned using a change in the surface of the horizontal tail (or distance from the aerodynamic center). Indeed, the value of the pitching moment coefficient for zero angle of attack can be finely calibrated by acting on the settling angle of the horizontal tail. An increase

in the dimensions of the aircraft longitudinal control surfaces (stabilizers and/or elevators) leads to reduced control surfaces deflections to trim (or to an extension of the possible angle of attack range for which trimming is ensured).

Practically same observations made for Mach number 0.31 could be made for the other flight conditions evaluated for Mach numbers 0.45, 0.54, 0.66 and 0.79. Indeed, it could be observed that in Figure 3.13, Figure 3.14, Figure 3.15 and Figure 3.16 (a), the aerodynamic polar corresponding to the aircraft equipped with an adaptive winglet (in "pink" color) is located on the left-top hand side of the reference aerodynamic polar. Moreover, these aerodynamic polar were obtained with a winglet deflection angle that is almost located within the range ξ= -25 deg to ξ= 10 deg.

For α = -2 deg, the winglet position that offered the maximum lift-to-drag ratio is usually close to -73 deg, which is far from the other "optimal winglet deflection positions". This could be explained by the fact that aerodynamic coefficients C_L and C_D obtained for α = -2 deg are very close for each winglet deflection position. Polynomial fitting surfaces (displayed in section 3.2.4.2 for α = 0 deg) obtained for α = -2 deg were relatively "flat" according to the winglet deflection angle axis. Indeed, if the winglet deflection was "forced" to another position, similar results could have been observed (this fact was only observed for α = -2 deg).

3.3.3 Drag Improvement Summary

A last results section has been added in order to highlight the drag reduction permitted using the adaptive winglet with respect to the fixed winglet (reference). In other words, the difference in terms of drag was computed between aerodynamic polar of the two aircraft configurations (fixed and adaptive winglet) and was displayed on Figure 3.17.

The drag absolute (Figure 3.17 (a)) and relative (Figure 3.17 (b)) differences were shown using blue bars while the "normal" distribution of the differences was displayed using red curves.

These results were obtained for the 25 flight conditions that were used to display the aerodynamic polar on Figure 3.12 (a) to Figure 3.16 (a).

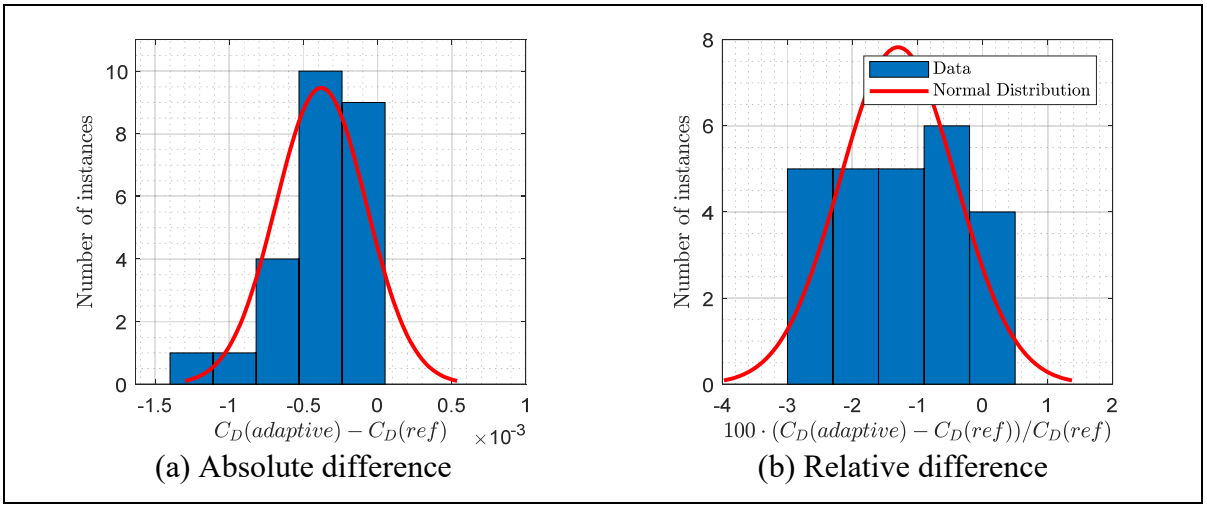

Figure 3.17 Drag benefits observed between the new aerodynamic polar (adaptive winglet) and the reference polar (fixed winglet)

Figure 3.17 (a) shows that using an adaptive winglet, the drag coefficient could be reduced by up to 0.0015. In 95% of cases, the drag coefficient has been reduced by 0.00038±0.00031, which is corresponding to a reduction of -1.30 ± 0.89 % using relative values. Moreover, Figure 3.17 (b) shows that the adaptive winglet allows to reduce the drag by up to 2.90% for several flight conditions. These encouraging results confirms that using an adaptive winglet allow to reduce the drag generated and therefore improve aerodynamic characteristics of the aircraft. As a result, a fuel burn reduction is also expected for future performance studies.

3.3.4 Evolution of the Winglet Position during a Generic Cruise Profile

In order to highlight the motion of the adaptive winglet during cruises, the best winglet deflections angles for three optimization criteria: the maximum lift coefficient, the minimum drag coefficient and the maximum lift to drag ratio. These optimum winglet deflections angles were found for two typical cruise profiles at Mach number 0.50 (low-speed), and Mach number 0.75 (high-speed).

Results obtained for a low speed cruise profile (Mach number 0.50) have been exposed in Figure 3.18 (a), (b) and (c). It was considered that at Mach number 0.50, due to the weight reduction during the flight, the angle of attack should change from 4 deg to 1 deg. On Figure 3.18 (a), it could be observed that the maximum lift coefficient is obtained when the winglet is varying between -11 and -23 degrees. On Figure 3.18 (b), the minimum of drag coefficient have been obtained for winglet deflection angles from 41 to 72 deg. This range of winglet position obtained for a "minimum drag" criterion is as large as for a "maximum lift" criterion. Finally, for an optimal criterion based on the lift to drag ratio, it could be observed on Figure 3.18 (c) that the maximum fitness was obtained for a winglet position between 16 and 18 degrees, which is close to 0 deg.

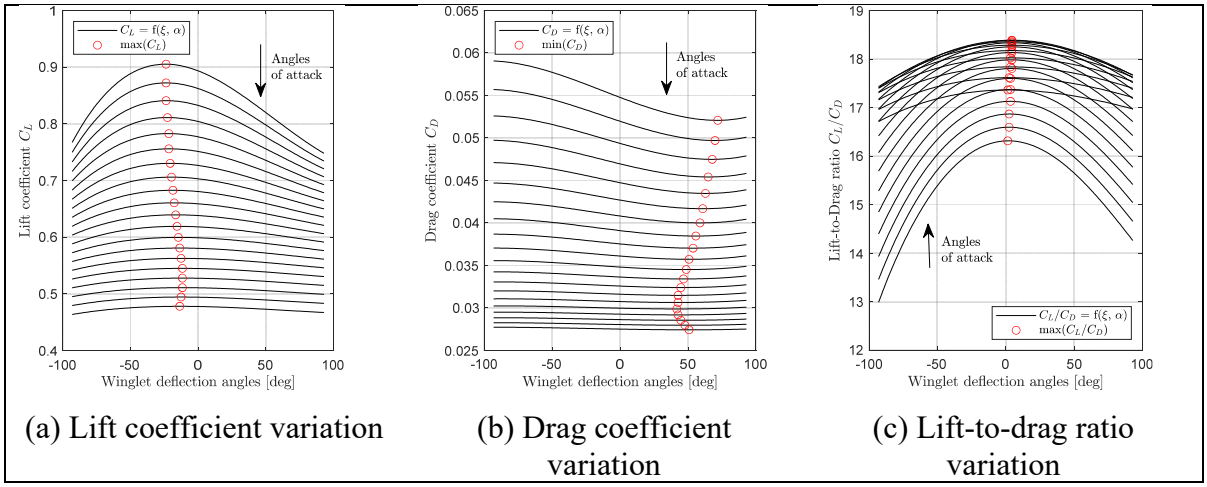

(a) Lift coefficient variation (b) Drag coefficient variation (c) Lift-to-drag ratio variation

Figure 3.18 Aerodynamic characteristics variation during a generic cruise mission at Mach number 0.5 (angle of attack variation from 4 deg to 1 deg)

From these observations, it could be concluded that for a low speed cruise profile at Mach number 0.50, a winglet deflection motion from 16 to 18 degree is required to fly using the maximum lift-to-drag criterion. If the minimum drag coefficient is preferred to optimized the cruise, the winglet deflection angle should be moved from 41 to 72 deg.

The similar study was conducted for a typical cruise profile at Mach number 0.75. In this case, due to the fuel burn during the flight and therefore the weight reduction induced, it was considered that the angle of attack varying from 1 deg to -1 deg during this profile. Results that

were obtained in terms of lift, drag and pitching moment coefficients were displayed in Figure 3.19 (a), (b) and (c).

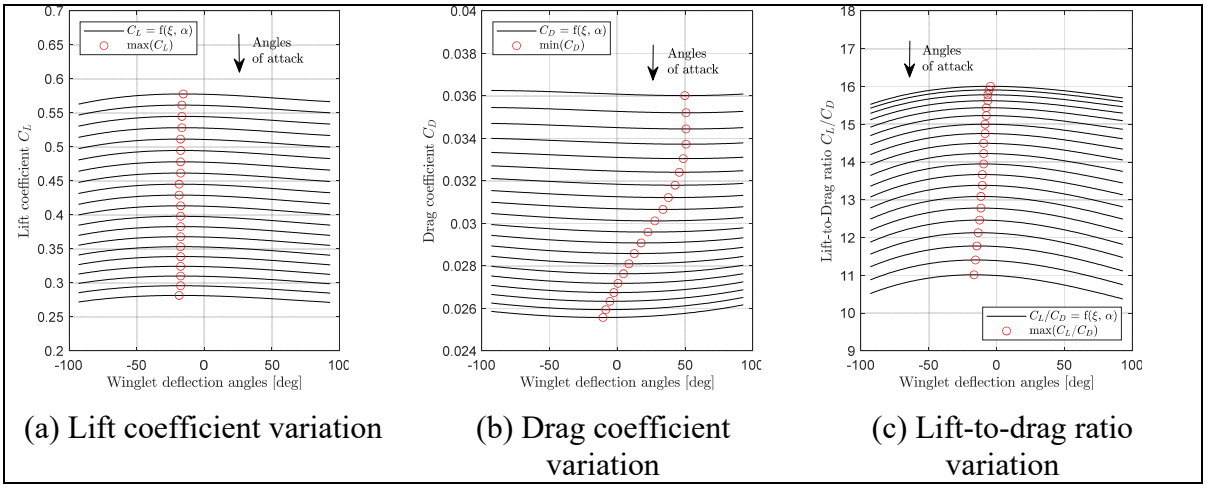

(a) Lift coefficient variation (b) Drag coefficient variation (c) Lift-to-drag ratio variation

Figure 3.19 Aerodynamic characteristics variation during a generic cruise mission at Mach number 0.75 (angle of attack variation from 1 deg to -1 deg)

From Figure 3.19 (a) it was observed that the winglet needs to remain close to -15 degrees along the flight in order to offer the maximum lift coefficient. However, it needs to move from -10 deg to 50 deg in order to offer the minimum drag coefficient along the flight (Figure 3.19 (b)). Finally, to optimize the lift to drag ratio of the aircraft, the winglet deflection angles need to move from -16 to -4 degrees, which is very close to degrees (Figure 3.19 (c)).

More generally, by observing the general trend of curves it could be supposed that the winglet position has a higher influence for low speed cruises (Figure 3.18) than for high speed cruises (Figure 3.19). Indeed, the curves shown in Figure 3.19 are flatter than those observed in Figure 3.18. It signifies that aerodynamic coefficients are very close, regardless of the winglet position. From this fact, it is expected that using an adaptive winglet, a higher improvement is achieved at low speed than at high speed

3.4 Conclusion

The research presented here is a part of a larger project on the way in which an adaptive winglet can improve aircraft performance during flight. This paper has presented the aerodynamic aspects of the study applied on the Bombardier Regional Jet CRJ700.

An adaptive winglet that has only one degree of freedom was designed from a Computer-Aided-Design (CAD) model of the original CRJ700 aircraft. The adaptive winglet can move from deflection angles ξ = -93 deg to ξ = +93 deg measured from the ground and the winglet planform.

To compute the lift, drag and pitching moment coefficients of this new aircraft design, a high-fidelity aerodynamic model designed using OpenFoam tools and validated using a highly qualified flight simulator (level D) was used (Marine Segui, Abel, et al., 2021a).

A wide range of winglet deflection angles were simulated for the most commonly used flight conditions of this aircraft (i.e., for Mach numbers 0.31 to 0.79). Very promising results were obtained; for instance, the lift-over-drag ratio (i.e., the fitness) was increased by up to 6.10% by moving the winglet from -35 deg to 35 deg on the entire aircraft flight envelope.

Using fitting polynomial surfaces, it was possible to compare aerodynamic polar of both aircraft configurations, based on the maximum lift-to-drag ratio optimization criterion. It was observed that the aerodynamic polar of the Bombardier CRJ700 equipped with an adaptive winglet were always located on the left-hand-side of the original aerodynamic polar. This fact indicates that for a given lift coefficient required by the aircraft trim, the generated drag would be reduced. The drag reduction was predicted using a last study which demonstrated an averaged drag reduction of 1.30 ± 0.89 %.

With these promising results, it will be interesting to realize performance studies of this aircraft equipped with adaptive winglets and verify how much fuel could be saved for typical flight

profiles. It would also be interesting to investigate the benefits that could be gained by using the adaptive winglet di-symmetrically from one side to the other of the aircraft, for example, during a turn. An evaluation of the size and power of the actuation system of the adaptive wings, and additional components weight could contribute to assess the usefulness of the concept here developed. Finally, an optimization design of the junction (i.e., the “pod”) and aeroelastic studies should be conducted in future studies as they were not considered into this paper due to a lack of structural data. However, it is expected that it should improve the results observed.

On another hand, it should be interesting to conduct a cost study especially concerning the weight penalty induced by the adaptive mechanism, as well as the maximum fuel consumption that could be induced in case of a winglet motion failure.

In spite of the maintenance costs that could be induced by such a system, the authors would like to conclude that this adaptive winglet system is very interesting for an aircraft. For this purpose, we would like to take the example of the new generation of aircraft, equipped with oversized wingspan, requiring a foldable wingtip to reach the airport facilities (such as the 777-9x). Indeed, since these aircrafts will in all cases be equipped with a mechanism to allow wingtip movement, the added maintenance costs to make it move during flight are minimal compared to the aerodynamic performance improvements provided.

CHAPTER 4

PERFORMANCES IMPROVEMENT OF THE REGIONAL JET CRJ700 AIRCRAFT EQUIPPED WITH ADAPTIVE WINGLETS

Marine Segui [a] and Ruxandra Mihaela Botez [b]

[a, b] Department of System Engineering, École de Technologie Supérieure,
1100 Notre-Dame West, Montréal, Québec, Canada H3C 1K3

Paper published in *AIAA Journal of Aerospace Information Systems*, June 2022.
DOI: https://doi.org/10.2514/1.I011099

Résumé

Cette recherche s'inscrit dans la continuité d'une étude qui consistait à analyser les performances aérodynamiques d'un avion équipé d'ailettes adaptatives (*winglets*) par rapport à un avion équipé d'ailettes fixes. En se basant sur les méthodes RANS (Reynold-Averaged Navier-Stokes), il a été observé que les ailettes adaptatives permettent au CRJ700 de réduire sa traînée jusqu'à 2,90% (Marine Segui, Abel, Botez, & Ceruti, 2021b ; Marine Segui, Botez, Abel, & Ceruti, 2021). À partir de ces résultats aérodynamiques, la recherche consiste maintenant à analyser les gains de performance en montée et en croisière obtenus par un avion équipé d'ailettes adaptatives. La méthodologie présentée dans cet article détaille les modèles aérodynamiques et de performance utilisés pour obtenir ces nouveaux résultats. Une nouvelle méthodologie pour calculer l'angle de déflexion du *downwash* à partir de simulations OpenFoam a également été développée. Les résultats montrent qu'une ailette adaptative peut réduire le débit de carburant d'un avion jusqu'à 1,99% en croisière par rapport à un avion équipé d'une ailette fixe. Des avantages intéressants ont également été trouvés pour les segments de montée, tels qu'une réduction du temps de montée allant jusqu'à 128,11 secondes.

Abstract

This research follows a previous study which consisted in analyzing the aerodynamic performance of an aircraft equipped with adaptive winglets compared to an aircraft equipped with fixed winglets. Based on Reynold-Averaged Navier-Stokes (RANS) methods, it was observed that adaptive winglets help the CRJ700 to reduce its drag by up to 2.90% (Marine Segui, Abel, et al., 2021b ; Marine Segui, Botez, et al., 2021). Using these aerodynamic results, this research now involves analyzing the climb and cruise performance benefits achieved by an aircraft equipped with adaptive winglets. The methodology presented in this paper details the aerodynamic and performance models used to obtain these new results. A new methodology for calculating the downwash deflection angle from OpenFoam simulations was also developed. The results show that an adaptive winglet can reduce the fuel flow of an aircraft by up to 1.99% in cruise with respect to an aircraft equipped with a fixed winglet. Interesting benefits were also found for climb segments, such as a climb time reduction of up to 128.11 seconds.

4.1 Introduction

This study is part of the development of an improved aircraft design needed to increase its efficiency and thus reduce its carbon footprint. Indeed, the International Civil Aviation Organization (ICAO) has committed to achieve a reduction of carbon dioxide (CO2) emissions by 50% from 2005 levels by 2050 (International Civil Aviation Organization (ICAO), 2010). This measure was subsequently supported by the Carbon Offsetting and Reduction Scheme for International Aviation (CORSIA) program in January 2019 by obliging the polluting actors to "compensate" the planet for their pollution (ICAO, 2018). Faced with the challenge of these two measures, aerospace engineers have launched themselves towards the design and the development of the least polluting aircraft.

4.1.1 Aircraft Improvement

The research efforts are mainly oriented towards a change in the type of motorization, essentially from fuel to electric or hydrogen. This change will make these new motorized aircraft completely different, while the certification process would be complex and very long. While this new generation of aircraft appears to be a very good strategy to limit air pollution in a long-term vision, finding shorter-term solutions is of utmost importance.

Shorter-term solutions could be provided via improvements applied to existing aircraft. This process could allow aircraft trajectories design and/or control procedures to be improved, thereby reducing the amount of fuel burnt during a complete flight (B. Dancila & Botez, 2018 ; R. Dancila & Botez, 2019 ; Murrieta-Mendoza, Beuze, Ternisien, & Botez, 2017 ; Murrieta-Mendoza & Botez, 2020 ; Murrieta-Mendoza, Ternisien, et al., 2018). For instance, up to 7.44% of the fuel cost can be saved using a 4D trajectory prediction (Murrieta-Mendoza, 2017).

In another approach for improving flight costs and reducing greenhouse gas emissions, some parts of an aircraft, such as winglets, could be replaced by more efficient ones. Among the geometry-based improvements of winglets, Whitcomb's contributions, which improve the cruise efficiency of a National Aeronautics and Space Administration (NASA) test aircraft from 6% to 9% (Freestone, 1988), are impressive. Since the publication of his work, aircraft designers (i.e., Airbus, Boeing, Bombardier, etc.) have followed strategies focused on winglet shapes design and have developed blended, fences, split-scimitar, raked, and other types of winglet shapes (Heathers, 2002 ; Hitchens, 2015 ; The Boeing Company, 2009 ; United Airlines, 2014). Indeed, the behavior of the air around the winglet is very complex, given its high level of turbulence generated (Anderson, 2017b ; Haddad, 2015). As a result, to reduce the induced drag generated by turbulence, there are multiple convenient shapes for a given aircraft as the most convenient shape depends on the flight condition.

Several studies have shown that aircraft wings with a high aspect ratio lead to the best aerodynamic performances. However, the wing aspect ratio is limited by airport gate size. A

particularly interesting solution would be to move the winglet during the flight, so that it would make the aircraft as efficient as possible for each flight condition encountered. During ground phases, the winglet could be folded, as proposed by Boeing for its latest version of the Boeing 777x, which had its first flight on January 2020 (Boeing, 2013 ; Federal Aviation Administration, 2018).

Studies seeking to imitate the flight of birds by equipping aircraft with changing shapes surfaces, usually called “Morphing-Wings”, have led to important improvements (Ameduri & Concilio, 2020 ; SARISTU (Project), Final Conference, & Papadopoulos, 2016). Some adaptive structures have already shown their efficiency, such as adaptive wing airfoil, tips, winglets, leading and trailing edges, flaps or horizontal tails. To give some examples, wing airfoil shape improvements have allowed to reduce the wing drag by up to 14% based on CFD aerodynamic calculations (R. M. Botez et al., 2018 ; Koreanschi, Sugar Gabor, & Botez, 2016c ; Sugar Gabor et al., 2014). Similarly, adaptive work targeted on trailing edges improvement has demonstrated that it was possible to replace an aileron by a morphing surface and validated with wind tunnel data (Communier et al., 2019). Aerodynamic improvements were also obtained using adaptive wing flaps, developed for a regional aircraft. Indeed, a research team has found interesting results in terms of increased lift-to-drag ratio and drag reduction by equipping adaptive wing flaps on regional aircraft, while considering structural aspects of the wing (Pecora, 2021 ; Pecora, Amoroso, Amendola, & Concilio, 2014). Another original study applied on the Cessna Citation X business jet has shown that an adaptive horizontal tail could reduce its fuel consumption by up to 100 lb per hour during cruise segments based on Vortex Lattice Method (VLM) calculations and a performance model of the aircraft validated using flight simulator data (Marine Segui, 2018 ; Marine Segui, Mantilla, Ghazi, et al., 2018).

The literature offers many aircraft improvements thanks to moveable surfaces, which justify that using moveable surface could be an interesting solution to improve existing aircraft performances. It has been shown that the moveable system could be applied to several parts of the aircraft (wing, horizontal tail, flaps, and trailing edges), however those applied to the

winglet and wingtip should be easier to implement from a manufacturing point of view. The following section presents the corresponding literature review in more details.

4.1.2 Literature Review: Aircraft Equipped with Moveable Wingtips

Even if adaptive design focusing on the wingtip research started many decades ago (e.g., Mak-10 research aircraft in 1931), research in this field is still limited (P. Bourdin, Gatto, & Friswell, 2008 ; Patrick Bourdin, Gatto, & Friswell, 2006 ; Guerrero, Sanguineti, & Wittkowski, 2020 ; Panagiotou, Efthymiadis, Mitridis, & Yakinthos, 2018 ; D. D. Smith, Lowenberg, Jones, & Friswell, 2014 ; Ursache, Melin, Isikveren, & Friswell, 2007). Very interesting projects assessed the advantages of inflight-controllable winglets, as well as those that aimed to conduct free motion winglet research with the aim to reduce the wing load. Each of these concepts offered significant advantages.

One of the most advanced studies evaluating winglets that are free to rotate on themselves during flight is presented in the Airbus AlbatrossONE project (Wilson, 2019). Flight tests conducted in 2019 with the Airbus Albatross ONE demonstrator gave some interesting benefits, including a lower hinge moment at the wing root during gusts. By bending the whole wing less in gusty winds (thanks to free winglets), researchers believe they can achieve an 8% to 9% reduction in fuel consumption compared to that of the aircraft with a conventional fixed wingtip (Castrichini et al., 2017 ; Cheung et al., 2018). In addition, by use of less load, the wing structure could be lightened, which would result in a significant reduction of the aircraft's empty weight (which is connected to lift, induced drag and therefore to fuel consumption). This free-folding wingtip concept has also led to some advantages in roll performance, another interesting aspect offered by this system (Healy et al., 2021).

From 2011 to 2017, the European consortium "Smart Intelligent Aircraft Structures" (SARISTU) included improvement research projects on winglets. SARISTU was one of the largest European programs dedicated to study morphing systems applied to aeronautics, with the goal of enhancing existing air fleets (Gianluca Amendola et al., 2017 ; Concilio et al.,

2021). An adaptive winglet was developed and applied on a regional aircraft (the TP90, used for Clean Sky 2 projects) in the Adaptive Trailing Edge Device (ATED) research project (Carossa et al., 2016 ; Cedric Liauzun et al., 2018). This adaptive winglet had a “finger-like” mechanism; the main part of the winglet was considered as fixed, while its trailing edge was moveable during flight. Performance studies have shown that this system could reduce drag by up to 3% in climb conditions. It was also estimated that the moveable part of the winglet could be used as a control surface of the aircraft and it could directly influence lift coefficient values. As part of determining the limits of this approach, a structural analysis demonstrated that a maximum weight of 50 kg should be added to the aircraft when integrating this new system, which could be a disadvantage for small aircraft (Dimino et al., 2021).

NASA and Boeing collaborated on a project to control winglets during flight in an effort to improve aircraft performance (Ortiz & Alley, 2018). Entitled “Spanwise Adaptive Wing” (SAW), this project tested a wing that folded spanwise during flight. Flight tests performed using the Prototype-Technology Evaluation and Research Aircraft PTERA in 2017 showed that the optimal positions (i.e., angles) of the winglet were located between -15 deg and +15 deg (angle measured between the winglet platform and the ground) while the dihedral angle was tested from -75 deg to +75 deg. Subsequent dynamic studies have shown that some changes could happen in roll damping dynamic, but no changes appeared concerning the original yaw damping or longitudinal stability (M. S. Smith et al., 2018).

Based on the bibliographical research that was presented in the previous Section 4.1.1 and Section 4.1.2, the objectives of this research will be specified in the following section.

4.1.3 Project and Paper Objectives

In our effort to improve civil aircraft performance using morphing wing principles, this research aims to compute the inflight performance gains that can be achieved by an aircraft equipped with adaptive winglets.

Since aircraft design based on morphing-wing principles has been able to realize important flight performance improvements, we wonder how effective an aircraft such as the Boeing 777x could be if it was possible to mechanically adapt its wingtips (or the winglets) in-flight to a desired position (between unfolded and folded). The Boeing 777x is already equipped with a folding wingtip, capable of moving to two positions: "unfolded" and "folded"; therefore, it is assumed that no significant weight would need to be added for the wingtip control mechanism, as it is already installed in the aircraft (additional actuators or sensors were considered negligible compared to the weight of the overall mechanism).

This study was evaluated on the CRJ700 aircraft, as a large and accurate flight dynamics and aerodynamics dataset for this aircraft is available at the Laboratory of Active Controls, Avionics and AeroServoElasticity (LARCASE). An adaptive winglet was designed and then adapted to the CRJ700 Regional Jet. An adaptive winglet is a winglet that would be able to move during flight in order to be in a position that is always its "ideal" position. The "ideal" criterion may change depending on the phase of flight (i.e., climb, cruise, descent, or takeoff) or the operator's requirements (need to reduce fuel consumption, flight time, maximize payload, etc.). Figure 4.1 shows the adaptive winglet design for the CRJ700.

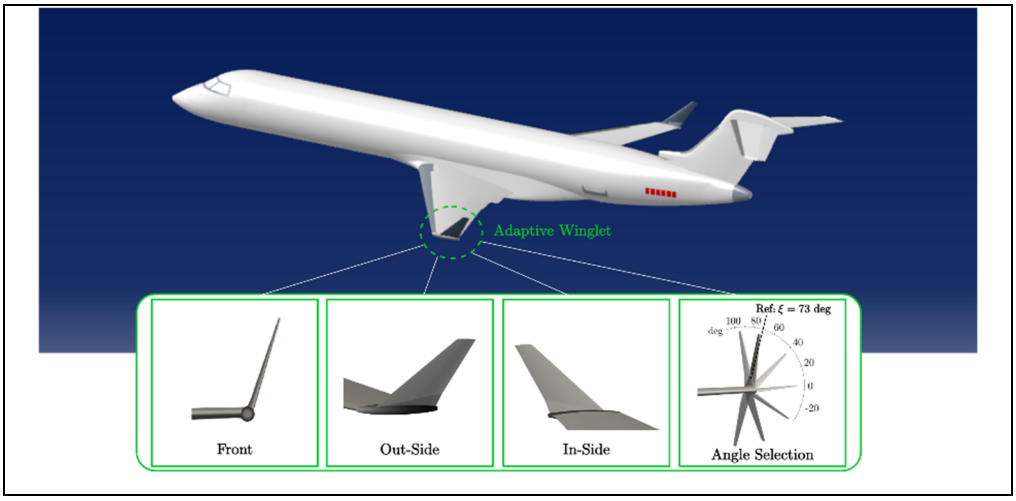

Figure 4.1 Adaptive winglet design for the CRJ700

The adaptive winglet developed moves by an angle ξ from -93 deg to +93 deg, between the winglet platform and the ground. For its integration, the aircraft design was kept in its initial geometry and modified only at the wingtip by including a “pod” (Marine Segui, Abel, et al., 2021b ; Marine Segui, Botez, et al., 2021). Therefore, to compute its benefits, the adaptive winglet set at 73 degrees was considered as the baseline configuration. Using an aerodynamic model based on CFD principles (M. Segui, Abel, Botez, & Ceruti, 2021), many advantages from an aerodynamic perspective were found (Marine Segui, Abel, et al., 2021b ; Marine Segui, Botez, et al., 2021). Depending on the optimization criteria, an adaptive winglet improved the lift-to-drag ratio by up to 6.10%, or reduced the drag coefficient by up to 2.90% (if the lift coefficient remained constant) (Marine Segui, Abel, et al., 2021b ; Marine Segui, Botez, et al., 2021). While the adaptive winglet was varied from -93 deg to +93 deg, its most efficient positions were found for -35 deg to +35 deg. These results were obtained for several flight conditions, for which the Mach numbers ranged from 0.31 to 0.79 and the angle of attack from -2 to 4 deg (Marine Segui, Abel, et al., 2021b).

Based on the promising results obtained during the above-mentioned aerodynamic studies (Marine Segui, Abel, et al., 2021b ; Marine Segui, Botez, et al., 2021), it was decided to continue these studies and to measure the benefits in terms of climb and cruise performances, that an aircraft equipped with an adaptive winglet could achieve. These studies will allow the flight performances of an aircraft equipped with an adaptive winglet system to be estimated in terms of its range, fuel consumption and climb performance.

4.2 Methodology

The methodology utilized to compute the cruise and climb performances of an aircraft equipped with adaptive winglets is outlined here. A mathematical model of the aircraft, composed of an aerodynamic model and an engine model, was used to compute its in-flight performance. The mathematical model considers a “static” aircraft state, estimated at several positions along a flight. Consequently, the aircraft forces were computed “statically”.

Since the study aims to highlight the aircraft's performance improvement using an adaptive winglet (an exclusively aerodynamic modification), the engine data of the CRJ700 remain the same for the simulations of the adaptive and the fixed winglet. The aerodynamic model is presented next in the first sub-section (Section 4.2.1), followed by the performance (mathematical) model in the second section (Section 4.2.2).

4.2.1 Presentation of the Aerodynamic Model

Aerodynamic forces L, D and moment M_y applied on a designated aircraft can be computed from the aerodynamic lift C_{L_S}, drag C_{D_S} and pitching moment C_{M_S} coefficients using Eqs. (4.1), (4.2) and (4.3), where ρ is the air density, *S* is the reference wing area, *V* is the True Air Speed (TAS), $\bar{c}$ is the Mean Aerodynamic Chord (MAC), α is the angle of attack, and *M* is the Mach number.

$$L = 0.5\,\rho.\mathrm{S}.\mathrm{V}^2.C_{L_s}(\alpha, M, \delta_{\mathrm{stab}}, \delta_{\mathrm{elev}}) \tag{4.1}$$

$$D = 0.5\,\rho.\mathrm{S}.\mathrm{V}^2.C_{D_s}(\alpha, M, \delta_{\mathrm{stab}}, \delta_{\mathrm{elev}}) \tag{4.2}$$

$$M_y = 0.5\,\rho.\mathrm{S}.\mathrm{V}^2.\bar{c}\,.C_{M_s}(\alpha, M, \delta_{\mathrm{stab}}, \delta_{\mathrm{elev}}) \tag{4.3}$$

The aerodynamic coefficients (C_{L_S}, C_{D_S} and C_{M_S}) depend upon the flight conditions (angles of attack α and Mach number M) and the longitudinal control surfaces deflections angles (stabilizer δ_{stab} and elevators δ_{elev}). As low-speed maneuvers such as take-off and landing are not considered here, flaps and slats are assumed to be retracted. Moreover, only the control surfaces used during longitudinal flight were considered, and therefore, the rudder, ailerons and the spoiler deflections were excluded.

The Navier-Stokes (NS) equations resolution method is considered as the most accurate to numerically compute aerodynamic forces applied on an aircraft. However, this high-fidelity method is very costly, as the computations require a specific computer memory configuration and takes a very long time to be performed. To analyze the aerodynamic characteristics of an

aircraft equipped with an adaptive winglet using high-fidelity methods requires a significant amount of resources (Cédric Liauzun, 2006b ; Cedric Liauzun et al., 2018).

To minimize the computational cost, a specific aerodynamic model was developed in a previous research using medium-mesh qualities and low computational resources (8 cores and 64GB RAM memory) (M. Segui et al., 2021). Based on these aspects, and on the fact that static aerodynamic study was required, Reynold-Averaged Navier-Stokes (RANS) methodology was preferred.

Then, to smooth the integration of the aerodynamic model into the mathematical model of the aircraft (presented in the Section 4.2.2), the aerodynamic contributions of the *wing-body* (*wb*) (i.e., the wing, fuselage and vertical tail) and the *horizontal-tail* (*ht*) (i.e., the horizontal tail including the stabilizer) must be entered independently.

Simulating different flow conditions for several winglet deflection positions to assess the different contributions of the *wb* and the *ht* configurations would require a huge investment in computation time. In order to perform computations with minimal costs, the methodology was developed in order to minimizing the number of simulations. For this purpose, global aerodynamic coefficients (C_{L_s}, C_{D_s} and C_{M_s}) where computed using an aerodynamic model presented in the subsection 1. Then the methodology has consisted in separating aerodynamic contributions applied on the *wing-body* from those applied on the *horizontal-tail* using Eqs. (4.4) to (4.6).

$$C_{L_s} = C_{L(wb)} + \frac{S_{ht}}{S_{wb}}\left[C_{L(ht)}.\cos(\varepsilon) - C_{D(ht)}.\sin(\varepsilon)\right] \quad (4.4)$$

$$C_{D_s} = C_{D(wb)} + \frac{S_{ht}}{S_{wb}}\left[C_{D(ht)}.\cos(\varepsilon) - C_{L(ht)}.\sin(\varepsilon)\right] \quad (4.5)$$

$$C_{M_s} = C_{M(wb)} + \frac{S_{ht}.z_{ht}}{S_{wb}.\bar{c}}\left[C_{D(ht)}.\cos(\varepsilon) - C_{L(ht)}.\sin(\varepsilon)\right] - \frac{S_{ht}.x_{ht}}{S_{wb}.\bar{c}}\left[C_{L(ht)}.\cos(\varepsilon) + C_{D(ht)}.\sin(\varepsilon)\right] \quad (4.6)$$

where S_{wb} and S_{ht} designate the reference areas of the wing and horizontal tail, respectively. Subscripts wb, ht and s refer to the *wing-body*, *horizontal-tail* and global aircraft aerodynamic contributions in the *stability* axis, respectively. Lengths x_{ht} and z_{ht} are the Cartesian projections of the distance between the aerodynamic center of the wing and the horizontal tail. Finally, ε defines the downwash angle.

The downwash angle represents the deviation angle of the flow induced by the wing. Indeed, the flow angle interacting with the wing is usually called the angle of attack α; however, by passing through the wing, the flow is deviated by a downwash angle ε. The downwash angle depends upon the *wing-body* geometry, and therefore the horizontal tail interacts with the flow by an angle of $\alpha - \varepsilon + \delta_{\text{stab}}$ (δ_{stab} is the stabilizer platform angle with respect to the body line). To distinguish the *wb* of the *ht* contributions, the downwash deviation angle must be calculated.

Therefore, after computing global aerodynamic coefficient (presented in subsection 4.2.1.1), the downwash estimation methodology was developed in subsection 4.2.1.2 and finally the subsection 4.2.1.3 explains the methodology used to separate aerodynamic contributions applied on the *wing-body* from those applied on the *horizontal-tail*.

4.2.1.1 Computation of global aerodynamic coefficients

A high-fidelity aerodynamic model of the Bombardier CRJ700 was designed by us using OpenFoam toolbox. This model was designed to compute the aerodynamic forces and moments of the CRJ700 Regional Jet equipped either with its original winglet or with the new adaptive winglet. An illustration of the model is shown in Figure 4.2. It is important to notice

that different choices have been made to develop the aerodynamic model, and all of them have been presented in details in (M. Segui et al., 2021). In order to remain consistent in the methodology, it was preferred to present the aerodynamic model as concisely as possible. Therefore, the reader is invited to consult the reference (M. Segui et al., 2021) for further details concerning the aerodynamic model.

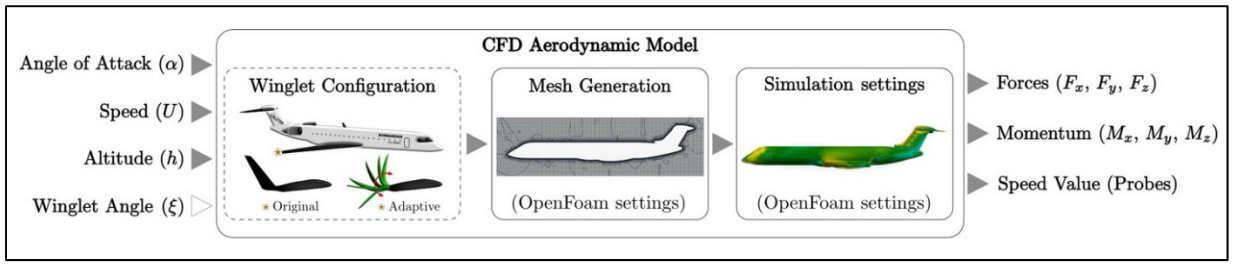

Figure 4.2 CRJ700 CFD Aerodynamic Model developed using OpenFoam toolbox

Meshes were designed using *blockMesh* and *snappyHexaMesh* OpenFoam utilities. The domain dimensions used to design the model are indicated in Figure 4.3. It is important to add that it was preferred to rotate the aircraft instead of the flow to simulate a different angle of attack; as a consequence of this, it was necessary to define a different mesh for each angle of attack (M. Segui et al., 2021, p. 700). In addition, one mesh was designed per winglet deflection angle because of the geometric modification. In an effort to limit the aerodynamic computations, seven winglet deflections angles {-93, -73, -35, 0, 35, 73 and 93 deg} were considered. On average, the meshes have 11.14×10^6 cells. It would be important to specify that to model the motors, a large number of cells is necessary to keep the simulations stable. Therefore, in order to keep the mesh as light as possible, the motors have not been considered in aerodynamic simulations.

Based on several observations made during the aerodynamic model design, a specific methodology was developed to reach stable and robust flow simulations for the CRJ700 aircraft, more explanations were provided in (M. Segui et al., 2021). Stable and robust flow simulations were targeted as the flow solutions needed to converge for several aircraft geometry variations (different winglet cant angles).

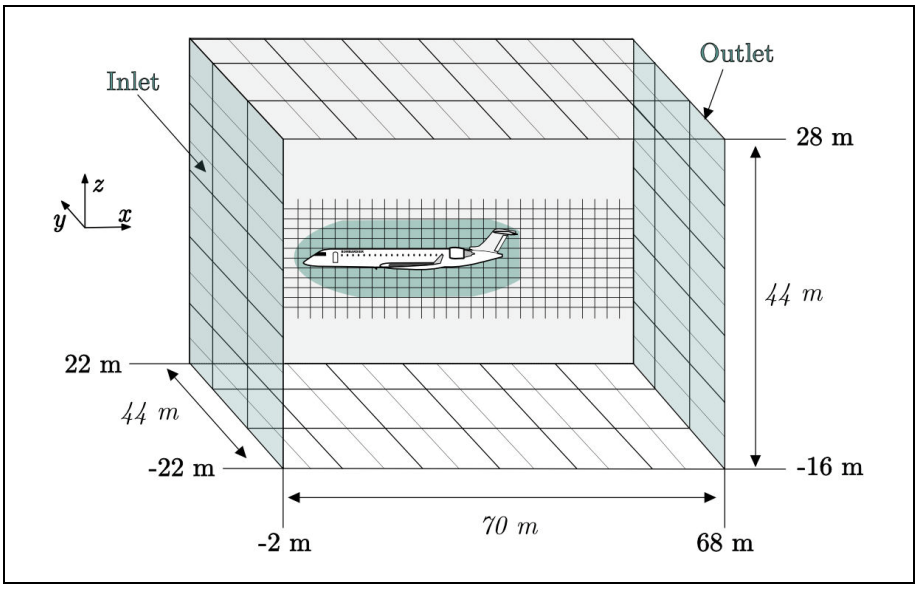

Figure 4.3 Drawing of the CFD Aerodynamic Model mesh domain

The aerodynamic model has been designed using two successive simulations, the first simulation used an incompressible solver *simpleFoam* and the second simulation used the compressible solver *rhoSimpleFoam*. The incompressible solver was initialized using International Standard Atmosphere (ISA) equations at the domain boundaries (i.e., inlet, outlet, etc.), and then the converged solution obtained was used to initialize the compressible simulation.

The first simulation (with the incompressible solver) uses Spalart-Allmaras (SA) turbulence model and a Spalding wall function to compute turbulence parameters close to the wall. The usage of wall function was mainly made from the perspective of memory use as less cells should to be added close to the wall. The second simulation (with the compressible solver) uses $k-\omega$ SST turbulence model and its corresponding wall functions, that were able to predict the universal turbulence profile close to the wall (M. Segui et al., 2021). Finally, the forces and moments considered were those obtained using the second simulation.

To optimize the computational time and therefore, minimize the number of CFD simulations, a strategy was used to simulate a wide range of aircraft configurations (i.e., different winglet deflection angles and flight conditions (α, M)). CFD simulations were performed for the

different conditions specified in Table 4.1, while the horizontal tail was maintained in a constant position ($\delta_{\text{stab}} = 0$ deg). The aerodynamic coefficients (C_{L_S}, C_{D_s} and $C_{M_s y}$) obtained in this step were displayed using black squares in Figure 4.4, (a), (b) and (c).

Table 4.1 Global aerodynamic coefficients computation parameters

Aircraft dimensions				
Reference area:		68.6269 m^2		
Mean aerodynamic chord:		3.3829 m		
Aerodynamic computations				
Altitude	**Mach**	**Air density**	**Angle of attack**	**Winglet deflection angle**
5,000 ft	0.31	1.0555 kg.m^3	-2, -1, 0, 1, 2 deg	-93, -73, -35, 0, 35, 73, 93 deg
10,000 ft	0.45	0.9046 kg.m^3		
20,000 ft	0.54	0.6527 kg.m^3		
25,000 ft	0.66	0.5489 kg.m^3		
30,000 ft	0.79	0.4583 kg.m^3		

Then, to predict the aerodynamic coefficients for intermediate flight conditions and winglet deflection angles, an interpolation technique was used. In order to reduce the number of degrees of freedom in the analysis (attack angle, Mach number and winglet deflection angle), it was considered as known the variation of the coefficients as a function of the angle of attack for a fixed Mach number and winglet position. Indeed, the lift and pitching moment coefficients should be considered as linear and the drag coefficient should be considered as parabolic due to their equation shape versus α (Raymer, 2012b ; Marine Segui, Abel, et al., 2021b).

Therefore, the variation of C_{L_S}, C_{D_s} and C_{M_s} (only for a fixed angle of attack) according to the Mach number and the winglet deflection position were identified using the polynomial surface technique. The polynomial surface that has the closest correlation factor to 1 was defined in Eq. (4.7).

$$C_{L,D,M_y}(M,\xi) = \sum_{i=0}^{n=4} \sum_{j=0}^{m=3} a_{ij}.M^i.\ \xi^j \tag{4.7}$$

where a designates a polynomial coefficient, M the Mach number, ξ the winglet deflection angle, and i and j are the mathematical indices. It was found that the Mach number polynomial order was $n = 4$ and the winglet deflection polynomial order was $m = 3$.

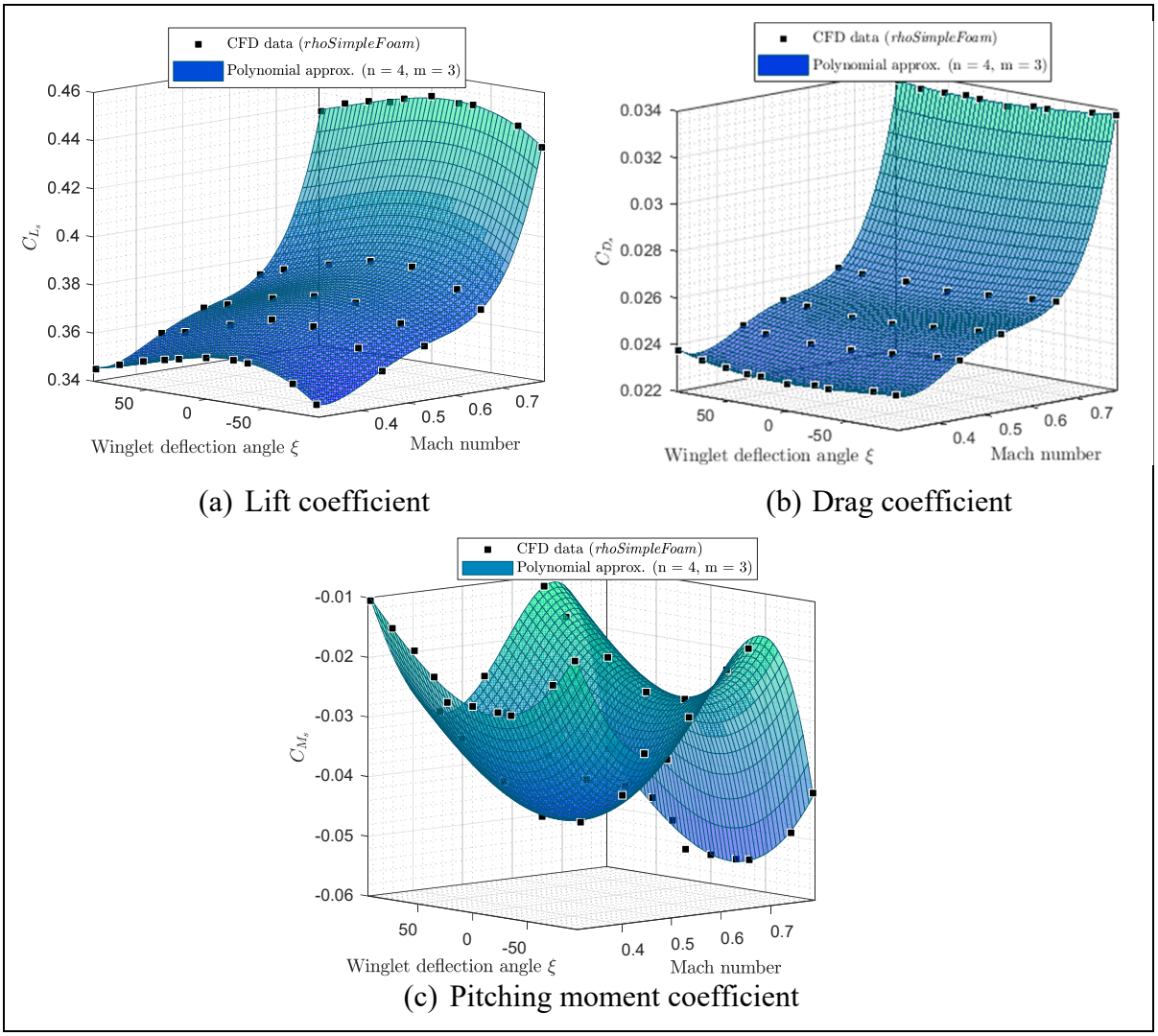

Figure 4.4 Global aerodynamic coefficient variation versus the winglet deflection angle and the Mach number for an angle of attack of 0 deg

Figure 4.4 (a), (b) and (c) show the variations of the aerodynamic coefficients (lift, drag and pitching moment, respectively) with the winglet deflection angle and the Mach number. Black squares indicate the values obtained using the aerodynamic model through different simulations, as indicated in Table 4.1. The polynomial approximation surfaces show the prediction of the aerodynamic coefficients using their polynomial approximation in Eq. (4.7).

It is important to remind the fact that the adaptive winglet set at 73 degrees was considered as the baseline for aerodynamic characteristics comparisons (Marine Segui, Abel, et al., 2021b ; Marine Segui, Botez, et al., 2021).

It can be observed on Figure 4.4 (a), (b) and (c) that the polynomial approximation surface is very close to the black squares, which are the values obtained during CFD simulations. It can be seen that some points slightly deviate from the surface, which may be due to small "noises" in the simulations. In order to "smooth" these irregularities, for the rest of the study, it was considered that the aerodynamic coefficients were all predicted according to Eq. (4.7), and that the polynomial coefficients a depend on the angle of attack considered and on the nature of the aerodynamic coefficient to be predicted (lift, drag or pitching moment coefficient).

At this point we have described the methodology to obtain the global aerodynamic coefficients. The next step is to explain the computation of the downwash deflection angle.

4.2.1.2 Downwash deviation angle computation

The downwash deviation angle was estimated by computing the difference of the velocity flow angle between the front and the back of the wing. The velocity flow angles were evaluated from the magnitude of the flow velocity (U_x, U_y and U_z) that were recorded when OpenFoam simulations converged. A total of fourteen probes $\mathbf{P_X}(x, y, z)$ were used for each simulation, seven were located in front of the CRJ700 wing (P_1 to P_7) and seven others were located behind the wing (P_8 to P_{14}), as illustrated in Figure 4.5. Engines were not studied in the aerodynamic simulations, therefore, only the flow deviation due to the wing was considered in this research.

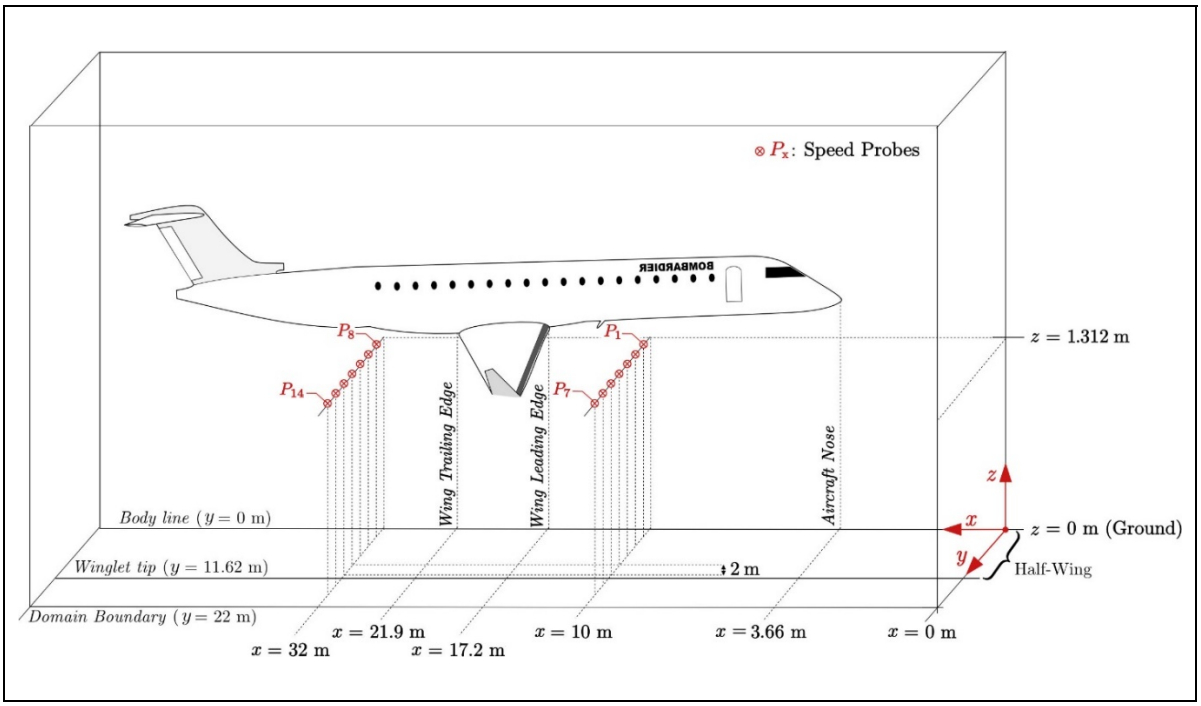

Figure 4.5 Flow velocity measurement location when CRJ700 is rotated with an angle of attack of 0 degrees

According to Figure 4.5, P_1 to P_{14} were located at the same height of 1.312 m, and spaced at distances of 2 m. Therefore, probes P_1 and P_8 were located at 2 m according to the "body line" (i.e., the fuselage axis), while the probes P_7 and P_{14} were located at 14 m from the "body line". As the half-wing span length is 11.62 m, probes P_6, P_7, P_{13} and P_{14} were located outside the streamlines that pass through the aircraft wing.

The streamline that passes through the Mean Aerodynamic chord (MAC) location as a lateral reference is often used to measure the downwash angle (Cantwell, 2014, p. 12 ; Levy, 1992). For the CRJ700, the MAC is located 5.35 m from the body line, and therefore, we should be able to estimate the speed deviation angle between the 4 probes P_2, P_3, P_9 and P_{10}. However, the streamlines located precisely around the MAC location present some fluctuations of the flow speed due to the fuselage interaction. Therefore, to stabilize the measurements, a larger number of measurement than 4 were used. The downwash angle was thus successfully computed using five probes located in front of the wing, P_1 to P_5, and five probes located behind the wing, P_8 to P_{12}.

The downwash ε (in degrees) was calculated using the average presented in Eq. (4.8), in which $front$ and $back$ refer to probes located in front of and in back of the wing, respectively. U_z and U_x represent the velocities, that were recorded in m/s by measurements taken in the z and x directions (shown in Figure 4.3 and Figure 4.5), respectively.

$$\varepsilon = \left[\sum_{i=1}^{5} \tan^{-1}\left(\frac{U_{z\,(i)}}{U_{x\,(i)}}\right)_{back} - \tan^{-1}\left(\frac{U_{z\,(i)}}{U_{x\,(i)}}\right)_{front}\right]/5 \tag{4.8}$$

To validate this downwash calculation methodology, downwash angles computed for the original shape of the CRJ700 (without the adaptive winglet) were compared to downwash angles provided by the flight simulator VRESIM in Figure 4.6. The VRESIM is a flight simulator qualified by a level D degree, that was given by the Federal Aviation Administration (FAA). Therefore, the VRESIM provides accurate flight dynamics data for validation. It is important to remind here that the aerodynamic model does not consider the engines geometry, nor their interactions with the flow, while the reference system (VRESIM) does.

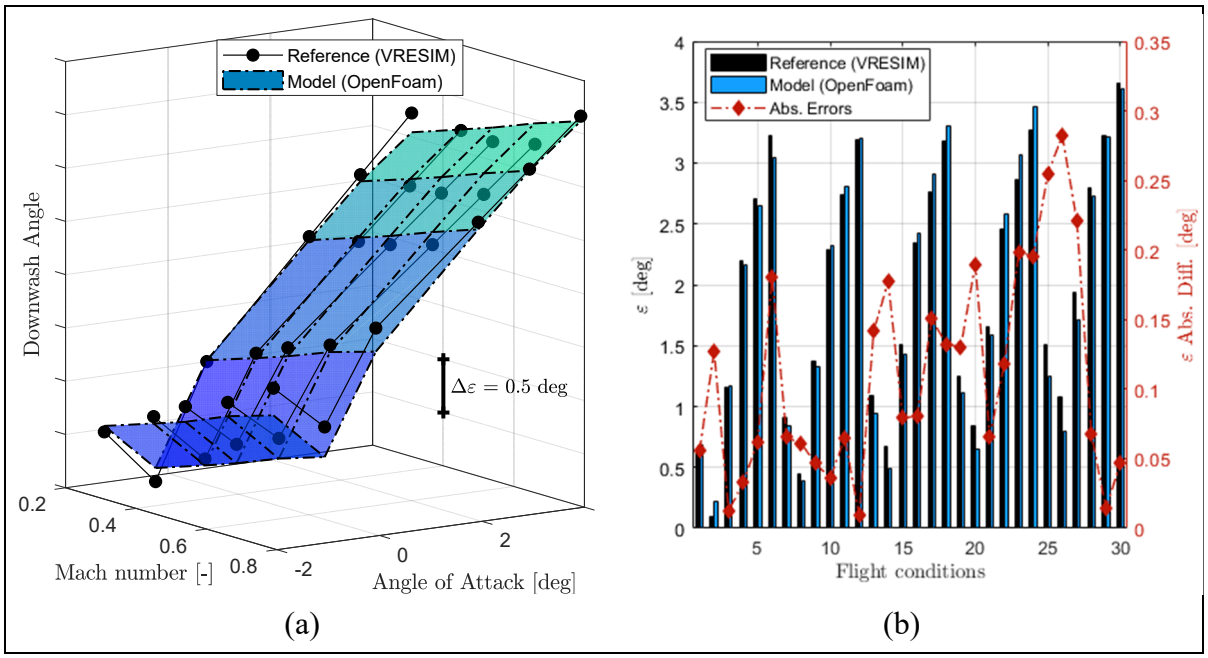

Figure 4.6 Results obtained for downwash calculation validation

Figure 4.6 (a) shows the downwash angles variations with the Mach number (from 0.31 to 0.79) and the angle of attack (from -2 deg to 4 deg). The reference values of the downwash angles provided by the VRESIM are indicated using solid black lines and black circles, while the downwash angle values computed using the OpenFoam aerodynamic model of the CRJ700 with Eq. (4.8) are represented using a colored surface. For confidentiality reasons, it is not possible to publish the reference values given by the VRESIM. Therefore, the downwash angle values have been hidden in Figure 4.6 (a). In order to appreciate the difference between the model and its reference, a grid reference of 0.5 deg has been added.

Figure 4.6 (a) shows that the downwash angles estimated are very close to their reference values and follow the same trend, especially around angle of attack of -1 deg, where downwards trend can be seen. More details in terms of the differences between the model and the VRESIM (reference) results are presented in Figure 4.6 (b), according to the flight conditions. The *y* axis located on the left of Figure 4.6 (b) indicates the downwash angle values, and the *y* axis on the right indicates the absolute errors in degrees (in red color) computed between the VRESIM reference ("black" color bars) and the model ("blue" color bars). The *x* axis presents the number of flight conditions.

The downwash angle value was estimated with less than 0.28 deg of error for all flight conditions tested. A majority of errors had less than 0.15 deg, which was a very good result, especially from the fact that the aerodynamic model did not considered engines geometry, therefore a small deviation (error) was expected. More generally, using a statistical study, the downwash value predicted by the model was found within a margin error of 0.110 ± 0.075 deg in 95% of cases using a normal distribution. These excellent results validated the model used to compute the downwash from Eq. (4.8), and the probes location used during OpenFoam simulations.

The methodology presented in this Section 4.2.1.2 explained how the downwash deviation angle was estimated and validated using the original CRJ700 data (without adaptive winglets).

Figure 4.7 shows the variation of downwash deflection angle values as a function of the adaptive winglet positions ξ and Mach numbers M, for angles of attack α of -1 deg (using red color), 0 deg (using blue color) and +1 deg (using cream color).

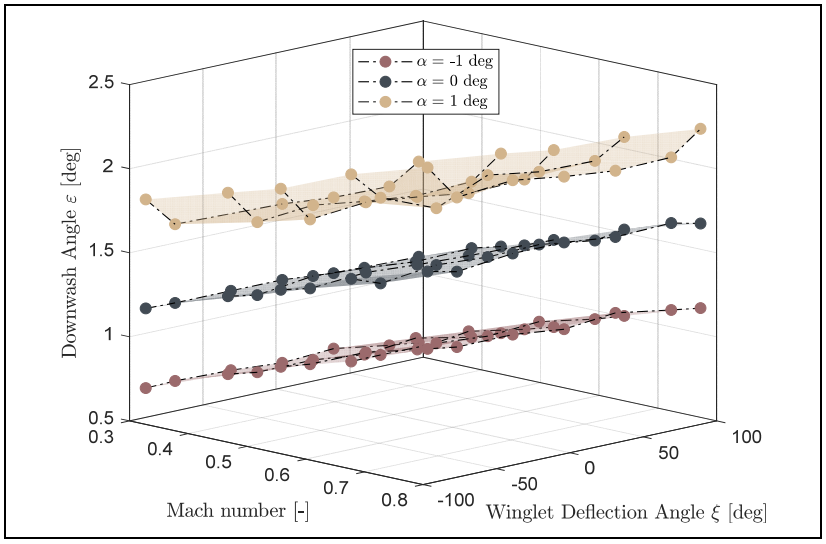

Figure 4.7 Downwash angle variation with respect to the Mach number, the winglet deflection angle and the angle of attack

It can be seen from Figure 4.7 that the downwash deviation angle values did not change too much as a function of the winglet position angle for incidence angles of -1 deg and 0 deg. However, the winglet position seems to change the value of the downwash deviation angle for the angle of attack of 1 deg, especially for ξ = 100 deg and ξ = -100 deg.

At this point, it has been explained how to calculate the essential aerodynamic parameters in order to determine further the aerodynamic contributions of the wing-body (wb) and horizontal-tail (ht). Indeed, subsection 4.2.1.1 has shown how to obtain the global aerodynamic coefficients. Subsection 4.2.1.2 was dedicated to present the methodology used to calculate the downwash. Finally, the next subsection 4.2.1.3 will show how to isolate the contributions.

4.2.1.3 Decomposition of the wing-body (*wb*) and horizontal-tail (*ht*) aerodynamic contributions

To compute the "wing-body" aerodynamic coefficients, Eqs. (4.4), (4.5) and (4.6) were manipulated to isolate the *wing-body* contributions ($C_{L_{(wb)}}$, $C_{D_{(wb)}}$, $C_{M_{(wb)}}$) of the aircraft from the global *aircraft* contributions (C_{L_s}, C_{D_s}, C_{M_s}) obtained in subsection 4.2.1.1. To perform the computations, the downwash values obtained in subsection 4.2.1.2 have been used, in addition, it is also necessary to know the aerodynamic coefficients of the horizontal tail ($C_{L_{(ht)}}$, $C_{D_{(ht)}}$).

Two methods can be considered to obtain $C_{L_{(ht)}}$ and $C_{D_{(ht)}}$. The first method would be to compute the aerodynamic coefficient variations of the horizontal tail wing (isolated) for several angles of attack α_{ht} using a high-fidelity method. For the second method, the original horizontal tail characteristics of an aircraft could be maintained while its wing design was geometrically (and aerodynamically) improved. This second method considers the original aircraft characteristics as known values, and was preferred for this study as it saved computational costs.

The aerodynamic coefficients of the CRJ700 horizontal tail $C_{L(ht)}$ and $C_{D(ht)}$ were extracted from the VRESIM, as it provided aerodynamic data derived from the original model designed by the aircraft manufacturer, Bombardier. Certified with the highest qualification degree (level D), the VRESIM is an accurate source from which $C_{L(ht)}$ and $C_{D(ht)}$ were obtained.

To validate this approach, the initial configuration of the CRJ700 aircraft (i.e., without adaptive winglets) was considered. Aerodynamic coefficients computed through the methodology (*model*) were compared to coefficients provided by the VRESIM for the wing-body contributions (*reference*). The absolute errors between the *model* and *reference* (VRESIM) data are displayed on Figure 4.8.

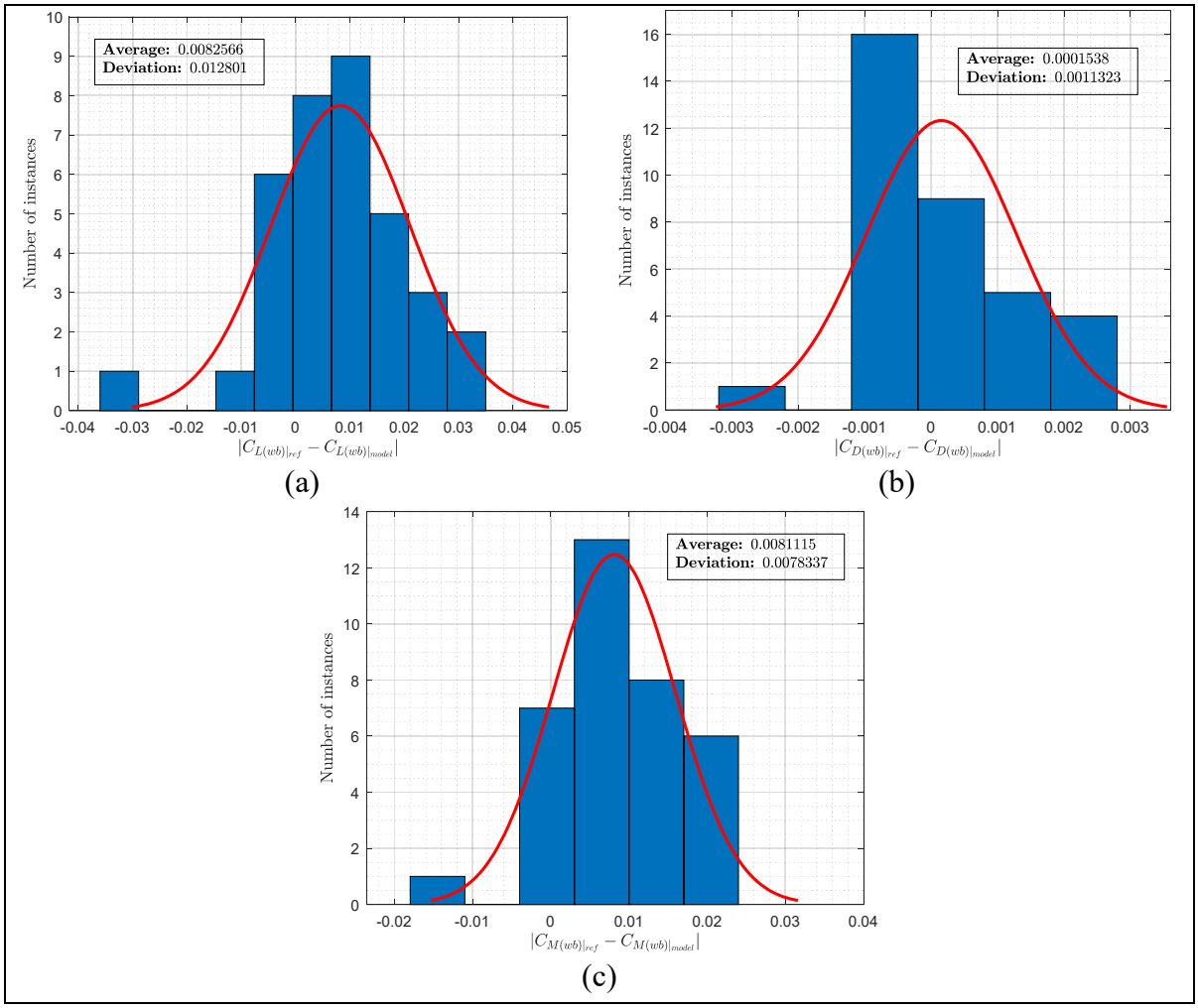

Figure 4.8 Validation of the methodology for the wing-body contribution calculation for the lift (a), drag (b) and pitching moment (c) coefficients

Figure 4.8 (a) shows the errors obtained for the *wing-body* lift coefficient ($C_{L\,(wb)}$) prediction. The majority of errors are located between -0.01 and 0.02, which is very low. On average, the estimation error of the lift coefficient is 0.008 with a standard deviation of 0.012. Using a "normal" law, the lift coefficient was predicted with a margin of error of 0.008±0.013 in 95% of cases. Similar results were found for the C_{L_s} that was validated with an error margin of -0.007±0.045 in 95% of cases. The $C_{L\,(wb)}$ error was slightly higher, but had the same order of magnitude. Indeed, by computing the $C_{L\,(wb)}$ from the C_{L_s} values, it was normal that errors have been propagated. Moreover, the use of the *horizontal-tail* (*ht*) aerodynamic coefficients

values provided by the VRESIM to obtain the *wing-body* aerodynamic contributions, limited the error propagation in the estimation of aerodynamic coefficients.

Figure 4.8 (b) shows the absolute errors obtained for the *wing-body* drag coefficient ($C_{D\ (wb)}$) prediction. Errors were distributed between -0.003 and 0.003, with most of them located around an error margin of -0.001. Using a Gauss distribution, the model could predict the *wing-body* drag coefficient within an error margin of 0.00015±0.00113 in 95% of cases. As a reminder, the aerodynamic model was able to predict the *aircraft* drag coefficient (C_{D_s}) within a margin of error of -0.00015±0.0014 in 95% of cases (using a Gauss distribution). Thus, it can be argued that the errors in predicting the drag coefficient were slightly greater for the *wing-body* contributions ($C_{D\ (wb)}$) than for the *aircraft* contributions (C_{D_s}). However, the errors maintained a similar order of magnitude (for $C_{D\ (wb)}$ or for C_{D_s}), which confirmed that the method of calculation of the *wing-body* contributions limited the propagation of errors.

Finally, the pitching moment coefficients computed for the *wing-body* contributions were compared to the VRESIM values on Figure 4.8 (c). Errors obtained for the pitching moment coefficients were a little bit higher than those obtained for the lift and drag coefficients, respectively, in Figure 4.8 (a) and (b). However, the errors obtained for the *wing-body* contribution calculations remained in the same order of magnitude as those obtained for the *aircraft* contributions (for the aerodynamic model validation). The $C_{M(wb)}$ was estimated with a margin of error of 0.0081±0.078 in 95% of cases, while C_{M_s} was estimated with a margin of error of -0.0077±0.0079 in 95% of cases (both errors were obtained using a Gauss distribution). Therefore, the same observations as those made previously for the $C_{L(wb)}$ and $C_{D(wb)}$ could be made; the error margin obtained for the $C_{M(wb)}$ was a little bit larger than that of the C_{M_s}, which was normal because $C_{M(wb)}$ was estimated from C_{M_s}, and the final error could not be less than the first one. However, the error margin of $C_{M(wb)}$ was limited because both errors (for $C_{M(wb)}$ or C_{M_s}) remain in the same magnitude order.

In order to compute the climb and cruise performance of the CRJ700 aircraft equipped with deformable winglets, the aerodynamic data obtained previously (Section 4.2.1), were integrated into the performance model that was presented in the following section (Section 4.2.2).

4.2.2 Performance Modelling

To correctly model the climb and cruise performances of a CRJ700 equipped with fixed or adaptive winglets, we first review the procedures that generally apply to this aircraft and which were considered in this research. Figure 4.9 indicates the complete climb profile in "purple" color and shows the cruise trajectory in "green" color.

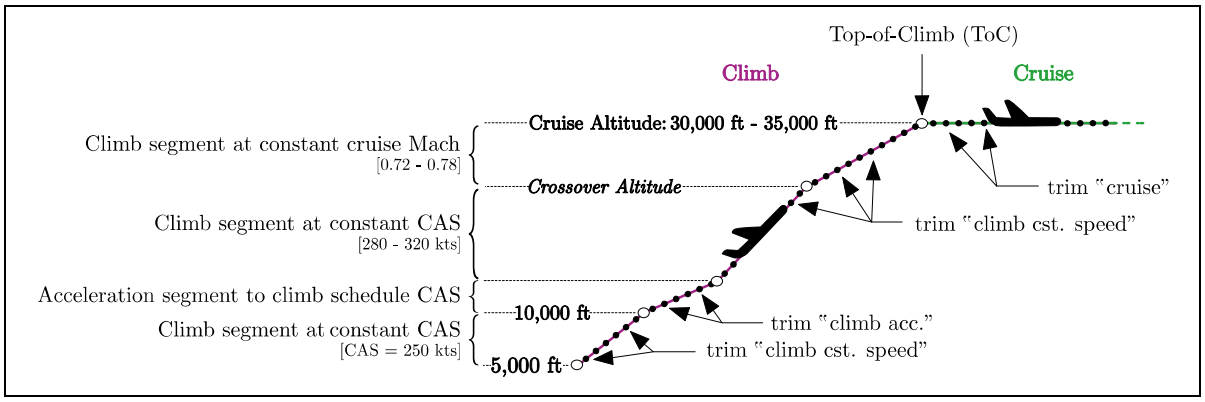

Figure 4.9 Climb and cruise speed schedules

For the cruise segments, the altitude and the Mach number were considered as constant along the cruise. However, for the climb segments, flight profiles were considered starting at the flaps' retraction altitude, estimated at 5,000 ft, to the expected cruise altitude of 30,000 ft to 35,000 ft (for the CRJ700 aircraft) (Blake, The performance Training Group, & Flight Operations Engineering, 2009).

The typical CRJ700 climb schedule must follow certain rules as shown on Figure 4.9. The CRJ700 aircraft must first climb using a constant CAS speed of 250 kts to an altitude of 10,000 ft, in accordance with FAA regulations. The aircraft should then perform an acceleration from

250 kts to its intended CAS speed, typically from 280 kts to 320 kts (CRJ700 Flight Crew Operating manual - FCOM). For this acceleration step, a vertical speed of 1000 ft/min was assumed. Two flight segments at constant speeds were then performed: one segment at a constant CAS speed until reaching the crossover altitude, and a second segment at a constant Mach speed from the crossover to the cruising altitudes (Blake et al., 2009).

In order to calculate the overall performance of an aircraft equipped with adaptive winglets during a complete climb and/or cruise, Section 4.2.2 was divided into two subsections. The first subsection (subsection 4.2.2.1) presents the performance model used for a conventional aircraft, while the second subsection (subsection 4.2.2.2) explains how the model was modified to consider an aircraft equipped with adaptive winglets.

4.2.2.1 Performance model developed in-house at our laboratory LARCASE

To evaluate performance of an aircraft along a climb and/or cruise, it was considered to discretize whole segments in several "steps", indicated by "black" color dots on Figure 4.9. The discretization was made differently according to the flight segment (i.e., acceleration climb, constant speed climb, cruise, etc.). For climb segments using constant speed schedule (CAS or Mach), the discretization was performed every 1000 ft. For acceleration climb segments, an Euler integration was used every 2 seconds. For each step, the flight condition changes (i.e., altitude, speed, weight, etc.), and therefore the *Aircraft State* needs to be updated.

The *Aircraft State* corresponds to the global aircraft configuration (i.e., the control surfaces' setting) required to be statically trimmed (i.e., balanced) for the flight condition provided as input. To compute the *Aircraft State* at each step, we used the performance model shown in Figure 4.10, developed and validated at our laboratory LARCASE (Ghazi, Botez, Bourrely, & Turculet, 2021). The performance toolbox can then provide the desired output information, including the angle of attack α, the thrust required F_N, stabilizer δ_{stab} and elevators δ_{elev} angles, the fuel flow w_f, the rate of climb *R/C*, as shown on Figure 4.10.

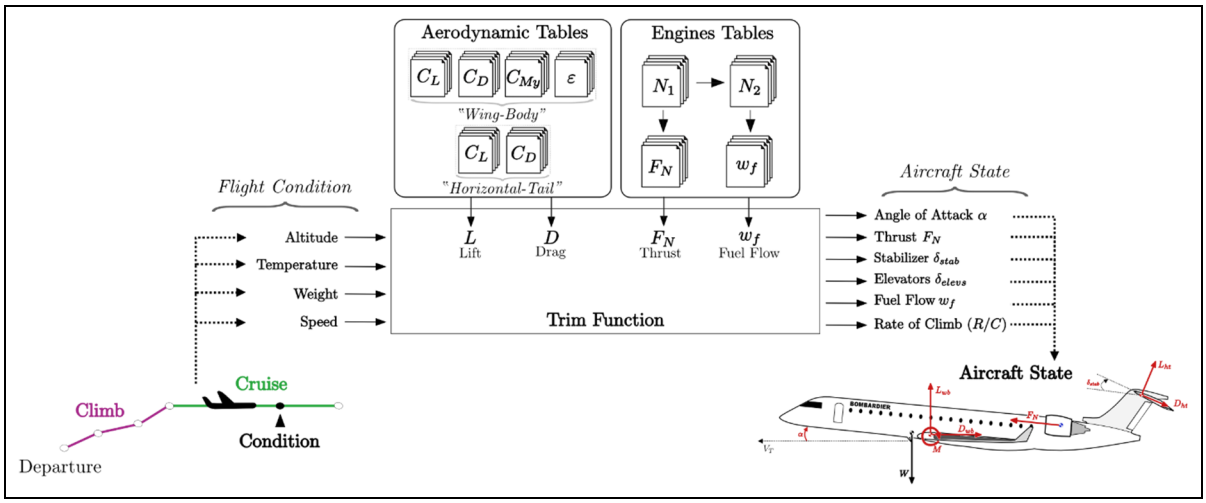

Figure 4.10 Drawing of the performance model developed in-house at LARCASE

Throughout the flight, the pilot (or an autopilot) is constantly trimming the lift surfaces and the Throttle Lever Angle (TLA) to make the flight as efficient as possible. The performance model (Figure 4.10) is designed to reproduce this action by predicting the aircraft's static state for a given flight condition provided as input using a "trim function".

The "trim" function manages all the "trim parameters", including the angle of attack, the vertical path angle, the longitudinal control surfaces (i.e., stabilizer and elevators' positions, etc.) and the thrust, in order to balance the aircraft for a given flight condition (altitude, speed and weight). To be considered as balanced, all forces and moments projected in a Cartesian axis must follow Newton's second law (Eq. (4.9)). It is important to note that winds were neglected in this study. The trim function was thus expressed as:

$$\text{Trim function} \begin{cases} \sum \overrightarrow{F_x} = m.\vec{a} \\ \sum \overrightarrow{F_z} = m.\vec{a} \\ \sum \overrightarrow{M_y} = \vec{0} \end{cases} \Rightarrow \begin{cases} L + F_N.\sin(\alpha + \phi_T) = m.g_0.\cos(\gamma) \\ F_N.\cos(\alpha + \phi_T) - D - m.g_0.\sin(\gamma) = m.\dot{V}_T \\ M_{\text{aero}} + M_{\text{engine}} = 0 \end{cases} \quad (4.9)$$

where F_N is the thrust force, ϕ_T is the engine inclination angle (between the engines and the body axis), V_T is the aircraft True Air Speed (TAS), m is the aircraft mass, g_0 is the

gravitational constant, γ is the aircraft path angle, α is the angle of attack, and M_{aero} and M_{engine} are the aerodynamic and engine moments, respectively, induced by their corresponding forces and application locations relevant to the aircraft gravity center (CG). *L* and *D* define the total lift and drag forces, respectively, including the *wing-body* and *horizontal-tail* contributions. Therefore, *L* and *D* are dependent upon the angle of attack α, the stabilizer angle δ_{stab} and the aircraft TAS (i.e., Eqs. (4.1), (4.2), (4.4) and (4.5)).

The general trim function expressed in Eq. (4.9) is valid for all aircraft flight scenarios. However, by developing the forces and moments, it is possible to simplify these equations by using the assumptions corresponding to the flight scenario being considered ("climb constant speed", "climb acceleration" or "cruise").

To find the aircraft's trim state, the trim algorithm solves Eqs. (4.9) by adjusting the angle of attack α, the stabilizer angle δ_{stab}, and the thrust force value F_N at cruise conditions. During climbs, the Throttle Lever Angle (TLA) was considered to be set in the "Maximum Climb Thrust Position (MCLT)" (Blake et al., 2009 ; Flight Operations Support & Line Assistance teams & Customer Service, 2002 ; Ghazi et al., 2021 ; Marine Segui & Botez, 2018b). This implies that the thrust force F_N is always at its maximum capacity for the corresponding flight condition. Consequently, for climb scenarios (constant speed or acceleration), the performance trim algorithm can determine the combination of the angle of attack α, the stabilizer angle δ_{stab} and the flight path angle γ that best balances the forces and moments.

The performance model was developed as a tool, that can be adapted to several different types of aircraft. Therefore, to calculate the forces and moments (i.e., the aerodynamics and the engines' performances), applied to an aircraft, this model stores all the aircraft-specific data using two types of lookup tables: *Aerodynamic* (aerodynamic coefficients) and *Engine* (engine parameters) (see Figure 4.10). Geometrical data were also provided to the model, such as the chords, surface areas, gravity center positions, etc.

The performance toolbox used two *Engine* lookup tables to compute the forces, moments and performances relative to the engines. One lookup table was utilized to estimate the thrust force F_N delivered by the engines, and the other was used to compute the corresponding fuel flow W_f. These engine lookup tables require the altitude *h,* the Mach number *M*, the temperature deviation from the International Standard Atmosphere (ISA) ΔISA, the speed rotation of the fan N_1 and the Thrust Rating Parameter *TRP* (i.e., 'Max Climb', 'Max Continuous', 'Idle', etc.) for their inputs, as indicated in Eqs. (4.10) and (4.11) for the lookup tables F_N and W_f, respectively.

$$F_N = f(h, M, \Delta\text{ISA}, N_1(TRP)) \tag{4.10}$$

$$W_f = f(h, M, \Delta\text{ISA}, N_1(TRP)) \tag{4.11}$$

It is important to specify that the values resulting from these lookup tables made possible the trimming of the aircraft (thrust F_N lookup table), but also to calculate the corresponding fuel flow W_f. Knowing the fuel flow for each *Aircraft trim state*, the fuel consumed was thus calculated by adding the "delta of time" Δt necessary for the aircraft to reach the next trim evaluation (integration in time for a cruise segment and in altitude for a climb segment).

Six *Aerodynamic* lookup tables were used by the performance toolbox to compute the forces and moments relative to specific aerodynamic properties. The first three lookup tables obtained the *wing-body* (*wb*) lift $C_{L(wb)}$, drag $C_{D(wb)}$, and pitching moment $C_{My\,(wb)}$ coefficients. Each of these tables require the angle of attack of the wing α_{wb} and the Mach number M for their inputs, as indicated in Eq (4.12).

$$\left[C_{L(wb)}, C_{D(wb)}, C_{My\,(wb)}\right] = f(\alpha_{wb}, M) \tag{4.12}$$

The next two tables are needed to store the *horizontal tail* (*ht*) aerodynamic contributions in terms of the lift $C_{L(ht)}$ and drag $C_{D(ht)}$ coefficients. Both of these lookup tables require the

values of the tail angle of attack α_{ht}, the Mach number M and the elevator deflection position δ_{elev}, as detailed in Eq. (4.13).

$$\left[C_{L(ht)}, C_{D(ht)}\right] = f(\alpha_{ht}, M, \delta_{\text{elev}}) \tag{4.13}$$

The sixth and last lookup table provides the values of the downwash angles ε to the performance toolbox, with the wing angle of attack α_{wb} and the Mach number M as its input.

The information contained in the *Aerodynamic* and *Engine* tables must be as accurate as possible, highlighting the importance of a reliable source of data. To develop and validate this performance toolbox, the LARCASE has used the *Aerodynamic* and *Engine* data provided by the two flight simulators displayed in Figure 4.11.

(a) Cessna Citation X RAFS

(b) Bombardier CRJ700 VRESIM

Figure 4.11 Level D flight simulators available at LARCASE

Figure 4.11 (a) shows the Research Aircraft Flight Simulator (RAFS), and Figure 4.11 (b) shows the Virtual Research Simulator (VRESIM). The RAFS is an Integrated Procedures Trainer (IPT) product of CAE Inc. that simulates the Cessna Citation X business jet, while the VRESIM is a Virtual Simulator (VSIM) that was designed for the LARCASE team's research needs by CAE Inc. This second flight simulator simulates a larger aircraft, the Bombardier CRJ700 Regional Jet.

Together, these two flight simulators provide a highly accurate and large source of information. The information provided by these simulators relative to flight dynamics is guaranteed to have less than 5% of error with respect to the real aircraft flight test, as they satisfy all criteria for the level D provided by the Federal Aviation administration (FAA).

A validation study completed the development of the performance toolbox model. For this purpose, the performance model was used to compute each parameter of the *Aircraft State* (i.e., α, δ_{stab}, F_N, W_f, γ, etc.) and then to compute the global performances of the aircraft, such as the time to climb, the ground distance covered during climb, or the fuel burnt for a given segment. For 60 climb scenarios, the performance model estimated the time to climb within an error of -0.23±0.52% (between -10s to 10s) in 95% of cases, using a Gauss distribution. Similarly, the ground distance covered was estimated within an error of -0.32±0.61% (between -1.5 nautical miles (nmi) to 1 nmi) and the amount of fuel burnt within an error of -0.33±0.54% (between -10lb to +10lb) in 95% of cases, using a Gauss distribution (Ghazi et al., 2021).

The accuracy of the performance model for computing cruise parameters was demonstrated via complete flight scenarios (climb, cruise and descent). For 60 complete flight scenarios, the performance model estimated the total fuel burnt with less than 2% of error. It is clear that if the model was able to predict the fuel burned over a complete flight within an error smaller than 2%, the error for the cruise phase will be even smaller.

Based on these very low prediction errors, the performance model can be qualified as very accurate. Therefore, this mathematical model was used in this study to estimate the cruise and climb performances of an aircraft equipped with an adaptive winglet.

This performance model was developed by our laboratory LARCASE during previous research. From the fact that this paper has for objective to present performances obtained for an aircraft equipped with adaptive winglets, the performance model was concisely presented. However, the reader is invited to refer to references (Ghazi & Botez, 2017 ; Ghazi et al., 2021 ;

Ghazi, Botez, & Maniette, 2020) for all the details of the trim algorithms and trajectory predictions used in the performance model, as well as for the validation results.

4.2.2.2 Adaptation of the performance toolbox for the adaptive winglet computations

This sub-section presents the methodology used to apply the performance toolbox (presented in subsection 4.2.2) to an aircraft that has an adaptive winglet. The performance toolbox was originally developed for conventional aircraft, which have all the common conventional longitudinal control surfaces (i.e., flaps, slats, elevators, and stabilizer). Therefore, to predict the flight performance of an aircraft equipped with an adaptive winglet, the performance model must be adapted and the winglet deflection should be selected in the process.

As a reminder, only the wingtip geometry has been changed in this effort to design an adaptive winglet for the CRJ700. Given that limited design change in the "adaptive" version of the CRJ700, the engines remain the same as those of the initial version of the aircraft. Therefore, *Engine* lookup-tables of the original CRJ700 aircraft (obtained by the VRESIM) were used in the performance toolbox.

In addition, the original horizontal tail design has been kept in the "adaptive" version of the CRJ700, and therefore the *horizontal-tail* aerodynamic coefficients (i.e., $C_{L(ht)}$, $C_{D(ht)}$) could be taken from the VRESIM data.

Nevertheless, the wing geometry was changed (due to the adaptive winglet modification), and therefore, the *Aerodynamic* tables of the performance toolbox were also updated. This update was accomplished by arranging the *wing-body* aerodynamic coefficients (i.e., $C_{L(wb)}$, $C_{D(wb)}$ and $C_{My\,(wb)}$) computed in section 4.2.1.3 as lookup tables that can then be provided to the performance toolbox model. Similarly, the downwash deviation angle ε computed in section 4.2.1.2 was arranged into a lookup table, and then it was provided to the performance toolbox model.

It is important to note that the *wing-body* aerodynamic coefficients and the downwash deviation angle ε now depends on the winglet deflection angle ξ in addition to the angle of attack α_{wb} and the Mach number M. Due to the additional dimension of the winglet deflection parameter (i.e., ξ) added to the *wing-body* aerodynamic coefficients and downwash deviation angle lookup tables, an optimization process must be performed to select the "optimal" winglet deflection for each flight condition and "trim" state.

An exhaustive research was performed to compute the *Aircraft State* for each winglet position considered and for each flight conditions according to an optimization criterion. For cruise scenarios, the *Aircraft State* leading to the minimum fuel consumption was selected and then saved, as well as the corresponding winglet deflection angle. Concerning climb phases, there are a several targets depending on an airliner's optimization criteria or the climb schedule imposed by control towers or airport procedures. Sometimes, it is better to reach the Top of Climb (ToC) as soon as possible, and thus maximize the rate of climb. In other cases, it could be advantageous to maximize the ground distance before reaching cruise altitude, which could be defined as the "Minimum Trip Time" trajectory by considering the global flight (climb, cruise and descent phases) (Blake et al., 2009). In order to highlight the advantages that an aircraft equipped with adaptive winglets can offer during climb, two optimization criteria were established: the "Minimum Time" to reach ToC and the "Maximum Ground Distance" to reach ToC.

4.3 Results – Performance Calculations

This third section presents the results obtained for the aerodynamic study of an adaptive winglet application for the Bombardier CRJ 700 regional jet. To better evaluate the advantages of equipping the CRJ 700 with adaptive winglets, the performance of the CRJ700 equipped with an adaptive winglet and with a fixed winglet (i.e., its original configuration) were both computed using the performance toolbox algorithm. The results are displayed in three subsections; the first subsection (4.3.1) shows the results obtained for climb segments, the

second subsection (4.3.2) highlights the benefits obtained for cruise segments, and the third subsection (4.3.3) presents the results obtained for the combined climb and cruise segments.

4.3.1 Climb Segments

Several climb segments were simulated according to the flight envelope of the original CRJ700. To better explain the results, it was preferred to first show the results obtained for one specific climb scenario.

The results obtained for the climb scenario 320/0.72 (i.e., CAS = 320 kts and Mach number set to 0.72) are displayed in Figure 4.12 (a). The vertical profile corresponding to the two strategies “Minimum Time” (using “blue” color) and “Maximum Ground Distance” (using “green” color), performed using the aircraft equipped with an adaptive winglet, were compared to the reference vertical profile (using “black” color), performed with the reference configuration of the aircraft (fixed winglet). It is important to note that for the three vertical profiles, the engines were the same, each of them was set at the “Maximum Climb” regime. Consequently, the differences observed between the three climb schedules were only due to the different aerodynamic properties obtained from the adaptive winglet aspects.

Globally, the three strategies show different trajectories above the crossover altitude, while some minor differences can be observed for the trajectories under the crossover altitude.

Using a strategy that focuses on maximizing the rate of climb R/C in order to minimize the time to climb (climb to the Top of Climb-ToC) (data represented in “blue” on Figure 4.12 (a)), the ToC was reached 47.22s before that of the reference aircraft (1516.65s), that is an encouraging performance indicator (time to climb to ToC reduced by 3.1% in this case).

It can also be observed on Figure 4.12 (a) that the “Maximum Ground Distance” strategy takes longer time to reach the ToC, since this was not the objective; however, this strategy allows the aircraft to fly 4.81 nautical miles more than the reference aircraft (which, in this example,

needed 167.07 n miles to climb). In this case, the adaptive winglet could improve the horizontal distance by up to 2.8%. Therefore, improving the "Maximum Ground Distance" using an adaptive winglet could also be promising, depending upon the situation.

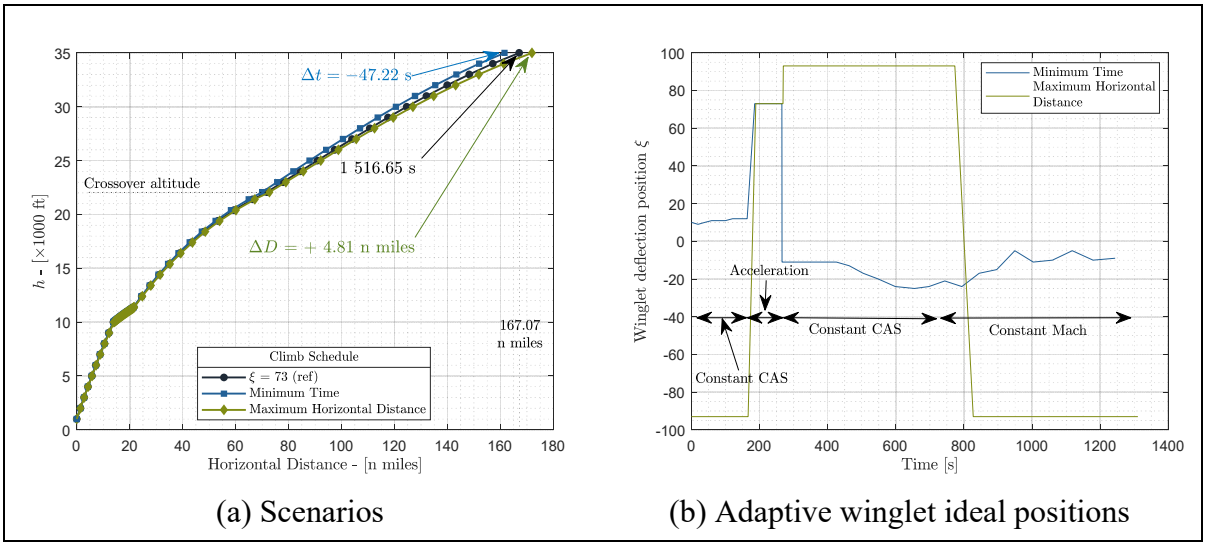

(a) Scenarios (b) Adaptive winglet ideal positions

Figure 4.12 Performances obtained during the climb scenario 320/0.72 for the CRJ700 aircraft model equipped either with fixed or with adaptive winglets

Figure 4.12 (b) shows the optimum winglet positions that were used during the climb and for the two strategies ("minimum time" and "maximum horizontal distance") versus time. It could be observed that the winglet moves from -25 deg to 12 deg most of time to offer a "minimum time" strategy, so around the horizontal position of 0 deg. For the acceleration climb segment, the best winglet positions were found for 73 deg (which is the original configuration) for both strategies. Finally, using a "maximum horizontal distance" strategy, it could be observed that the adaptive winglet needs to move close to its extreme angle values (-93 degrees and +93 degrees).

Table 4.2 Conditions for the combination of the 10 climbing scenarios

CAS segment	Cruise altitude	Cruise Mach	Crossover altitude
260 kts to 320 kts	30,000 ft to 35,000 ft	0.72 to 0.78	≈22,000 ft to ≈32,500 ft

Similar remarks can be made for 10 different climb scenarios by using the parameter combinations shown in Table 4.2. It is important to precise that for all simulations, the initial aircraft weight and the gravity center remain unchanged, thus, they were set for a heavy (70,000 lb) configuration of the aircraft. The results obtained in terms of time, distance and fuel burnt for the “Maximum Ground Distance” and “Minimum Time” strategies are displayed on Figure 4.13, Figure 4.14 and Figure 4.15, respectively.

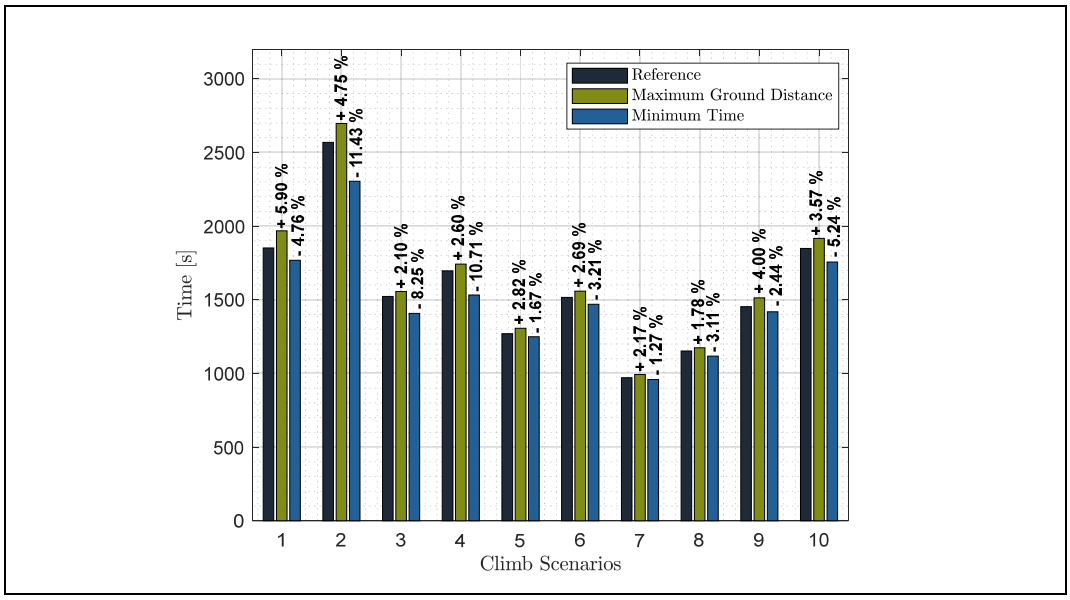

Figure 4.13 Results obtained in terms of time for 10 climb speed schedules for the CRJ700 aircraft model equipped with adaptive ("Maximum Ground Distance" (green) and "Minimum Time" (blue) strategies) and fixed winglets (black)

For all 10 scenarios performed, it was observed that by using the “Minimum Time” strategy (results indicated by the blue bars), the ToC was reached in from 1.21% to 11.43% (5.2% on average) less time than with the reference (Figure 4.13).

For the other strategy, that, of covering the “Maximum Ground Distance” before reaching the ToC, (shown in green), the time to reach the ToC is longer than the time required by the reference aircraft. This time is as expected, given that this strategy seeks to increase the horizontal distance travelled, and not to optimize the time. In this case, while the aircraft took

more time to reach the ToC, it had already covered a part of the “cruise” distance by that time. The resulting cruise distance is therefore smaller when using the “Maximum Ground Distance” strategy than that of the reference vertical climb profile.

Figure 4.14 shows that using the “Maximum Ground Distance” strategy of the aircraft equipped with adaptive winglets allows the aircraft to cover from 1.86% to 6.38% (3.44% on average) more distance than the reference aircraft equipped with a fixed winglet. This increased distance could be especially advantageous for some flights.

Being able to maximize the ground distance using the adaptive winglet strategy is a very interesting advantage for a flight, as it increases the possibility to save time from the global flight time perspective. However, this strategy is not the most ecological approach, as the “Maximum Climb” engine regime must be used for a longer period than that of the reference flight. This engine regime (MXCL) consumed more fuel than the engine regimes typically used during cruise, which explains why fuel burnt using the “Maximum Ground Distance” strategy is greater by 1.66% to 5.13% than that of the reference. However, the longer an aircraft can fly further than the reference, the greater the amount of time is saved at the end of the flight (Figure 4.14 and Figure 4.15). On the contrary, the “Minimum Time” strategy should reduce the fuel burnt while also reducing the time to reach the ToC. Indeed, Figure 4.15 shows that the fuel burnt to reach the ToC could be reduced by 1.16% to 10.34% with respect to the reference.

Globally, the results have shown that the adaptive winglet offers airliners different strategies. According to the chosen strategy, adaptive winglets improve the original aircraft performances by either increasing the ground distance traveled during the climb or reducing the time and the fuel burnt to reach the ToC.

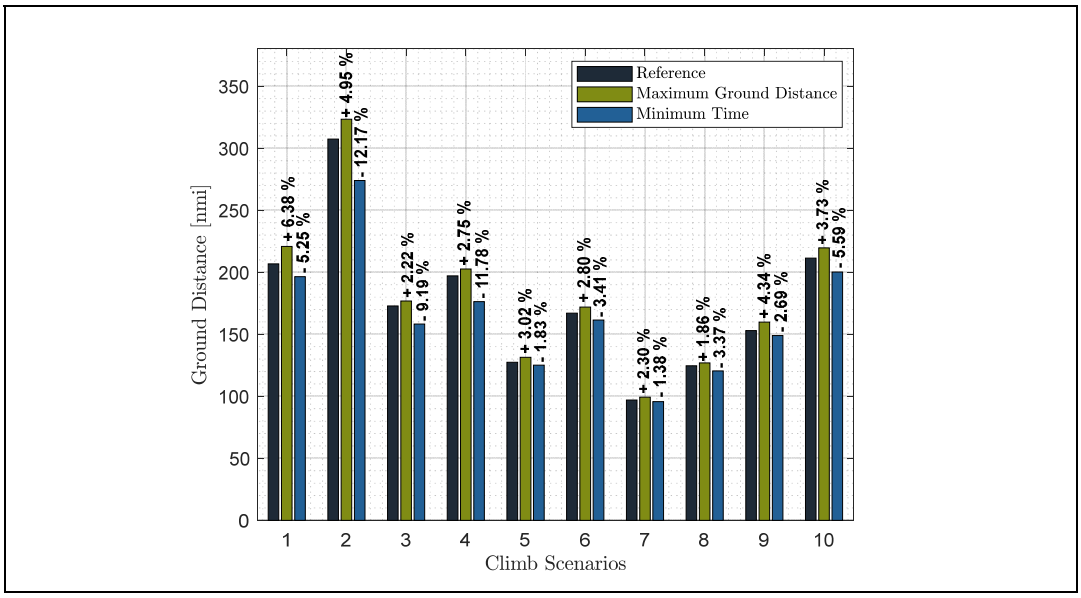

Figure 4.14 Results obtained in terms of distance for 10 climb speed schedules for a CRJ700 aircraft model equipped with adaptive ("Maximum Ground Distance" (green) and "Minimum Time" (blue) strategies) and fixed winglets (black).

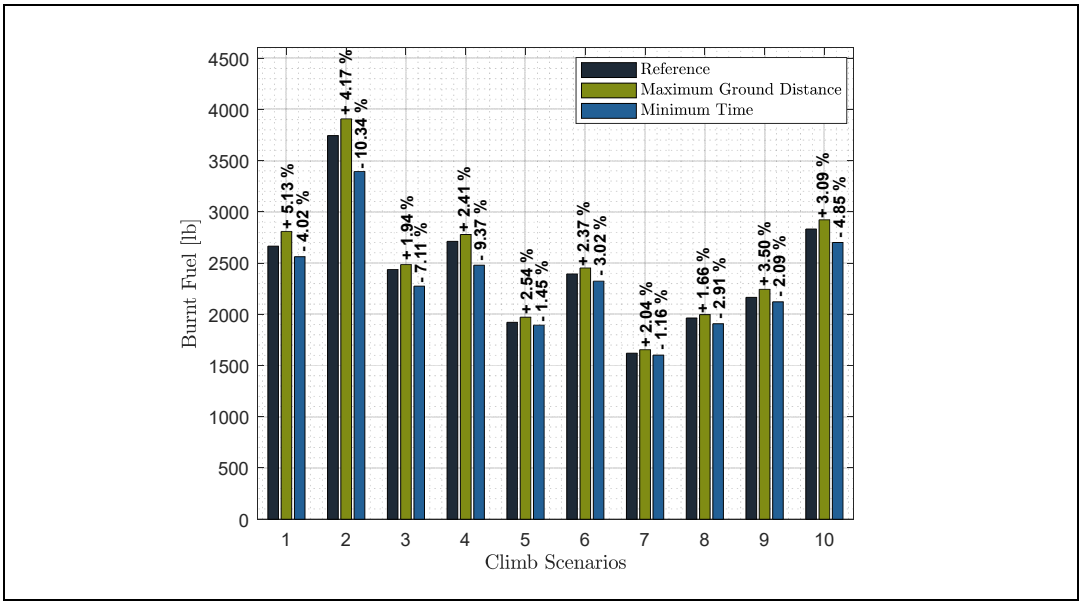

Figure 4.15 Results obtained in terms of fuel burnt for 10 climb speed schedules for a CRJ700 aircraft model equipped with adaptive ("Maximum Ground Distance" (green) and "Minimum Time" (blue) strategies) and fixed winglets (black).

To obtain statistically significant results, 69 climb scenarios were then evaluated. For these 69 scenarios, the first segment was always identical due to the FAA restriction (CAS = 250kts from 5,000ft to 10,000 ft) and the maximum initial aircraft weight was standard (70,000 lbs). The following climb segments were defined by varying the top of climb (ToC) between 30,000 ft and 35,000 ft, the constant Mach number climb from 0.72 to 0.78, the constant CAS climb from 280 to 320 kts, and the center of gravity (CG) from 25 to 30% of the chord. The performances in terms of ground distance, time and fuel burnt obtained for the CRJ700 model equipped with the original fixed winglet and the adaptive winglets were recorded.

A Gauss distribution of the absolute and relative differences between the performances of the aircraft equipped with fixed or adaptive winglets was computed. The results obtained for 95% of the cases are reported in Table 4.3. The equations used to compute the absolute ΔX_{val} and relative errors $\Delta X_{\%}$ are expressed in Eqs. (4.14) and (4.15), respectively:

$$\Delta X_{\mathrm{val}} = X_{\mathrm{ref}} - X_{\mathrm{opt}} \tag{4.14}$$

$$\Delta X_{\%} = 100 \times \frac{\Delta X_{\mathrm{val}}}{X_{\mathrm{ref}}} \tag{4.15}$$

where X_{ref} is the reference value (of distance, time or fuel burnt) obtained for the CRJ700 model equipped with the fixed winglet, and X_{opt} is the value obtained for the CRJ700 model equipped with the adaptive winglet configuration.

Table 4.3 presents several different types of results. First of all, there are “negative” and “positive” signs in both the “Minimum Time” and “Maximum Ground Distance” columns, which indicates that either the time and fuel consumption have been improved, or the distance achieved, all with respect to the reference (fixed winglets). Once again, the performances presented in these two columns are those obtained for a CRJ700 aircraft model equipped with adaptive winglets with respect to that of its initial configuration (fixed winglets). Consequently, according to the desired flight optimization, an aircraft equipped with adaptive

winglets could, using the same speed schedule, either reduce the time and the fuel burnt to reach the ToC or maximize the ground distance covered during climb.

Table 4.3 Statistical performance differences obtained in 95% of cases for the CRJ700 model equipped with adaptive winglets compared to standard fixed winglets for 69 climb scenarios

	Minimum Time	**Maximum Ground Distance**
Δt_s	71.25 ± 63.27 s	-45.22 ± 27.98 s
$\Delta t_{\%}$	4.21 ± 2.60 % (*reduced*)	-2.79 ± 0.97 % (*increased*)
ΔD_{nmi}	8.71 ± 8.09 nmi	-5.35 ± 3.55 nmi
$\Delta D_{\%}$	4.54 ± 2.80 % (*reduced*)	-2.95 ± 1.04 % (*increased*)
ΔF_b	98.62 ± 83.12 lb	-61.72 ± 33.41 lb
$\Delta F_{b\%}$	3.79 ± 2.32 % (*reduced*)	-2.49 ± 0.80 % (*increased*)

For 95% of the 69 cases evaluated, the adaptive winglet configuration allowed the CRJ 700 aircraft to reduce the time to reach the ToC by 71.25 s ± 63.27s and reduce the corresponding fuel burnt by 3.79 ± 2.32 %. Reaching the ToC with a difference of more than 1 minute while consuming on average 3.79% of less fuel than the reference (fixed aircraft) represents a very promising result. However, if optimizing the time or the fuel burnt to reach the ToC is not considered a priority for some reason by an airline, the aircraft equipped with adaptive winglets can also increase the ground distance covered during climb by 5.35 ± 3.55 n miles, an improvement of 2.95 ± 1.04 % with respect to the reference aircraft.

The results presented in Table 4.3 confirm the statements summarizing the information on 10 scenarios graphically presented in Figure 4.12 to Figure 4.15. The adaptive winglet clearly allows the CRJ700 to improve its climb performance. The range of improvement is impressively large (distance, time or fuel burnt), as the adaptive winglets can be set according

to the desired climb strategy (“Minimum Time” or “Maximum Ground Distance”). By choosing an adaptive winglet configuration, the strategy can be changed from one flight to another and lead to globally more efficient aircraft performance.

4.3.2 Cruise scenarios

A flight trajectory can be optimized by choosing the best compromise between the fuel burnt and the time required for its scheduled arrival (Blake et al., 2009 ; Flight Operations Support & Line Assistance teams & Customer Service, 2002). For the same fixed crew costs, the flight cost can be expressed using Eq. (4.16), where W_f is the fuel flow in lb/h, CI is the Cost Index of the flight in lb/h ($/h / $/lb) and GS is the aircraft Ground Speed in kts (Ghazi & Botez, 2017 ; Ghazi et al., 2021 ; Ghazi, Botez, et al., 2020).

$$FC = \frac{W_f + 100 \times \mathrm{CI}}{\mathrm{GS}} \tag{4.16}$$

The Cost Index is a value that ranges from 0 to 999 lb/h. It represents an “optimization criteria” for airliners, as this value is used to find the balance between the flight time constraint and the total fuel needed to operate a flight. If CI = 0 lb/h, minimizing the flight cost *FC* is similar to reducing the fuel consumption; contrarily, if CI = 999 lb/h, minimizing the flight cost *FC* is similar to reducing the flight time.

To consider both time and fuel advantages during cruise, a first study was conducted to analyze the flight cost corresponding to an aircraft equipped with adaptive or fixed winglets for a typical cruise schedule. This analysis considered a cruise where the aircraft weight was varied between 70,000lb (heavy) to 50,000 lb (light), the Mach number was fixed to 0.75, and the altitude fixed to 30,000 ft. The results were obtained for a Cost Index variation of from 0 lb/h to 999 lb/h, and they are presented in Figure 4.16.

Figure 4.16 shows the flight costs computed for three weight configurations: heavy (70,000lb), indicated in “purple” color, medium (60,000lb) in “grey” color and light (50,000lb) in “blue” color according to the winglet deflection angle, which varied from -93 to 93 deg. The reference flight cost for each of the three weight configurations is illustrated using a white square, corresponding to a winglet deflection angle of 73 deg.

The dashed green line in Figure 4.16 connects, for a given Cost Index (CI) value, the minimum cost that can be obtained using an adaptive winglet. For all Cost Index studied, the minimal flight cost for a heavy configuration (purple) was obtained for a winglet deflection angle ξ of close to 0 deg, while this minimum cost for a light configuration (blue) required a winglet deflection angle ξ of close to -30 deg.

The relative difference between the optimal and the reference winglet deflection angle is indicated in green, just below where the green dashed line shows the minimum flight cost value. It is clear that the highest flight cost reduction occurs when the aircraft has a medium to light weight. When a flight is optimized from the perspective of fuel consumption, and thus for a very low Cost Index(CI) of 0 lb/h, we can observe that the flight cost can be reduced from 7.04% to 12.37% when the aircraft has a medium or light weight, respectively (Figure 4.16(a)).

An increasing cost index value means that the cost of a flight will depend more and more on the required flight time. We have observed that the improvement brought by adaptive winglets becomes less significant in these conditions. For instance, by considering a medium weight of 60,000 lb, the flight cost reduction allowed by the adaptive winglet varies from 7.04% to 0.27% for a Cost Index of 0 lb/h to 999 lb/h (the extremum values of this parameter). This aspect can be explained from the strategy used. Indeed, to optimize a flight, the aircraft as well as the speed schedule can be optimized. To optimize the flight time, it is imperative to improve the speed schedule. This aspect was considered as fixed in this research in order to highlight the performance improvement of an aircraft equipped with adaptive winglets compared to the same flight plan as an aircraft equipped with fixed winglets. However, the flight cost may be further reduced if optimal trajectories’ prediction and/or improved speed schedules can be

utilized (R. M. Botez et al., 2018 ; Communier et al., 2019 ; Koreanschi et al., 2016c ; Sugar Gabor et al., 2014).

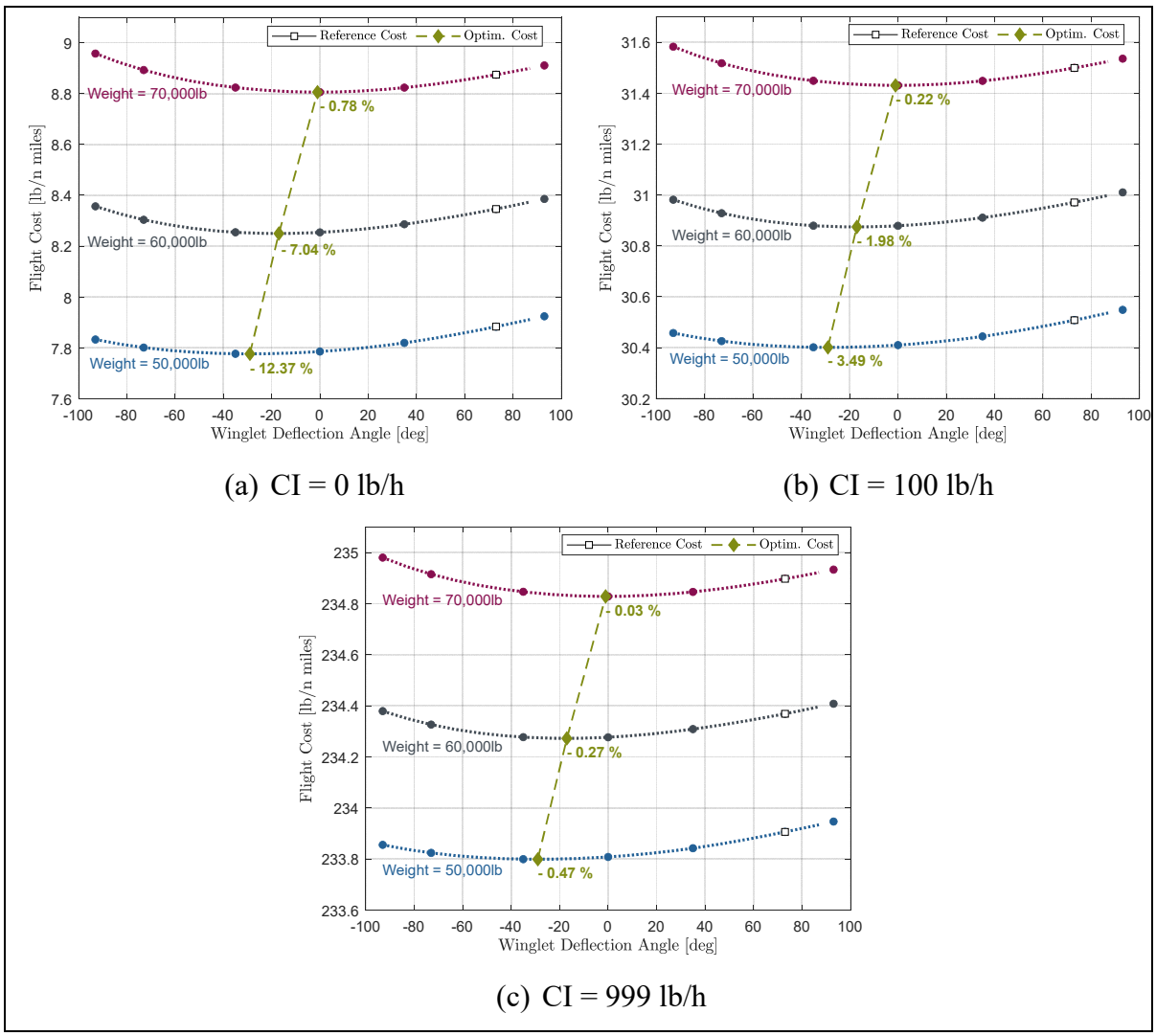

Figure 4.16 Flight costs obtained for different winglet deflection angles during a cruise performed at Mach number 0.75 and altitude 30,000 ft.

To study the statistical results, 86 different cruise scenarios were considered, in which the aircraft weight varied from 70,000lb (heavy) to 50,000 lb (light), the cruise Mach number from 0.60 to 0.79, and the altitude from 15,000 ft to 35,000 ft (this range includes a cruise step performed at low altitude). As indicated earlier, the adaptive winglet helps to improve the fuel consumption during cruise, but not (directly) the time to reach an aircraft's destination.

Therefore, only the fuel flow was studied subsequently, as it evaluates the flight cost using a Cost Index of 0 lb/h.

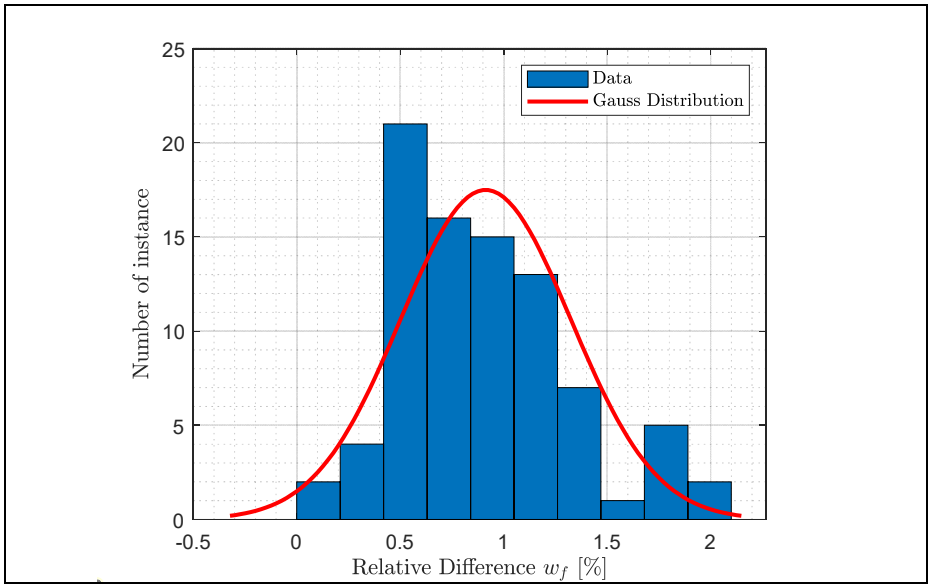

Figure 4.17 The relative difference of the fuel flow for aircraft equipped with adaptive or fixed winglets for 86 cruise conditions

Figure 4.17 shows that the fuel flow was reduced by up to 1.99 % when the aircraft was equipped with an adaptive winglet with respect to an aircraft equipped with fixed winglets. Overall, the fuel flow was reduced from 0.53% to 1.16%, a promising result. Using a Gauss distribution, the fuel flow was reduced by 0.91±0.42% in 95% of cases.

4.3.3 Climb and Cruise scenarios

Finally, a last analysis was performed by combining climb and cruise segments. A “minimum time” strategy was chosen for the climb segment, while a horizontal distance of 600 nautical miles was set to end the complete cruise segment. The 10 scenarios shown on Figure 4.18 (a) were simulated. At the end of these simulations, the total fuel consumed by the reference aircraft and by the aircraft equipped with an adaptive winglet was collected, and the difference of these values was displayed in Figure 4.18 (b).

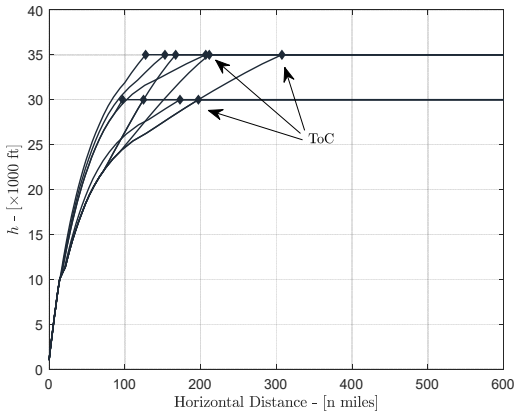

(a) Climb-Cruise scenarios simulated

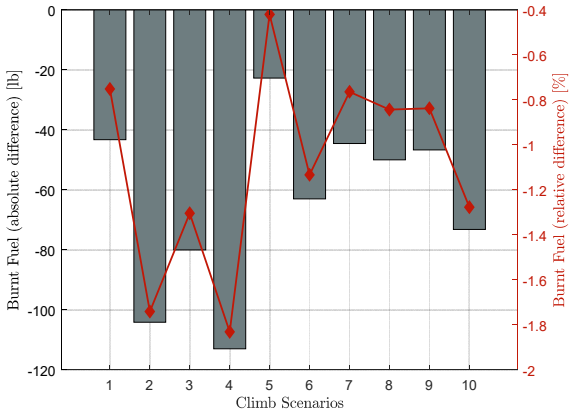

(b) Fuel difference obtained (fixed winglet-adaptive winglet)

Figure 4.18 Fuel burnt difference obtained for different climb/cruise scenarios between the CRJ700 equipped with fixed or adaptive winglets

Typical flight performed by the CRJ700, such as climbing to cruise altitude between 30,000 ft and 35,000 ft, and a constant Mach speed maintained during cruise between 0.72 and 0.78, were chosen for this analysis. Therefore, the results obtained in this context could be very representative of performance that could be obtained in the operational condition of the aircraft. Figure 4.18 (b) shows that the fuel burn differences are all negative, meaning that an aircraft equipped with adaptive winglets always consumes less fuel than the original aircraft (equipped with fixed winglets). Fuel savings of up to 113 lb (1.83%) were achieved using an adaptive winglet with respect to an aircraft equipped with a fixed winglet. It was also observed that results obtained in Figure 4.18 (b) were close to those obtained previously for the 86 cruise scenarios in Figure 4.17, which confirm the benefits observed separately for the climb or cruise segments.

4.4 Conclusion

The aerodynamic characteristics of an aircraft equipped with adaptive winglets compared to the original configuration of the aircraft (fixed winglets) have been emphasized through a previous study. To summarize the results, the lift-to-drag ratio had been improved up to 6.10% and the drag coefficient had been reduced up to 2.90% for an equivalent lift coefficient

(CHAPTER 3). Following this aerodynamic analysis, the objective of this new study was to analyze the performances in climb and cruise of an aircraft equipped with adaptive winglets.

The methodology has illustrated how the aerodynamic properties of the “wing-body” of the CRJ700 aircraft model were computed from global aerodynamic coefficients obtained using the OpenFoam software (the CFD computation method). A methodology to compute the downwash deviation angles using OpenFoam was also shown.

The second part of the methodology presented the performance model utilized to compute the performances of a CRJ700 aircraft equipped with adaptive winglets. This performance toolbox was validated in a previous study, in which errors of less than 5% were obtained with respect to data provided by level D flight simulators (Ghazi et al., 2021). Based on this reliable and accurate performance model, some modifications were made in order to integrate the winglet deflection selection for aircraft equipped with adaptive winglets.

The results obtained in this paper show that the adaptive winglet configuration of the aircraft allows for the choice of different climb strategies, such as “Minimum Time” or “Maximum Ground Distance”. For a strategy that minimizes the time to climb, the adaptive winglet allows the aircraft to reach the ToC from 7.98s to 134.52s (71.25 ± 63.27 s) sooner than an aircraft equipped with fixed winglets in 95% of cases. Moreover, it was found that this strategy makes it possible to reach the ToC with a fuel reduction of 1.47% to 6.11% (3.79 ± 2.32 %), a very interesting result.

The other strategy was to maximize the horizontal distance covered during the whole climb profile. The ground distance covered by the aircraft equipped with fixed winglets was increased by up to 5.35 ± 3.55 n miles in 95% of cases for the aircraft with adaptive winglets.

Both of these strategies can be considered by an airline for any given flight. The aircraft equipped with adaptive winglets has shown real advantages in terms of time, fuel or distance depending on the strategy used for the climb to the ToC. During the cruise phase, the use of

adaptive winglets can also allow an aircraft to reduce its fuel flow by 0.91±0.42% in 95% of cases.

Globally, this research has shown that adaptive winglets could greatly improve the original aircraft configuration (equipped with fixed winglets). Possible future work would be to compute the inertia generated for each winglet deflection motion, and to study the dynamic aircraft behavior with the objective of certifying aircraft stability throughout a flight. Stability analysis should be performed by considering flutter phenomenon that could occur due to aircraft configuration change (i.e., adaptive winglet). Indeed, the flutter impact need to be investigated as it may represent an obstacle to develop adaptive winglets for civil aircrafts.

CONCLUSION AND RECOMMENDATIONS

This thesis has presented a literature review and the methodology developed to optimize aircraft flight performances using adaptive winglet technology.

The last 20 years of research have shown that morphing wing technologies can significantly improve aircraft performance. However, most of them have some disadvantages, as they may increase the weight to integrate the new morphing system or reduce the fuel tanks' capabilities because the new system is usually located inside of the main wing of an aircraft and therefore the fuel tanks' size would have to be reduced.

The literature review revealed that different winglet shapes can change aircraft cruise efficiency by up to 9%. That led to the supposition that there could be different winglet shapes that allow to optimize a specific aircraft design, according to the varying flight conditions of its flight envelope.

The solution proposed consisted of a winglet design that could be adapted during the flight in order to perform most efficiently at each point of the flight. The choice of an adaptive winglet was supported by the fact that the winglet is one of the last surfaces added during the assembly of an aircraft. Consequently, an adaptive winglet concept represents an efficient, rapid and cost-effective solution to implement, since it could reduce aircraft fuel consumption and thus achieve the objectives of the International Civil Aviation Organization (ICAO) in a short time.

The challenge of this thesis is to design this new adaptive winglet design, and to analyze the advantages and benefits that can be provided to an aircraft during its flight. The complete methodology was applied on the regional jet CRJ700 aircraft because the LARCASE has complete and accurate data for this aircraft. A precise CAD drawing provided by the manufacturer Bombardier and a level-D flight simulator designed by the CAE company are the tools that were essential to obtain the geometrical and flight test data, respectively.

Another advantage of using the CRJ700 aircraft is that it is widely operated in North America and in Europe for 2-to 4-hour flights. Therefore, it is a very representative aircraft of the world air fleet. In other words, the benefits found in this research could also indicate the benefits of using the same adaptive system on other similar type of aircraft.

The methodology developed to reach the objective of this thesis was detailed in the last three chapters, making it possible to analyze the aerodynamic characteristics and flight performances of an aircraft equipped by an adaptive winglet for several climb and cruise scenarios.

To analyze the adaptive winglet advantages, it was first necessary to design a high-fidelity computational tool. This research was developed in CHAPTER 2. As suggested by preliminary studies, an aerodynamic model based on the resolution of Navier-Stokes equations was developed. Indeed, adaptive winglets have a major impact on lift-induced drag, which can be highlighted using low fidelity calculation method, such as the Vortex Lattice Method (VLM). However, high fidelity methods were required to analyze the turbulence effects and some disturbances of the fluid around the winglets.

The high-fidelity aerodynamic model was designed using OpenFoam toolbox software. Widely used, this CFD code was chosen to investigate this research for its accuracy and parameterized properties. The meshes were designed using *blockMesh* and *snappyHexMesh* utilities (available in OpenFoam tools), and they considered several parameters. Simulations were set to be run for these generated meshes using several criteria that can offer a good compromise between convergence and accuracy. Indeed, a new methodology was developed by using two successive flow solvers coupled with different properties. A first simulation was performed with an incompressible solver, *simpleFoam*, coupled with a Spalart-Allmaras (S-A) turbulence model. The S-A turbulence model is a one-equation model that verifies that a property is accurate, especially in an aircraft flight context. *SimpleFoam* solver deals with incompressible flow equations, which are simpler to solve than compressible flow equations because there are fewer unknown values (e.g., temperature, air density and turbulence

parameters). Consequently, this first simulation using *simpleFoam* provided good convergence in the computed performances.

Next, to reach a more accurate solution, especially for high Mach number simulations, a second simulation was developed, using the compressible solver *rhoSimpleFoam*. Simulations were initialized using the converged solution obtained in the first incompressible simulation, which helped to be very close to a good solution. A two-equation turbulence model, $k-\omega$ SST, commonly used for the range of conditions used for an aircraft (subsonic and transonic), was coupled with a *rhoSimpleFoam* solver simulation. This second simulation provided accurate results.

Globally, the methodology developed to design this aerodynamic model was very efficient, as accurate results were obtained in a relatively short computational time (22h on average). Simulations were performed for 35 flight conditions where the altitude varied from 5,000 ft to 35,000 ft and the Mach number from 0.31 to 0.79. The aerodynamic coefficients obtained by the model have been compared to those provided by the flight simulator VRESIM. The lift, drag and pitching moment coefficient were predicted by the model within -0.007±0.045%, -0.00015±0.00114% and -0.0077±0.0079% margin of error, respectively, in 95% of cases.

This accurate model developed for the original CRJ700 design was then used to analyze the aerodynamic forces applied on the aircraft equipped with adaptive winglet. The same parameters used to design the aerodynamic model (mesh and simulation settings) were used by assuming that the aircraft geometry has similar shape when is equipped with a fixed or an adaptive winglet. As computational cost was expensive, the methodology consisted of analyzing specific winglet deflection angles for several flight conditions. A total of 25 flight conditions for 7 winglet deflections angles (175 cases) were simulated. These simulations made it possible to design aerodynamic coefficient predictions for all winglet deflection angles and all the conditions available in the flight envelope. The adaptive winglet advantages listed in the preliminary study were verified with these analyses. The lift-to-drag ratio was increased

by up to 6.10%, which indicated that for a constant lift coefficient, the drag coefficient has been reduced by up to 1.30% on average using an adaptive winglet.

Encouraged by the very promising results obtained during the aerodynamic analysis (CHAPTER 3), a performance analysis was done to analyze the climb and cruise benefits observed using an adaptive winglet. An in-house performance model was set up to be used for the "new" CRJ700 equipped with an adaptive winglet. A methodology was developed to compute the aerodynamic contributions of the aircraft wing and tail and of the downwash deviation angle produced by the wing. Several climb scenarios generally utilized by the CRJ700 were simulated for the CRJ700 equipped with fixed and with adaptive winglets. Performance comparisons showed that the adaptive winglet provided a time advantage (reduction) to reach the top of climb of 4.21s ± 2.68% (71.25 ± 63.27s) on average and a fuel burn advantage (reduction) of 3.79 ± 2.32% (98.62 ± 83.12lb) on average, with respect to the original aircraft configuration (fixed winglet). Similarly, cruise simulations were performed at several conditions usually operated by the aircraft. The CRJ700 equipped with adaptive winglets consumed on average 1.99% less fuel flow than a CRJ700 equipped with fixed winglets.

Descent phases were not analyzed, as they do not consume much energy. Therefore, trying to reduce fuel consumption during these phases would not be significant or worth the investment.

In this thesis different methodologies were developed to analyze aircraft equipped with adaptive winglets. These methodologies have been validated and it was shown to be very accurate. In addition, the advantages of equipping an aircraft with adaptive winglets were demonstrated. Aerodynamic and performance evaluations were the two aspects to be studied in the first objectives.

Based on these very promising results, it is recommended to continue this work and perform some complementary analyses. Structural analyses could be conducted to estimate the exact weight required to be added to an aircraft not initially equipped with a rotating winglet (all

aircraft, except the Boeing 777x). This kind of study could also allow the new inertia of an aircraft to be computed.

Another recommendation would be to perform lateral analysis, especially of a non-symmetrical rotation of the winglets on both sides of a wing. This analysis could highlight some specific benefits, specifically during turns. It should also be interesting to include operational challenges analysis such as icing phenomenon.

Adaptive winglets could also be incorporated in take-off and landing phases, as they could offer performance advantages. For the take-off phase, downward winglets could offer a larger wing surface than usually and thus more lift. Consequently, aircraft equipped with adaptive winglets could take off on shorter runways than originally specified or carry a higher payload. Similarly, for landing, an aircraft could reach a lower speed than the original stall speed, which could lead to a softer landing. A reduction of maintenance costs, especially in terms of landing gear fatigue, could then be expected, as well as some noise reduction.

By coupling the study performed in this thesis with the proposed future analyses, a longitudinal and lateral stability analysis could be developed to specify aircraft stability performance. Finally, a controller could be designed to control the adaptive winglet motion during flight.

LIST OF BIBLIOGRAPHICAL REFERENCES

Air Transport Action Group (ATAG). (2018). *Aviation: Benefits Beyond Borders report* (Rapport No. 2018 edition). Retrieved from https://www.aviationbenefits.org/media/166711/abbb18_full-report_web.pdf

Airbus. (2020). *Airbus' "BLADE" laminar flow wing demonstrator makes first flight*. Retrieved from https://www.airbus.com/newsroom/press-releases/en/2017/09/airbus_-_blade_-laminar-flow-wing-demonstrator-makes-first-fligh.html

Airbus. (2020, 8 avril). The E-Fan X puts its aerodynamic design to the test. *Airbus*. Retrieved from https://www.airbus.com/en/newsroom/stories/2020-02-the-e-fan-x-puts-its-aerodynamic-design-to-the-test

Ameduri, S., & Concilio, A. (2020). Morphing wings review: aims, challenges, and current open issues of a technology. *Proceedings of the Institution of Mechanical Engineers, Part C: Journal of Mechanical Engineering Science*, *1*(1), 1-19. https://doi.org/10.1177/0954406220944423

Amendola, G., Dimino, I., Concilio, A., Pecora, R., & Amoroso, F. (2019). A linear guide-based actuation concept for a novel morphing aileron. *The Aeronautical Journal*, *123*(1265), 1075-1097, https://doi.org/10.1017/aer.2019.35

Amendola, G., Dimino, I., Concilio, A., Andreutti, G., Pecora, R., & Cascio, M. L. (2017). Preliminary Design Process for an Adaptive Winglet. *International Journal of Mechanical Engineering and Robotics Research*, *6*(6), 83-92. https://doi.org/10.18178/ijmerr.7.1.83-92

Anderson, J. D. (2017). *Fundamentals of aerodynamics* (Sixth edition). New York, NY : McGraw Hill Education.

Ashton, N., & Skaperdas, V. (2019). Verification and Validation of OpenFOAM for High-Lift Aircraft Flows. *Journal of Aircraft*, *56*(4), 1641-1657. https://doi.org/10.2514/1.C034918

Ashton, N., Unterlechner, P., & Blacha, T. (2018). Assessing the Sensitivity of Hybrid RANS-LES Simulations to Mesh Resolution, Numerical Schemes and Turbulence Modelling within an Industrial CFD Process, In WCX World Congress Experience. https://doi.org/10.4271/2018-01-0709

Aviation: Benefits Beyond Borders. (2018). *Aviation: Benefits Beyond Borders report*, Retrieved from https://www.aviationbenefits.org/media/166711/abbb18_full-report_web.pdf

Bacchini, A., & Cestino, E. (2020). Key aspects of electric vertical take-off and landing conceptual design. *Proceedings of the Institution of Mechanical Engineers, Part G: Journal of Aerospace Engineering*, *234*(3), 774-787. https://doi.org/10.1177/0954410019884174

Bacchini, A., Cestino, E., Van Magill, B., & Verstraete, D. (2021). Impact of lift propeller drag on the performance of eVTOL lift+cruise aircraft. *Aerospace Science and Technology*, *109*, 106429. https://doi.org/10.1016/j.ast.2020.106429

Bardela, P.-A., Botez, R. M., Bournisien, T., & Rusovici, R. (2018). Identification and Validation of the Cessna Citation X Turbofan Modelling with Flight Tests. In *2018 AIAA Modeling and Simulation Technologies Conference*. Kissimmee, Florida, USA : American Institute of Aeronautics and Astronautics. https://doi.org/10.2514/6.2018-1920

Bashir, M., Longtin-Martel, S., Botez, R. M., & Wong, T. (2021). Aerodynamic Design Optimization of a Morphing Leading Edge and Trailing Edge Airfoil–Application on the UAS-S45. *Applied Sciences*, *11*(4), 1664. https://doi.org/10.3390/app11041664

Behrens, A., Grund, T., Ebert, C., Luckner, R., & Weiss, J. (2020). Investigation of the aerodynamic interaction between two wings in a parallel flight with close lateral proximity. *CEAS Aeronautical Journal*, *11*(2), 553-563. https://doi.org/10.1007/s13272-019-00435-9

Blake, W., The performance Training Group, & Flight Operations Engineering. (2009). *Jet Transport Performance Methods* (Rapport No. D6-1420). Seattle, Washington, USA : Boeing Company.

Boeing. (2013). the 777x aircraft. Boeing commercial. Retrieved from https://www.boeing.com/commercial/777x/

Bombardier. (2019). *CRJ Series*, CRJ700. Canada. Retrieved from: commercialaircraft.bombardier.com

Botez, R. (2018). Morphing Wing, UAV and Aircraft Multidisciplinary Studies at the Laboratory of Applied Research in Active Controls, Avionics and AeroServoElasticity

LARCASE. *AerospaceLab Journal*, *Issue 14*, September 2018; ISSN: 21076596. https://doi.org/10.12762/2018.AL14-02

Botez, R. M. (2018). Morphing Wing, UAV and Aircraft Multidisciplinary Studies at the Laboratory of Applied Research in Active Controls, Avionics and AeroServoElasticity LARCASE. *AerospaceLab Journal*, *Issue 14*, September 2018; ISSN: 21076596. https://doi.org/10.12762/2018.AL14-02

Botez, R. M., Koreanschi, A., Sugar Gabor, O., Tondji, Y., Guezguez, M., Kammegne, J. T., Concilio, A. (2018). Numerical and experimental transition results evaluation for a morphing wing and aileron system. *The Aeronautical Journal*, *122*, 1-38. https://doi.org/10.1017/aer.2018.15

Botez, Ruxandra M., Bardela, P.-A., & Bournisien, T. (2019). Cessna Citation X Simulation Turbofan Modelling: Identification and Identified Model Validation Using Simulated Flight Tests. *The Aeronautical Journal*, *123*, 1-31. https://doi.org/10.1017/aer.2018.166

Bourdin, P., Gatto, A., & Friswell, M. I. (2008). Aircraft Control via Variable Cant-Angle Winglets. *Journal of Aircraft*, *45*(2), 414-423. https://doi.org/10.2514/1.27720

Bourdin, Patrick, Gatto, A., & Friswell, M. (2006). The Application of Variable Cant Angle Winglets for Morphing Aircraft Control. In *24th AIAA Applied Aerodynamics Conference*. San Francisco, California : American Institute of Aeronautics and Astronautics. https://doi.org/10.2514/6.2006-3660

Burdette, D. A., & Martins, J. R. R. A. (2019). Impact of Morphing Trailing Edges on Mission Performance for the Common Research Model. *Journal of Aircraft*, *56*(1), 369-384. https://doi.org/10.2514/1.C034967

Cantwell, B. (2014). *Chapter 12: Wings of finite span*, Stanford University, course notes, Retrieved from: https://web.stanford.edu

Caretto, L. S., Gosman, A. D., Patankar, S. V., & Spalding, D. B. *Two Calculation Procedures for Steady, Three-Dimensional Flows with Recirculation* (Rapport No. 197315). National Aeronautics and Space Administration (NASA).

Carossa, G. M., Ricci, S., De Gaspari, A., Liauzun, C., Dumont, A., & Steinbuch, M. (2016). Adaptive Trailing Edge: Specifications, Aerodynamics, and Exploitation. In *Smart Intelligent Aircraft Structures (SARISTU)* 143-158. Springer International Publishing. https://doi.org/10.1007/978-3-319-22413-8_7

Castrichini, A., Siddaramaiah, V. H., Calderon, D. E., Cooper, J. E., Wilson, T., & Lemmens, Y. (2017). Preliminary investigation of use of flexible folding wing tips for static and dynamic load alleviation. *The Aeronautical Journal*, *121*(1235), 73-94. https://doi.org/10.1017/aer.2016.108

Cestino, E., Frulla, G., Spina, M., Catelani, D., & Linari, M. (2019). Numerical simulation and experimental validation of slender wings flutter behaviour. In *Proceedings of the Institution of Mechanical Engineers, Part G: Journal of Aerospace Engineering*, *233*(16), 5913-5928. https://doi.org/10.1177/0954410019879820

cfdsupport. (2020). *CFDsupport OpenFoam for windows*. Retrieved from https://www.cfdsupport.com/openfoam-for-windows.html

Cheung, R. C. M., Rezgui, D., Cooper, J. E., & Wilson, T. (2018). Testing of a Hinged Wingtip Device for Gust Loads Alleviation. *Journal of Aircraft*, *55*(5), 2050-2067. https://doi.org/10.2514/1.C034811

Chevalier, C., & Pellegrini, F. (2008). PT-Scotch: A tool for efficient parallel graph ordering. *Parallel Computing*, *34*(6-8), 318-331. https://doi.org/10.1016/j.parco.2007.12.001

Communier, D., Botez, R. M., & Wong, T. (2019). Experimental validation of a new morphing trailing edge system using Price – Païdoussis wind tunnel tests. *Chinese Journal of Aeronautics*, *32*(6), 1353-1366. https://doi.org/10.1016/j.cja.2019.03.016

Comparing CFD Software - Part 2: Open Source CFD Software Packages. *Resolved Analytics CFD Consulting and Simulation Strategy*. Retrieved from https://www.resolvedanalytics.com/theflux/comparing-cfd-software-part-2-open-source-cfd-software-packages

Concilio, A., Dimino, I., Lecce, L., & Pecora, R. (2018). *Morphing wing technologies: large commercial aircraft and civil helicopters*. United Kingdom ; Cambridge, MA : Butterworth-Heinemann, is an imprint of Elsevier.

Concilio, A., Dimino, I., & Pecora, R. (2021). SARISTU: Adaptive Trailing Edge Device (ATED) design process review. *Chinese Journal of Aeronautics*, *34*(7), 187-210. https://doi.org/10.1016/j.cja.2020.08.036

Cooper, J. E. (2020, 10 avril). Control and Alleviation of Loads in Advanced Regional Turbo Fan Configurations (CLARET) - Final Report Summary. Retrieved from https://cordis.europa.eu/project/id/287078/reporting

Cooper, J. E., Chekkal, I., Cheung, R. C. M., Wales, C., Allen, N. J., Lawson, S., Carossa, G. M. (2015). Design of a Morphing Wingtip. *Journal of Aircraft*, *52*(5), 1394-1403. https://doi.org/10.2514/1.C032861

Cummins, N. (2019). The A350 vs B787 Dreamliner: which plane is best? Retrieved from https://simpleflying.com/boeing-787-vs-the-airbus-a350/.

Dancila, B., Beulze, B., & Botez, R. M. (2019). Flight Phase and Altitude-Dependent Geometrical Vertical Flight Plan Optimization Minimizing the Total Number of Vertical Plan Segments. *Proceedings of the Institution of Mechanical Engineers*, *233*(13), 4825-4838. https://doi.org/10.1177/0954410019832127

Dancila, B., & Botez, R. M. (2018). Vertical Flight Path Segments Sets for Aircraft Flight Plan Prediction and Optimisation. *The Aeronautical Journal*, *122*, 1-54. https://doi.org/10.1017/aer.2018.67

Dancila, R., & Botez, R. M. (2019). Vertical Flight Profile Optimization for a Cruise Segment with RTA Constraints. *The Aeronautical Journal*, *123*(1265), 970-992. https://doi.org/10.1017/aer.2019.47

Daniele, E., De Fenza, A., & Vecchia, P. D. (2012). Conceptual adaptive wing-tip design for pollution reductions. *Journal of Intelligent Material Systems and Structures*, *23*(11), 1197-1212. https://doi.org/10.1177/1045389X12445030

Datta, K., & Lagoudas, D. (2021, février). Adaptive Aerostructures for Revolutionary Civil Supersonic Transportation. NASA TechPort. Retrieved from https://techport.nasa.gov/view/96121

Dimino, I., Andreutti, G., Moens, F., Fonte, F., Pecora, R., & Concilio, A. (2021). Integrated Design of a Morphing Winglet for Active Load Control and Alleviation of Turboprop Regional Aircraft. *Applied Sciences*, *11*(5), 2439. https://doi.org/10.3390/app11052439

Duvelleroy, M., Benquet, L., & Ramadier, S. (2020). Airbus reveals its blended wing aircraft demonstrator. *Airbus Newsroom*, *Innovation*.

Elelwi, M., Calvet, T., Botez, R. M., & Dao, T.-M. (2021). Wing component allocation for a morphing variable span of tapered wing using finite element method and topology optimisation – application to the UAS-S4. *The Aeronautical Journal*, *125*(1290), 1313-1336. https://doi.org/10.1017/aer.2021.29

Fangqing, L. (2016). A Thorought Description Of How Wall Function Are Implemented In OpenFOAM. In *CFD with OpenSource Software*. Chalmers University of Technology.

Federal Aviation Administration. (2018). *Special Conditions: The Boeing Company Model 777–8 and 777–9 Airplanes; Folding Wingtips*.

Federal Aviation Administration (FAA). (1991). *Airplane Simulator Qualification* (Rapport No. AC 120-40B). U.S Department of Transportation.

Filippone, A., Parkes, B., Bojdo, N., & Kelly, T. (2021). Prediction of aircraft engine emissions using ADS-B flight data. *The Aeronautical Journal*, 1-25. https://doi.org/10.1017/aer.2021.2

Filippone, A. (2010). Theoretical Framework for the Simulation of Transport Aircraft Flight. *Journal of Aircraft*, *47*(5), 1679-1696. https://doi.org/10.2514/1.C000252

Filippone, A, Zhang, M., & Bojdo, N. (2019). Validation of an integrated simulation model for aircraft noise and engine emissions. *Aerospace Science and Technology*, *89*, 370-381. https://doi.org/10.1016/j.ast.2019.04.008

Finite Volume Method: A crash introduction. *Wold Dynamics - Multiphyisics Simulations, Optimization & Data analytics*.

Firdaus Mohamad, Wirachman Wisnoe, Wahyu Kuntjoro, Nasir, R. E. M., Ali, Z. Mohd., & Nor Fazira Reduan. (2010). Wind Tunnel experiments of UiTM's blended wing body (BWB) Baseline-II unmanned aerial vehicle (UAV) at low subsonic speed. In *2010 International Conference on Science and Social Research (CSSR 2010)* 991-994. Kuala Lumpur, Malaysia : IEEE. https://doi.org/10.1109/CSSR.2010.5773934

Flight Operations Support & Line Assistance teams, & Customer Service. (2002). *Getting to Grips with Aircraft Performance*. Blagnac, France : Airbus company.

Freestone. (1988). *Aerodynamic Principles of Winglets*. Engineering Science Data Unit.

Friedlander, S., & Serre, D. (2007). *Handbook of mathematical fluid dynamics* (1st éd., Vol. 4). Amsterdam : Elsevier.

Galea, E. R., Filippidis, L., Wang, Z., Lawrence, P. J., & Ewer, J. (2011). Evacuation Analysis of 1000+ Seat Blended Wing Body Aircraft Configurations: Computer Simulations and Full-scale Evacuation Experiment. In *Pedestrian and Evacuation Dynamics*, 151-161, Boston, MA. https://doi.org/10.1007/978-1-4419-9725-8_14

Ghazi, G., Bosne, M., Sammartano, Q., & Botez, R. M. (2017). Cessna Citation X Stall Characteristics Identification from Flight Data using Neural Networks. In *AIAA Atmospheric Flight Mechanics Conference*. Grapevine, Texas, USA : American Institute of Aeronautics and Astronautics. https://doi.org/10.2514/6.2017-0937

Ghazi, G., & Botez, R. M. (2017). Method to Calculate Cessna Citation X Aircraft Climb and Cruise Trajectory using an Aero-Propulsive Model. In *AIAA Atmospheric Flight Mechanics Conference*. Denver, Colorado, USA : American Institute of Aeronautics and Astronautics. https://doi.org/10.2514/6.2017-3550

Ghazi, G., & Botez, R. M. (2019). Identification and Validation of an Engine Performance Database Model for the Flight Management System. *Journal of Aerospace Information Systems*, *16*, 1-20. https://doi.org/10.2514/1.I010663

Ghazi, G., Botez, R. M., Bourrely, C., & Turculet, A.-A. (2021). Method for Calculating Aircraft Flight Trajectories in Presence of Winds. *Journal of Aerospace Information Systems*, *18*(7), 442-463. https://doi.org/10.2514/1.I010879

Ghazi, G., Botez, R. M., & Maniette, N. (2020). Cessna Citation X Takeoff and Departure Trajectories Prediction in Presence of Winds. *Journal of Aerospace Information Systems*, *17*(12), 659-681. https://doi.org/10.2514/1.I010854

Ghazi, G., Botez, R. M., & Messi Achigui, J. (2015). Cessna Citation X Engine Model Identification from Flight Tests. *SAE International Journal of Aerospace*, *8*. https://doi.org/10.4271/2015-01-2390

Ghazi, G., Gerardin, B., Gelhaye, M., & Botez, R. M. (2020). New Adaptive Algorithm Development for Monitoring Aircraft Performance and Improving Flight Management System Predictions. *Journal of Aerospace Information Systems*, *17*(2), 97-112. https://doi.org/10.2514/1.I010748

Goold, I. (2018). Flight Tests To Resume on Airbus BLADE Project. *Air Transport* (Singapore Air Show). Retrieved from https://www.ainonline.com/aviation-news/air-transport/2018-02-03/flight-tests-resume-airbus-blade-project

Grigorie, T. L., & Botez, R. (2018). Control Techniques for a Smart Actuated Morphing Wing Model: Design, Numerical Simulation and Experimental Validation. In *Morphing Wing Technologies*, 351-397. https://doi.org/10.1016/B978-0-08-100964-2.00012-5

Grigorie, T. L., Khan, S., Botez, R. M., Mamou, M., & Mébarki, Y. (2019). Design and experimental testing of a control system for a morphing wing model actuated with miniature BLDC motors. *Chinese Journal of Aeronautics*. https://doi.org/10.1016/j.cja.2019.08.007

Grisval, J.-P., & Liauzun, C. (1999). Application of the finite element method to aeroelasticity. *Revue Européenne des Éléments Finis*, *8*(5-6), 553-579. https://doi.org/10.1080/12506559.1999.10511397

Guerrero, J. E., Sanguineti, M., & Wittkowski, K. (2020). Variable cant angle winglets for improvement of aircraft flight performance. *Meccanica*, *55*(10), 1917-1947. https://doi.org/10.1007/s11012-020-01230-1

Haddad, N. (2015). *Aerodynamic and Structural Design of a Winglet for Enhanced Performance of a Business Jet* (M.Sc.A Thesis). Embry-Riddle University.

He, P., Mader, C. A., Martins, J. R. R. A., & Maki, K. J. (2018). An aerodynamic design optimization framework using a discrete adjoint approach with OpenFOAM. *Computers & Fluids*, *168*, 285-303. https://doi.org/10.1016/j.compfluid.2018.04.012

Healy, F., Cheung, R. C., Neofet, T., Lowenberg, M. H., Rezgui, D., Cooper, J. E., Wilson, T. (2021). Folding Wingtips for Improved Roll Performance. In *AIAA Scitech 2021 Forum*. Virtually : American Institute of Aeronautics and Astronautics. https://doi.org/10.2514/6.2021-1153

Heathers, D. (2002, octobre). New Boeing 777 Raked Wing Tips Improve Fuel Efficiency, Good for the Environment. Boeing Mediaroom. Retrieved from https://boeing.mediaroom.com/2002-10-01-New-Boeing-777-Raked-Wing-Tips-Improve-Fuel-Efficiency-Good-for-the-Environment

Herrera, C. Y., Lung, S., Ervin, G., & Flick, P. (2015). Aeroelastic Airworthiness Assesment of the Adaptive Compliant Trailing Edge Flaps. *Patent Number AFRC-E-DAA-TN24639*. Lancaster, CA.

Hitchens, F. (2015). *The Encyclopedia of Aerodynamics*, Andrews UK Limited. (Google-Books-ID: izv0CgAAQBAJ).

Hou, Y., Angland, D., & Scotto, A. (2017). The Ability of a Weakly Compressible Solver to Predict Landing Gear Noise with Flow-Acoustic Interactions. In *23rd AIAA/CEAS Aeroacoustics Conference*. Denver, Colorado : American Institute of Aeronautics and Astronautics. https://doi.org/10.2514/6.2017-3008

How the 777X's folding wing tips work. (2018). *The Air Current*. Retrieved from https://theaircurrent.com/technology/how-the-777xs-folding-wing-tips-work/

Huvelin, F., Dequand, S., Lepage, A., & Liauzun, C. (2018). On the Validation and Use of High-Fidelity Numerical Simulations for Gust Response Analysis. *AerospaceLab Journal*, 16(14). https://doi.org/10.12762/2018.AL14-06

IATA. (2019). *Industry Statistics Fact Sheet* (Rapport No. December 2019). Retrieved from https://www.iata.org/en/iata-repository/publications/economic-reports/airline-industry-economic-performance---december-2019---data-tables/

ICAO. (2010). *Aviation's Contribution to Climate Change*. ICAO. Retrieved from https://www.icao.int/environmental-protection/Documents/EnvironmentReport-2010/ICAO_EnvReport10-Ch1_en.pdf

ICAO. (2016). *Environmental report - Aviation and climate change*. ICAO. Retrieved from https://www.icao.int/environmental-protection/Documents/ICAO%20Environmental%20Report%202016.pdf

ICAO. (2020). Annex 16 - Environmental Protection - Volume IV - Carbon Offsetting and Reduction Scheme for International Aviation (CORSIA). Retrieved from https://store.icao.int/products/annex-16-environmental-protection-volume-iv-carbon-offsetting-and-reduction-scheme-for-international-aviation-corsia

International Air Transport Association (IATA). (2019). *Industry Statistics Fact Sheet* (Rapport No. December 2019). Retrieved from https://www.iata.org/en/iata-repository/publications/economic-reports/airline-industry-economic-performance---december-2019---data-tables/

International Civil Aviation Organization (ICAO). (2010). *Aviation's Contribution to Climate Change*. Retrieved from https://www.icao.int/environmental-protection/Documents/EnvironmentReport-2010/ICAO_EnvReport10-Ch1_en.pdf

Koreanschi, A., Sugar Gabor, O., Acotto, J., Brianchon, G., Portier, G., Botez, R. M., … Mebarki, Y. (2017). Optimization and design of a morphing wing tip aircraft demonstrator for drag reduction at low speed, Part I – Aerodynamic optimizations using genetic, bee colony and gradient descent algorithms. *Chinese Journal of Aeronautics*, *30*. https://doi.org/10.1016/j.cja.2016.12.013

Koreanschi, A., Sugar Gabor, O., Acotto, J., Brianchon, G., Portier, G., Botez, R. M., … Mebarki, Y. (2017). Optimization and design of a morphing wing tip aircraft demonstrator for drag reduction at low speeds, Part II – Experimental validation using infra-red transition measurements during wind tunnel tests. *Chinese Journal of Aeronautics*, *30*. https://doi.org/10.1016/j.cja.2016.12.018

Koreanschi, A., Sugar Gabor, O., & Botez, R. M. (2016a). Drag Optimization of a Wing Equipped with a Morphing Upper Surface. *The Aeronautical Journal*, *120*, 473-493. https://doi.org/10.1017/aer.2016.6

Koreanschi, A., Sugar Gabor, O., & Botez, R. M. (2016). Numerical and Experimental Validation of a Morphed Wing Geometry Using Price-Païdoussis Wind Tunnel Testing. *The Aeronautical Journal*, *120*. https://doi.org/10.1017/aer.2016.30

Kota, S. (2016). Future Airplanes Will Fly On Twistable Wings. *IEEE*, *Spectrum*. Retrieved from https://spectrum.ieee.org/future-airplanes-will-fly-on-twistable-wings

Kota, S., Flick, P., & Collier, F. S. (2016). Flight Testing of FlexFloilTM Adaptive Compliant Trailing Edge. Dans *54th AIAA Aerospace Sciences Meeting*. San Diego, California, USA : American Institute of Aeronautics and Astronautics. https://doi.org/10.2514/6.2016-0036

Kuitche, M., Botez, R., Guillemin, A., & Communier, D. (2020). Aerodynamic Modelling of Unmanned Aerial System through Nonlinear Vortex Lattice Method, Computational Fluid Dynamics and Experimental Validation - Application to the UAS-S45 Bàlaam: Part 1. *INCAS BULLETIN*, *12*, 91-103. https://doi.org/10.13111/2066-8201.2020.12.1.9

Launder, B. E., & Spalding, D. B. (1974). The numerical computation of turbulent flows. *Computer Methods in Applied Mechanics and Engineering*, *3*(2), 269-289. https://doi.org/10.1016/0045-7825(74)90029-2

Le, N. T. P., Greenshields, Ch. J., & Reese, J. M. (2012). Evaluation of nonequilibrium boundary conditions for hypersonic rarefied gas flows. In *Progress in Flight Physics*, 217-230, Versailles, France. https://doi.org/10.1051/eucass/201203217

Lee, E. E., & Pendergraft, O. C. (1985). *Installation Effects of Long-Duct Pylon-Mounted Nacells on a Twin-Jet Transport Model with Swept Supercritical Wing* (Rapport No. 2457). Langley Memorial Laboratory, Hampton, Virginia, United-States : National Aeronautics and Space Administration (NASA).

Levy, D. (1992). Prediction of average downwash gradient for canard configurations. In *30th Aerospace Sciences Meeting and Exhibit*. Reno,NV,U.S.A. : American Institute of Aeronautics and Astronautics. https://doi.org/10.2514/6.1992-284

Li, S., & Paoli, R. (2019). Modeling of Ice Accretion over Aircraft Wings Using a Compressible OpenFOAM Solver. *International Journal of Aerospace Engineering*, *2019*, 1-11. https://doi.org/10.1155/2019/4864927

Liauzun, Cédric. (2006). Assessment of CFD Techniques for Wind Turbine Aeroelasticity. Dans *Volume 9: 6th FSI, AE and FIV and N Symposium*, 341-350, Vancouver, BC, Canada : ASMEDC. https://doi.org/10.1115/PVP2006-ICPVT-11-93800

Liauzun, Cedric, Le Bihan, D., David, J.-M., Joly, D., & Paluch, B. (2018). Study of morphing winglet concepts aimed at improving load control and the aeroelastic behavior of civil transport aircraft. *Aerospace Lab*, *10*(14), 1-15. https://doi.org/10.12762/2018.AL14-10

Liem, R. P., Mader, C. A., & Martins, J. R. R. A. (2015). Surrogate models and mixtures of experts in aerodynamic performance prediction for aircraft mission analysis. *Aerospace Science and Technology*, *43*, 126-151. https://doi.org/10.1016/j.ast.2015.02.019

Mangano, M., & Martins, J. R. R. A. (2021). Multipoint Aerodynamic Shape Optimization for Subsonic and Supersonic Regimes. *Journal of Aircraft*, *58*(3), 650-662. https://doi.org/10.2514/1.C036216

Martins, J. R. R. A. (2016). Fuel Burn Reduction Through Wing Morphing. Dans R. Blockley & W. Shyy (Éds), *Encyclopedia of Aerospace Engineering*, 1-7. Chichester, UK : John Wiley & Sons, Ltd. https://doi.org/10.1002/9780470686652.eae1007

Menter, F. R. (1994). Two-equation eddy-viscosity turbulence models for engineering applications. *AIAA Journal*, *32*(8), 1598-1605. https://doi.org/10.2514/3.12149

Menter, F. R., Kuntz, M., & Langtry, R. (2003). Ten Years of Industrial Experience with the SST Turbulence Model. *Turbulence, Heat and Mass Transfer*, *4*, 625-632.

Moukalled, F., Mangani, L., & Darwish, M. (2016). *The finite volume method in computational fluid dynamics: an advanced introduction with OpenFOAM and Matlab*. Springer.

Murrieta-Mendoza, A. (2017). *Application of Metaheuristic and Deterministic Algorithms for Aircraft Reference Trajectory Optimization* (Ph.D Thesis). Ecole de technologie superieure, Montreal, Quebec, Canada.

Murrieta-Mendoza, A., Beuze, B., Ternisien, L., & Botez, R. M. (2017). New Reference Trajectory Optimization Algorithm for a Flight Management System Inspired in Beam Search. *Chinese Journal of Aeronautics*, *30*. https://doi.org/10.1016/j.cja.2017.06.006

Murrieta-Mendoza, A., & Botez, R. M. (2020). Commercial Aircraft Trajectory Optimization to Reduce Flight Costs and Pollution: Metaheuristic Algorithms. In *Advances in Visualization and Optimization Techniques for Multidisciplinary Research: Trends in Modelling and Simulations for Engineering Applications,* 33-62, https://doi.org/10.1007/978-981-13-9806-3_2

Murrieta-Mendoza, A., Botez, R. M., & Bunel, A. (2018). Four-Dimensional Aircraft En Route Optimization Algorithm Using the Artificial Bee Colony. *Journal of Aerospace Information Systems*, *15*, 1-28. https://doi.org/10.2514/1.I010523

Murrieta-Mendoza, A., Romain, C., & Botez, R. M. (2016). Commercial Aircraft Lateral Flight Reference Trajectory Optimization. *IFAC-PapersOnLine*, *49*(17), 1-6. https://doi.org/10.1016/j.ifacol.2016.09.001

Murrieta-Mendoza, A., Ternisien, L., Beuze, B., & Botez, R. M. (2018). Aircraft Vertical Route Optimization by Beam Search and Initial Search Space Reduction. *Journal of Aerospace Information Systems*, *15*, 1-15. https://doi.org/10.2514/1.I010561

OpenCFD ltd (ESI Group). (2019). *OpenFoam The Open Source CFD Toolbox*. OpenCFD ltd (ESI Group). Retrieved from https://www.openfoam.com/documentation/user-guide/

OpenCFD ltd (ESI Group). OpenFoam User-Guide v1912.

Ortiz, P., & Alley, N. (2018). Spanwise Adaptive Wing - PTERA Flight Test [Technical presentation]. AIAA Aviation 2018. Retrieved from https://ntrs.nasa.gov/api/citations/20180004640/downloads/20180004640.pdf

Panagiotou, P., Efthymiadis, M., Mitridis, D., & Yakinthos, K. (2018). A CFD-aided investigation of the morphing winglet concept for the performance optimization of fixed-wing MALE UAVs. In *2018 Applied Aerodynamics Conference*. Atlanta, Georgia : American Institute of Aeronautics and Astronautics. https://doi.org/10.2514/6.2018-4220

Pecora, R. (2021). Morphing wing flaps for large civil aircraft: Evolution of a smart technology across the Clean Sky program. *Chinese Journal of Aeronautics*, *34*(7), 13-28. https://doi.org/10.1016/j.cja.2020.08.004

Pecora, R., Amoroso, F., Amendola, G., & Concilio, A. (2014). Validation of a smart structural concept for wing-flap camber morphing. *Smart Structures and Systems*, *14*(4), 659-678. https://doi.org/10.12989/SSS.2014.14.4.659

Popov, A. V., Grigorie, T. L., Botez, R. M., Mébarki, Y., & Mamou, M. (2010). Modeling and Testing of a Morphing Wing in Open-Loop Architecture. *Journal of Aircraft*, *47*(3), 917-923. https://doi.org/10.2514/1.46480

Raymer, D. P. (2012). *Aircraft design: a conceptual approach* (5th ed). Reston, VA : American Institute of Aeronautics and Astronautics.

République Française. (2005). *Maîtrise des émissions de gaz à effet de serre de l'aviation civile*. France : Ministère de l`équipement, des Transport, de l'aménagement du Territoire, du Tourisme et de la mer.

Rolls-royce. (2019). *Rolls-Royce completes acquisition of Siemens' Electric and Hybrid-Electric aerospace propulsion business*. Rolls-royce. Retrieved from https://www.rolls-royce.com/media/press-releases/2019/01-10-19-rr-completes-acquisition-of-siemens-electric-and-hybrid-electric-aerospace-propulsion.aspx

Rumsey, C. (2020). NASA Langley Research Center - Turbulence Modeling Resource. Retrieved from https://turbmodels.larc.nasa.gov/index.html

SARISTU (Project), Final Conference, W., Piet Christof, & Papadopoulos, M. (2016). *Smart Intelligent Aircraft Structures (SARISTU): proceedings of the Final Project Conference*.

Schrass, J. A., Leal, P. B., & Hartl, D. J. (2020). Structurally Feasible Morphing of a Low-Boom Supersonic Transport. In *AIAA Scitech 2020 Forum*. Orlando, FL : American Institute of Aeronautics and Astronautics. https://doi.org/10.2514/6.2020-0791

Secco, N. R., Kenway, G. K. W., He, P., Mader, C., & Martins, J. R. R. A. (2021). Efficient Mesh Generation and Deformation for Aerodynamic Shape Optimization. *AIAA Journal*, *59*(4), 1151-1168. https://doi.org/10.2514/1.J059491

Segui, M., Abel, F. R., Botez, R. M., & Ceruti, A. (2021a). High-fidelity aerodynamic modeling of an aircraft using OpenFoam – application on the CRJ700. *The Aeronautical Journal*, *126*(1298), 585-606. https://doi.org/10.1017/aer.2021.86

Segui, Marine. (2018). *Mesure de l'impact de la technologie d'aile deformable sur les performances en croisière de l'avion d'affaire Cessna Citation X*. M.Sc. École de technologie supérieure, Montréal, QC, Canada.

Segui, Marine, Abel, F. R., Botez, R. M., & Ceruti, A. (2021b). New Aerodynamic Studies of an Adaptive Winglet Application on the Regional Jet CRJ700. *Biomimetics*, *6*(4), 54. https://doi.org/10.3390/biomimetics6040054

Segui, Marine, Bezin, S., & Botez, R. M. (2018). Cessna Citation X Performances Improvement by an Adaptive Winglet during the Cruise Flight. *International Journal of Aerospace and Mechanical Engineering*, *12*(4), 423-430. https://doi.org/10.5281/zenodo.1316402

Segui, Marine, & Botez, R. M. (2018a). Aerodynamic Coefficients Prediction from Minimum Computation Combinations Using OpenVSP Software. *International Journal of Mechanical and Industrial Engineering*, *12*(1), 9-16. https://doi.org/10.5281/zenodo.1315609

Segui, Marine, & Botez, R. M. (2018b). Cessna Citation X Climb and Cruise Performance Improvement Using Adaptive Winglet. Dans *Advanced Aircraft Efficiency in a Global Air Transport System 18' (AEGATS)*, 13(1), Toulouse, France

Segui, Marine, & Botez, R. M. (2018c). Cessna Citation X Static Cruise Improvement using Morphing Wing Application on its Horizontal Tail. Dans *European Conference for Aeronautics and Space Sciences (EUCASS)*. Madrid, Spain. https://doi.org/DOI: 10.13009/EUCASS2019-494

Segui, Marine, Botez, R. M., Abel, F. R., & Ceruti, A. (2021). Improvement of the Regional Jet CRJ700 Winglet Design based on Morphing Wing Principles. In *Canadian Aeronautics and Space proceedings* (CASI).

Segui, Marine, Gabor, O. S., Koreanschi, A., & Botez, R. M. (2017). Morphing Wing Application on Hydra Technologies UAS-S4. In *Modelling, Identification and Control*. Innsbruck, Austria. https://doi.org/10.2316/P.2017.848-048

Segui, Marine, Ghazi, G., Botez, R. M., & Thompson, E. (2018). Design, Development and Validation of a Cessna Citation X Aerodynamic Model using OpenVSP Software. In *2018 Modeling and Simulation Technologies Conference* (No. AIAA 2018-3256). Atlanta, Georgia, USA : American Institute of Aeronautics and Astronautics. https://doi.org/10.2514/6.2018-3256

Segui, Marine, Kuitche, M., & Botez, R. M. (2017). Longitudinal Aerodynamic Coefficients of Hydra Technologies UAS-S4 from Geometrical Data. In *AIAA Modeling and Simulation Technologies Conference*. Grapevine, Texas : American Institute of Aeronautics and Astronautics. https://doi.org/10.2514/6.2017-0579

Segui, Marine, Mantilla, M., & Botez, R. M. (2018). Design and Validation of an Aerodynamic Model of the Cessna Citation X Horizontal Stabilizer Using both OpenVSP and Digital Datcom. *International Journal of Mechanical, Industrial and Aerospace Sciences*, *11.0*(1). https://doi.org/10.5281/zenodo.1315951

Segui, Marine, Mantilla, M., Ghazi, G., & Botez, R. M. (2018). New Economical Cruise Methodology for the Cessna Citation X Business Jet by an Original Morphing Horizontal Tail Application. In *2018 Modeling and Simulation Technologies Conference* (Vol. No: AIAA 2018-3895). Atlanta, Georgia, USA : American Institute of Aeronautics and Astronautics. https://doi.org/10.2514/6.2018-3895

Smith, D. D., Lowenberg, M. H., Jones, D. P., & Friswell, M. I. (2014). Computational and Experimental Validation of the Active Morphing Wing. *Journal of Aircraft*, *51*(3), 925-937. https://doi.org/10.2514/1.C032262

Smith, M. S., Sandwich, C., & Alley, N. R. (2018). Aerodynamic Analyses in Support of the Spanwise Adaptive Wing Project. NASA document 20180004609, Atlanta, Georgia, USA. Retrieved from https://ntrs.nasa.gov/citations/20180004609

Solar Impulse Foundation. (2016a). Around the world to promote clean technologies. *Solar Impulse*. Retrieved from https://www.solarimpulse.com/

Solar Impulse Foundation. (2016b). *The First Ever Round-The-World Solar Flight at a Glance* (Rapport No. Facts and Figures). SolarImpulse. Retrieved from https://aroundtheworld.solarimpulse.com/img/pdf/SI_RTW_FACTSHEET_PRESS.pdf

Sorribes-Palmer, F., Sanz Andres, A., Figueroa, A., Donisi, L., Franchini, S., & Ogueta, M. (2017). Aerodynamic Design of a Wind Turbine Diffuser with OpenFoam. Communication présentée au 7th European and African Conference on Wind Engineering, Liège, Belgium : European & African Conferences on Wind Engineering (EACWE).

Spalart, P. R., & Rumsey, C. L. (2007). Effective Inflow Conditions for Turbulence Models in Aerodynamic Calculations. *AIAA Journal*, *45*(10), 2544-2553. https://doi.org/10.2514/1.29373

Stańkowski, T. P., MacManus, D. G., Sheaf, C. T., & Christie, R. (2016). Aerodynamics of aero-engine installation. *Proceedings of the Institution of Mechanical Engineers, Part G: Journal of Aerospace Engineering*, *230*(14), 2673-2692. https://doi.org/10.1177/0954410016630332

Sugar Gabor, O. (2015). *Validation of Morphing Wing Methodologies on an Unmanned Aerial System and a Wind Tunnel Demonstrator*. Ph.D. École de technologie supérieure, Montréal, QC, Canada.

Sugar Gabor, O., Koreanschi, A., & Botez, R. (2016). A new non-linear vortex lattice method: Applications to wing aerodynamic optimizations. *Chinese Journal of Aeronautics*, *29*. https://doi.org/10.1016/j.cja.2016.08.001

Sugar Gabor, O., Koreanschi, A., Botez, R. M., Mamou, M., & Mebarki, Y. (2016a). Analysis of the Aerodynamic Performance of a Morphing Wing-Tip Demonstrator Using a Novel Nonlinear Vortex Lattice Method. In *34th AIAA Applied Aerodynamics Conference*. Washington, D.C. : American Institute of Aeronautics and Astronautics. https://doi.org/10.2514/6.2016-4036

Sugar Gabor, O., Koreanschi, A., Botez, R. M., Mamou, M., & Mebarki, Y. (2016b). Numerical simulation and wind tunnel tests investigation and validation of a morphing wing-tip demonstrator aerodynamic performance. *Aerospace Science and Technology*, *53*, 136-153. https://doi.org/10.1016/j.ast.2016.03.014

Sugar Gabor, O., Simon, A., Koreanschi, A., & Botez, R. M. (2014). Application of a Morphing Wing Technology on Hydra Technologies Unmanned Aerial System UAS-S4. In *Volume 1: Advances in Aerospace Technology*. Montreal, Quebec, Canada. American Society of Mechanical Engineers. https://doi.org/10.1115/IMECE2014-37619

Tchatchueng Kammegne, M. J., & Botez, R. (2019). A new hybrid control methodology for a morphing aircraft wing-tip actuation mechanism. *The Aeronautical Journal*, *123*, 1-31. https://doi.org/10.1017/aer.2019.106

Tchatchueng Kammegne, M. J., Botez, R. M., & Grigorie, T. L. (2016). A Fuel Saving Way in Aerospace Engineering based on Morphing Wing Technology – A New Multidisciplinary Experimental Model. *International Journal of Contemporary ENERGY*, 2(2), 11-21. https://doi.org/10.14621/ce.20160202

Tchatchueng Kammegne, M. J., Tondji, Y., Botez, R., Grigorie, T. L., Mamou, M., & Mebarki, Y. (2017). New control methodology for a morphing wing demonstrator. *Proceedings of the Institution of Mechanical Engineers, Part G: Journal of Aerospace Engineering*, *232*, 095441001769900. https://doi.org/10.1177/0954410017699003

The Boeing Company. (2009). AERO Magazine, Operational Efficiency and Environmental Performance. Retrieved from https://www.boeing.com/commercial/aeromagazine/

United Airlines. (2014). United Airlines is the First to Fly with New, Fuel-Efficient Split Scimitar Winglets. United Airlines Worldwide Media Relations. Retrieved from https://united.mediaroom.com/2014-02-19-United-Airlines-is-the-First-to-Fly-with-New-Fuel-Efficient-Split-Scimitar-Winglets

Ursache, N., Melin, T., Isikveren, A., & Friswell, M. (2007). Morphing Winglets for Aircraft Multi-Phase Improvement. In *7th AIAA ATIO Conf, 2nd CEIAT Int'l Conf on Innov and Integr in Aero Sciences,17th LTA Systems Tech Conf; followed by 2nd TEOS Forum*. Belfast, Northern Ireland : American Institute of Aeronautics and Astronautics. https://doi.org/10.2514/6.2007-7813

Vittadini, G. (2020). Our decarbonisation journey continues: looking beyond E-Fan X, *Airbus Newsroom*. Retrieved from https://www.airbus.com/en/newsroom/stories/2020-04-our-decarbonisation-journey-continues-looking-beyond-e-fan-x

Welcome to the Clean Sky | Clean Sky. (2020). Retrieved from https://www.cleansky.eu/

Whitcomb, R. T. (1976). *A design approach and selected wind tunnel results at high subsonic speeds for wing-tip mounted winglets* (Rapport No. NASA-TN-D-8260). NASA Langley Research Center Hampton : NASA. Retrieved from https://ntrs.nasa.gov/citations/19760019075

White, F. M. (2006). *Viscous fluid flow* (3rd ed). New York, NY : McGraw-Hill Higher Education.

Wilcox, D. C. (2006). *Turbulence Modeling for CFD* (third), DCW Industries, Inc.

Wildschek, A., Storm, S., Herring, M., Drezga, D., Korian, V., & Roock, O. (2015). Design, Optimization, Testing, Verification, and Validation of the Wingtip Active Trailing Edge, 219-255. https://doi.org/10.1007/978-3-319-22413-8_12

Wilson, T. (2019). The albatross is inspiring tomorrow's aircraft wings. *Airbus Innovation*. Retrieved from https://www.airbus.com/newsroom/stories/the-albatross-is-inspiring-tomorrows-next-generation-of-aircraft-wings.html

Yan, X., & Su, X. (2009). *Linear regression analysis theory and computing*.

Zhang, Z. J., Khosravi, S., & Zingg, D. W. (2017). High-fidelity aerostructural optimization with integrated geometry parameterization and mesh movement. *Structural and Multidisciplinary Optimization*, *55*(4), 1217-1235. https://doi.org/10.1007/s00158-016-1562-7

Zou, Y., Zhao, X., & Chen, Q. (2018). Comparison of STAR-CCM+ and ANSYS Fluent for Simulating Indoor Airflows. *Building Simulation*, *11*(1), 165-174. https://doi.org/10.1007/s12273-017-0378-8